Chapter 9

Double-Quantum ESR and Distance Measurements

Petr. P. Borbat and Jack. H. Freed
Baker Laboratory of Chemistry and Chemical Biology Cornell University, Ithaca, NY 14853

Abstract: "Allowed" double quantum coherences (DQC) can now be routinely generated in disordered and oriented solids containing nitroxide biradicals and random distributions of stable radicals. The Pake doublets obtained from DQC pathways can be effectively used to determine a broad range of distances in the former case whereas decay constants yield concentrations in the latter. The DQC signals are strong and often comparable to standard single quantum signals. They are free of any large undesirable signals, so the DQ experiment is easy to perform. Their strong intensity permits the study of low concentrations of spins in samples typical of those ordinarily met in the case of doubly-labeled macromolecules such as proteins and polypeptides. The upper range of distances for systems labeled with nitroxides is estimated to be ca. 80 Å. In the limit of non-selective pulses the interpretation of DQC signals becomes independent of complicating geometric features which affect other ESR distance methods. The method is compared to other existing pulse distance measurement techniques and future improvements are also discussed.

1. INTRODUCTION: MOTIVATION

Multiple quantum coherence (MQC) is a well-known phenomenon in modern NMR, with many useful applications (Ernst *et al.*, 1987). On the other hand, it has been a considerable challenge to generate MQC in pulsed ESR. In recent work, Saxena and Freed (1997a) showed how "forbidden" coherence (FC) pathways can be utilized to generate double quantum coherence (DQC) spectra from a doubly labeled nitroxide (Saxena and Freed, 1996, 1997a). These FC pathways could be generated even under spectrometer conditions that were not favorable for producing DQC in nitroxides by allowed pathways, [e.g. insufficiently large microwave magnetic (B_1) fields in resonators with wide bandwidths]. A useful feature of the FC pathways is

FROM:
Biological Magnetic Resonance
Vol. 19, Distance Measurements in
Biological Systems by EPR.
Edited by: Lawrence J. Berliner,
Sandra S. Eaton, and Gareth R. Eaton,
Kluwer Academic/Plenum Pub. 2000.

that they are able to provide some orientational selectivity with respect to the angle between the interspin vector, $\boldsymbol{r}$, and the static magnetic field $\boldsymbol{B}_0$. This enhances their utility for measuring the distance between electron spins. A disadvantage is in weaker signals, and the precise adjustment of the B_1 field to its optimum magnitude is a complicating factor.

Given recent developments in pulsed ESR capabilities in our laboratory (Borbat and Freed, 1997) consisting of shorter dead-times, increased B_1's without a loss in resonator bandwidth, and increased signal-to-noise ratio (SNR) at higher working frequency, it proved possible to directly produce MQC by "allowed" pathways using several pulse sequences similar to those employed in NMR, but specially tailored for the ESR challenges (Borbat and Freed, 1999). These challenges include short relaxation times, T_2. They also include the typically broad spectral extent arising from electron-nuclear dipolar and g-tensor interactions that requires very strong B_1-fields in order to irradiate all the electron spins. Our successful results show, that by "allowed" coherence pathways, DQC signals can be achieved that are 10-100 times greater than for FC pathways. They also indicate some of the potentially rich uses to which MQC ESR can be employed. More recent results show that DQC signals can be obtained with smaller B_1 fields, especially in the case of large distances, but at the expense of SNR and resolution. Also, smaller B_1's considerably increase the minimum distance that can be reliably measured, (Borbat and Freed, 2000).

In the present chapter we emphasize the use of DQC for measurements of broad range of distances, which is important in solid-state studies and in biophysics. In the latter context one can use nitroxide bilabeled macromolecules to study aggregation and conformations in peptides and proteins as well as movement of their fragments (Farhbakhsh *et al.*, 1997; Thorgeirsson *et al.*, 1997). However, these biophysical applications were limited by an upper range of distance of ca. 20 Å (Rabenstein and Shin, 1995) since they are based upon cw-ESR. Also, whereas fluorescence energy transfer is capable of measuring distances greater than 20 Å, it requires two different types of fluorescent probes, and it is often limited by the uncertainty in the κ^2 parameter, which depends on the relative orientation of the transition-moments of the two chromophores. In the case of ESR, electron spins are oriented along $\boldsymbol{B}_0$.

Pulsed ESR methods have been used in the past by Milov *et al.* (1981, 1985), Ichikawa *et al.* (1985), Raitsimring and Salikhov (1985), Borbat *et al.*, (1977); to yield spatial distributions in solids. Several methods of practical importance have emerged. They are based on modifying the single quantum (SQ) echo produced by a 2 or 3 pulse sequence with a pulse at either the same frequency (Kurshev *et al.*, 1989; cf. Ch. 10) or at a different frequency (Milov *et al.*, 1998; Pfannebecker *et al.*, 1996; Pannier *et al.*, 1998; Larsen

and Singel, 1993). The latter, based on selective pulses, which is known as DEER (double electron-electron resonance) or PELDOR, (Milov *et al.*, 1998; cf. Ch. 11), originated from a solid-state NMR concept (Emshwiller *et al.*, 1960). It has proven effective in a number of applications, including bi-labeled biomolecules. Unlike DQC, it is not based on coherent effects. While there are some similarities, we find that DQC based upon allowed pathways offers several advantages compared to DEER. For example, DQC with strong pulses can yield signals that are at least an order of magnitude greater, in fact comparable to single quantum (SQ) signals from non-selective pulses. This is a very desirable feature when working with small amounts of bila-beled biomolecule and/or when greater sensitivity is needed for measuring longer distances, up to ca. 80 Å.

Strictly speaking, the requirement of using strong (or nearly non-selective) pulses is not absolutely necessary for "allowed" DQC signals to be observed. However it is very beneficial to use pulses as strong as possible. Recent work has shown that some coherent SQ pulse sequences are also use-ful for distance measurements, but are not nearly as effective as the DQ sig-nals produced by strong pulses (Borbat and Freed, 1999a, 2000).

2. THEORY OF DOUBLE QUANTUM COHERENCE

2.1 Multiple Quantum Coherences in ESR

"Allowed" multiple-quantum coherences in ESR were not observed until recently (Borbat, and Freed, 1999) although a form of "forbidden" DQC was reported by Saxena and Freed (1996) and a general theoretical approach for "forbidden" and "allowed" DQC was given by these authors (Saxena and Freed, 1997a). MQC were predicted by Tang, Norris *et al.*, (1995) and ob-served by Dzyuba *et al.*, (1996) in spin-correlated radical pairs formed by laser-induced dissociation (cf. Ch. 13). The relevant zero quantum (ZQ) co-herence arises naturally from the initial polarized non-equilibrium state. This important special case is sufficiently different from the present study that we do not consider it further. The MQC experiment in ESR that we explore is based upon the same principles that were developed in pulsed NMR. In this section, we outline the basics of the double-quantum coherence ESR ex-periment using a simplified approach.

2.1.1 Double and Zero-Quantum Coherences

Multiple-quantum transitions and coherences have been treated in detail in numerous studies in the field of NMR. See for example the following ref-

erences (Ernst *et al.*, 1987; Slichter, 1990; Cavanagh, 1996; Corio, 1966). Here, we outline the basic concepts and definitions in a way that is appropriate for the ESR experiment.

For a quantum system in thermal equilibrium, only the diagonal density matrix elements are non-zero and they represent the populations of the corresponding energy levels. All off-diagonal density matrix elements are zero. This is the fundamental property of random phases between any two states of the quantum system at thermal equilibrium. Non-zero off-diagonal density matrix elements correspond to coherent non-equilibrium superposition of states and therefore must vanish as the system approaches the equilibrium state. These elements are often referred to as coherences, and they can be produced by a coherent perturbation, for example by an *rf* pulse acting on the system. The action of the pulse yields such a coherent superposition between the states involved in the transition, which will persist until the system relaxes to thermal equilibrium.

In summary, coherences may be generated by coherently inducing transitions between states, and they are represented by the corresponding off-diagonal elements of the density matrix. Consider for example a system of two coupled spins of 1/2. In Fig. 1 we have four possible single-quantum transitions.

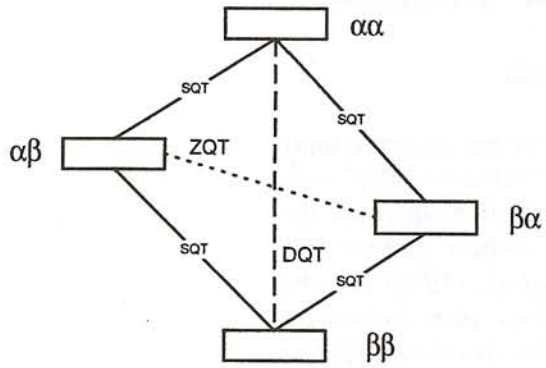

Figure 1. Energy level diagram for the two-spin system showing single (SQT), double (DQT), and zero (ZQT) quantum transitions.

These transitions are represented by the corresponding off-diagonal elements of the density matrix for the two spins. One can conveniently express the density matrix as the expansion in a complete set of the spin operators, (e.g. the density matrix for a single spin is given as a linear combination of the Pauli spin matrices and the unit operator; for many-spin systems one should take the direct product).

Then the coherences can be conveniently expressed by the spin operators corresponding to the elements of the density matrix for two spins defined in the product space $|m_1 m_2\rangle$. Single quantum transitions are represented by:

$$S_1^+ S_2^\alpha,\ S_1^+ S_2^\beta,\ S_1^- S_2^\alpha,\ S_1^- S_2^\beta \tag{1}$$

and those obtained by permuting the spins. Here,

$$S_i^\alpha \equiv \tfrac{1}{2} E_i + S_{iz},\quad S_i^\beta \equiv \tfrac{1}{2} E_i - S_{iz} \tag{2}$$

and E_i is the 2×2 unit operator for the i^{th} spin. Associated with these transitions are the single-quantum coherences (SQC), of which four are "inphase" coherences, which have the form:

$$S_1^\pm (S_2^\alpha + S_2^\beta) = S_1^\pm E_2 . \tag{3}$$

They correspond to the observable transverse magnetization. The other four are the antiphase coherences which cannot be directly detected but can evolve into observable SQC. They have the form:

$$S_1^\pm (S_2^\alpha - S_2^\beta) = 2 S_1^\pm S_{2z} . \tag{4}$$

The double- and zero-quantum coherences (DQC and ZQC, respectively) are associated with the remaining two transitions. DQC and ZQC correspond to transitions with simultaneous flips or flip-flops of both spins, respectively, and can be represented as follows (Ernst *et al.*, 1987; Cavanagh *et al.*, 1996):

$$\begin{aligned} DQ_x &= \frac{1}{2}(S_1^+ S_2^+ + S_1^- S_2^-) = \frac{1}{2}(2S_{1x}S_{2x} - 2S_{1y}S_{2y}) \\ DQ_y &= \frac{1}{2i}(S_1^+ S_2^+ - S_1^- S_2^-) = \frac{1}{2}(2S_{1x}S_{2y} + 2S_{1y}S_{2x}) \end{aligned} \tag{5a}$$

$$\begin{aligned} ZQ_x &= \frac{1}{2}(S_1^+ S_2^- + S_1^- S_2^+) = \frac{1}{2}(2S_{1x}S_{2x} + 2S_{1y}S_{2y}) \\ ZQ_y &= \frac{1}{2i}(S_1^+ S_2^- - S_1^- S_2^+) = \frac{1}{2}(2S_{1y}S_{2x} - 2S_{1x}S_{2y}) . \end{aligned} \tag{5b}$$

These coherences do not correspond to any experimental observables. They can only be detected indirectly in a pulse experiment. The multiple-quantum experiment is based on the fact that by a suitable pulse sequence, an antiphase SQC can be made to develop and can then be converted into higher orders of coherence and *vice versa*. The antiphase SQC also can be converted into an observable inphase SQC. These properties determine the strategy of the pulsed multiple-quantum experiment (Fig. 2). During the preparation period, the inphase SQC produced by the first pulse of the sequence evolves into an antiphase SQC due to the coupling between the spins. (More pulses can be applied during this period.) Then this coherence is converted by another pulse into ZQC, DQC or even higher orders of coherence (depending on the total spin of the system).

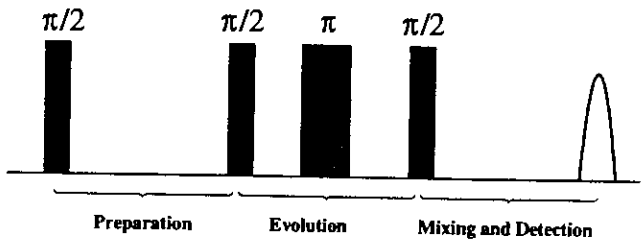

Figure 2. General scheme for the multiple-quantum experiment is exemplified by the 4-pulse sequence. The multiple-quantum pulsed experiment can be subdivided into the distinct periods:

1. During the preparation period single-quantum coherence evolves and becomes labeled by its interaction with other spins and then is converted into higher orders of coherence by the second pulse.
2. Evolution occurs when these newly created multiple-quantum coherences are allowed to evolve. (This period can, and normally will, include additional *rf* or field gradient pulses).
3. Mixing and detection starts with the last $\pi/2$ pulse, which transforms the higher orders of coherence into other orders of coherence including undetectable antiphase single-quantum coherence, which then evolves into observable inphase coherence.

At this stage, these higher orders of coherence evolve during the "evolution period" (with more pulses being applied during this period, as needed to complete the sequence or enhance performance). Finally, during the "mixing" and detection periods these coherences can be converted by an appropriate pulse into antiphase SQC, which evolves into the observable inphase SQC, that at last is detected as an FID or a spin-echo.

The incorporation of the evolution period for multiple-quantum coherence into the pulse sequence results in multiple-quantum filtering; i.e. the sequence transmits only those signals that directly involve the couplings between all of the spins involved in multiple-quantum transitions.

We illustrate these principles with specific examples that are relevant to the pulse schemes currently employed in multiple-quantum pulsed ESR experiments. We assume, for simplicity of presentation, that we have an isolated pair of weakly coupled spins of ½ and perfect, i.e. non-selective *rf* pulses. For a single pair of spins of ½ the highest order of coherence that can be produced is just two. Also we use a weak-coupling Hamiltonian (c.f. Sec. 2.2) in the rotating frame. We split the Hamiltonian into the two parts:

$$H = H_z + H_{zz} \tag{6a}$$

the first one contains the resonant offset terms

$$H_z = \Delta\Omega_1 S_{1z} + \Delta\Omega_2 S_{2z} \tag{6b}$$

while the last term is a dipolar coupling in the weak-coupling limit

$$H_{zz} = aS_{1z}S_{2z}\,. \tag{6c}$$

Here $\Delta\Omega_1$ and $\Delta\Omega_2$ represent the deviation of the resonant frequencies for the spins 1 and 2 respectively from the applied frequency, ω_{rf}. Also $aS_{1z}S_{2z}$ is the secular part of the spin-spin coupling. At this introductory stage, these assumptions are made to simplify the discussion.

2.1.2 Preparation

We describe the preparation of DQC by the use of 2 or 3 pulses. These pulse sequences are the standard preparation sequences in NMR (Ernst *et al.*, 1987) and were employed in the recent DQ ESR experiments by Borbat and Freed, (1999).

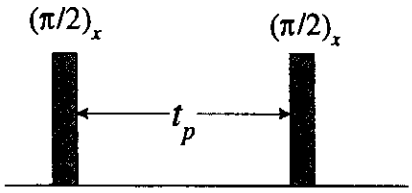

Figure 3. Preparation of multiple-quantum coherence with two pulses for the 4 and 5 pulse sequences.

For the two-pulse preparation sequence (cf. Fig. 3) the first pulse acts on both spins creating transverse magnetization that is proportional to inphase

SQC ($S_{1y} + S_{2y}$). Since S_{1y} and S_{2y} will yield equivalent results (but with subscripts permuted) we need only consider S_{1y} below. We shall employ, at this introductory stage, the standard Product Operator (PO) method (Sørensen *et al.*, (1983); Slichter, (1990); Ernst *et al.*, (1987); Cavanagh *et al.*, (1996); Shriver, 1992).

Here the pulses are taken as ideal $\pi/2$ or π pulses and according to Eqs. 6 the resonant offset terms in H_z commute with the dipolar coupling H_{zz} in the weak-coupling limit. For example, we find using the PO method that the effect of H_{zz} acting over a time, t on S_{1x} and S_{1y} is:

$$\begin{aligned} S_{1x} &\xrightarrow{H_{zz}t} S_{1x}\cos(at/2) + (2S_{1y}S_{2z})\sin(at/2) \\ S_{1y} &\xrightarrow{H_{zz}t} S_{1y}\cos(at/2) - (2S_{1x}S_{2z})\sin(at/2). \end{aligned} \tag{7}$$

One can see from Eq. 7 that the action of a finite spin-spin coupling term a during the time interval t will cause the inphase SQC's S_{1x}, S_{1y} to evolve as $\cos(at/2)$, whereas antiphase SQC's $S_{1x}S_{2z}$, $S_{1y}S_{2z}$ evolve as $\sin(at/2)$. That is, there are "coherent oscillations" between these two coherences. When we include the resonant offset terms as well, we find:

$$\begin{aligned} S_{1y} \xrightarrow{Ht} &(S_{1y}\cos\Delta\Omega_1 t + S_{1x}\sin\Delta\Omega_1 t)\cos(at/2) \\ &+ 2(S_{1x}S_{2z}\cos\Delta\Omega_1 t - S_{1y}S_{2z}\sin\Delta\Omega_1 t)\sin(at/2)\,. \end{aligned} \tag{8}$$

At the end of the time interval $t = t_p$ the second $\pi/2$-pulse converts the relevant antiphase SQ coherence into the sum of DQC and ZQC.

$$\begin{aligned} &2S_{1x}S_{2z}\cos\Delta\Omega_1 t_p \sin(at_p/2) \xrightarrow{(\pi/2)_x} \cos\Delta\Omega_1 t_p \sin(at_p/2) \\ &\times[\underbrace{(2S_{1x}S_{2y} + 2S_{1y}S_{2x})}_{DQ_y}/2 - \underbrace{(2S_{1y}S_{2x} - 2S_{1x}S_{2y})}_{ZQ_y}/2]. \end{aligned} \tag{9}$$

In this case the DQC and ZQC will be produced in equal amounts. (In the case of $\Delta\Omega_1 = \Delta\Omega_2$ the ZQ_y term vanishes when we consider the similar expression derived for S_{2y}). In. 9 we do not consider any of the other terms on the rhs, since they will lead to unwanted coherence pathways, that must be canceled out by "phase cycling", cf. below. With the 3-pulse preparation sequence, which we consider next, we can obtain better conditions for generation of DQC. In this sequence, the first pulse again produces SQ coherence $S_{1y}+S_{2y}$.

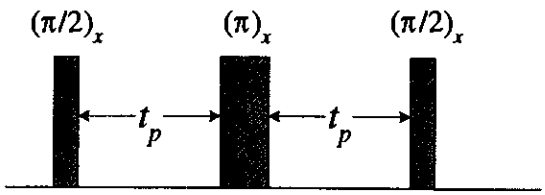

Figure 4. Preparation of DQC with three pulses used in the six-pulse sequence.

This coherence under the combined action of the spin-spin interaction, and the refocusing π-pulse, evolves into the sums of SQ inphase $S_{1y}+S_{2y}$ and antiphase $(S_{1x}S_{2z}+S_{1z}S_{2x})$ coherences:

$$(S_{1y}+S_{2y}) \xrightarrow{Ht_p} \xrightarrow{(x)_x} \xrightarrow{Ht_p} (S_{1y}+S_{2y})\cos at_p + 2(S_{1x}S_{2z}+S_{1z}S_{2x})\sin at_p . \tag{10}$$

Here, the refocusing π-pulse removes any dependence upon the frequency offsets $\Delta\Omega_1$ and $\Delta\Omega_2$. The last $(\pi/2)_x$ pulse in this three-pulse "sandwich" turns antiphase SQC into DQC:

$$2(S_{1x}S_{2z}+S_{1z}S_{2x})\sin at_p \xrightarrow{(\pi/2)_x} 2(S_{1x}S_{2y}+S_{1y}S_{2x})\sin at_p . \tag{11}$$

Thus all the SQC will be transformed into DQC when $\sin(at_p)=1$. For this case, there is no ZQC. Note, that if the last pulse in the sequence were applied along the y-axis, no DQC would be produced. Thus we see that in the case of non-selective pulses, and the preparation sequence of Fig. 4, only DQ_y is produced.

2.1.3 Evolution of DQC and ZQC due to the Frequency Offsets

During the evolution period the DQC and ZQC evolve due to resonant frequency offsets and are invariant with respect to the dipolar part of the Hamiltonian:

$$DQ_{x(y)} \xrightarrow{H_0 t} DQ_{x(y)}\cos[(\Delta\Omega_1+\Delta\Omega_2)t] \pm DQ_{y(x)}\sin[(\Delta\Omega_1+\Delta\Omega_2)t]$$
$$ZQ_{x(y)} \xrightarrow{H_0 t} ZQ_{x(y)}\cos[(\Delta\Omega_1-\Delta\Omega_2)t] \pm ZQ_{y(x)}\sin[(\Delta\Omega_1-\Delta\Omega_2)t]. \tag{12a}$$

For the case of a typical ESR spectrum where there are wide spectral extents, signals are detected in the form of echoes, and the FID's decay too fast to be

detected. To produce the maximum of the SQ echo at the final stage, the coherences in Eq. 12a should be refocused. The refocusing can be accomplished by a π-pulse placed at the middle of the DQC or ZQC pathway forming the sequence t_1 - π - t_1. From Eq. 5a it follows that

$$DQ_y \xrightarrow{\pi_x} -DQ_y\ , \qquad DQ_x \xrightarrow{\pi_x} DQ_x\ . \tag{12b}$$

Let us suppose that the second t_1 interval is changed by an amount δt. From Eqs. 12a and 12b one finds:

$$\begin{aligned} DQ_y(2t_1+\delta t) = DQ_y(0)\cos[(\Delta\Omega_1+\Delta\Omega_2)\delta t] \\ -DQ_x(0)\sin[(\Delta\Omega_1+\Delta\Omega_2)\delta t]. \end{aligned} \tag{12c}$$

Let us assume for simplicity that both spins have identical ESR spectra of the form $g(\Delta\Omega)=\pi^{-1/2}\Delta\Omega_0^{-1}\exp(-\Delta\Omega^2/\Delta\Omega_0^2)$ where $\Delta\Omega_0$ represents the spectrum width. Then we can integrate Eq. 12c over the distribution for both spins, to obtain the average signal for $DQ_y(2t_1+\delta t)$. We find:

$$DQ_y(2t_1+\delta t) = DQ_y(0)\exp(-\Delta\Omega_0^2\delta t^2/2)\ . \tag{12d}$$

The same result holds for ZQC. The reader can see that Eq. 12d describes an "echo" with maximum at δt = 0 and half width of $2(2\ln 2)^{1/2}\Delta\Omega_0^{-1}$. However, this DQ echo cannot be directly observed.

2.1.4 Mixing and Detection

At the end of the evolution period the final $\pi/2$ pulse (cf. Fig. 2) converts the refocused MQC (cf. previous Section) into SQ antiphase coherence. It will then evolve into observable inphase coherence. For the 6-pulse sequence described in Sec. 2.1.5 we have:

$$\begin{aligned} &\frac{1}{2i}(S_1^+S_2^+ - S_1^-S_2^-)\sin at_p \xrightarrow{(\pi/2)_x} \\ &-\frac{1}{2}(2S_1^+S_{2z} + 2S_2^+S_{1z} - 2S_1^-S_{2z} - 2S_2^-S_{1z})\sin at_p. \end{aligned} \tag{13}$$

This is essentially the reverse of Eq. 11. The antiphase coherences evolve during the mixing time into observable SQ coherences.

That is:

$$-\frac{1}{2}(2S_1^+S_{2z}+2S_2^+S_{1z}-2S_1^-S_{2z}-2S_2^-S_{1z})\sin at_p \xrightarrow{Ht} \xrightarrow{\pi} \xrightarrow{Ht_2}$$

$$-\frac{1}{2i}[S_1^+e^{-i\Delta\Omega_1\delta t_2}+S_2^+e^{-i\Delta\Omega_2\delta t_2}$$

$$-S_1^-e^{i\Delta\Omega_1\delta t_2}-S_2^-e^{i\Delta\Omega_2\delta t_2}]\sin at_p\sin(at+\delta t_2/2) \qquad (14)$$

where $\delta t_2 \equiv t_2$-t, ($t \equiv t_m$ - t_p). The π-pulse refocuses the SQC at $t_2 = t$. One of the two counter rotating components in the square brackets of Eq. 14 is sufficient for calculation of the signal. This follows because the observed signal is proportional to the precessing magnetization:

$$M(t_2)=-\frac{2\,\mathrm{Im}\{Tr(\hat{\rho}(t_2)S^+)\}}{Tr(S^-S^+)}M_0 \qquad (15a)$$

where M_0 is the static magnetization of the sample and $S \equiv S_1$+S_2. The DQ echo is singled out by appropriate phase cycling and/or by applying a sequence of pulsed field gradients. The echo signal becomes:

$$M(t_2)=M_0[\cos\Delta\Omega_1\delta t_2+\cos\Delta\Omega_2\delta t_2]\sin at_p\sin[a(t+\delta t_2/2)]/2. \qquad (15b)$$

The terms in the first set of square brackets, after averaging over all $\Delta\Omega_1$ and $\Delta\Omega_2$, produce an echo shape, with the maximum near $\delta t_2 = 0$. The echo envelope is modulated by $\sin(a\delta t_2/2)$. We see that the signal amplitude as a function of preparation and/or mixing times is modulated by $\sin(at_p)\sin(at)$. It is this modulation that is detected to obtain the modulation frequency a, from which the dipolar interaction, hence the distance, may be abstracted (cf. below), since for two coupled electron spins:

$$a = d(1-3\cos^2\theta)+2J \qquad (15c)$$

where $d \equiv 2D/3 = \gamma_e^2\hbar/r^3$, with D the dipolar coupling constant (cf. Ch. 1), and J is the exchange integral. The angle θ is the angle between r and the direction of the static magnetic field, $\boldsymbol{B}_0$. Fourier transformation of $\cos[a(t_p$-$t)]$, that emerges from the above product of two sin-functions, produces the dipolar spectrum, which (in the case of $J = 0$) has the shape of a Pake doublet (Pake, 1948) with a width of 2/3 of the classical Pake doublet. In general, the dipolar spectrum has two distinct canonical points corresponding to the orientations of interspin vector parallel and perpendicular to $\boldsymbol{B}_0$. We de-

note these frequencies as $\omega_{\parallel}$ and $\omega_{\perp}$, respectively. The dipolar spectrum will be symmetric with respect to zero frequency, hence from Eq. 15d one finds:

$$\omega_{\parallel} = |-2d + 2J|, \quad \omega_{\perp} = |d + 2J|. \tag{15d}$$

The frequency $\omega_{\perp}$ is a singular point of the dipolar line shape, and therefore is the most prominent feature in the spectrum. Typically, the observed echo modulation oscillates with the frequency $\omega_{\perp}$.

The point of following a particular coherence pathway and "filtering out" the other "unwanted" coherence pathways is to select the one that best provides the desired information, in this case the coupling between the electron spins. In addition, the DQC pathways guarantee that the signal is just from interacting spins, *viz.* the doubly labeled species.

2.1.5 The Pulse Sequences Employed in the DQ ESR Experiment; "Allowed" Coherence Pathways: 4, 5, & 6 pulses

We considered a variety of pulse sequences, but we found the three illustrated in Figure 5 to be the most useful. These pulse sequences have been used in the DQC distance measurements. We also show their associated coherence pathways with coherence orders p at each stage. Only the coherence pathways shown survive the phase cycling. In the 4-pulse sequence of Fig. 5(a) the first two pulses in the sequence: $(\pi/2)_x$ - t_p - $(\pi/2)_x$ generate DQ_y and ZQ_y coherences, as we have discussed above. These coherences are refocused by the π-pulse in the evolution sequence (t_1 - π - t_1), and the fourth pulse converts them into antiphase coherences, $S_1^- S_{2z}$, $S_2^- S_{1z}$ which then evolve into observable SQ coherences, S_1^- and S_2^-. The DQ signal is obtained by monitoring the echo height at $t_2 = t_p$ as t_p is stepped out.

Phase cycling selects the DQC pathway. The ZQC cannot be separated from the SQ pathway other than by "detuning" the refocusing conditions on the MQC pathway, (cf. below). This experiment can also be referred to as double-quantum filtered COSY. The $(\pi/2) - t_1 - \pi - t_1 - (\pi/2)$ three pulse "sandwich" plays the role of producing the DQC, refocusing it, and then returning it to SQC. Thus it acts like a **filter**, which selects only those coherence pathways that include evolution of double-quantum coherence. As a result, it is only sensitive to the modulation in echo amplitude due to coupling between electron spins. The phase cycling associated with this three pulse "sandwich" preserves the DQC pathway, while suppressing the other coherence pathways.

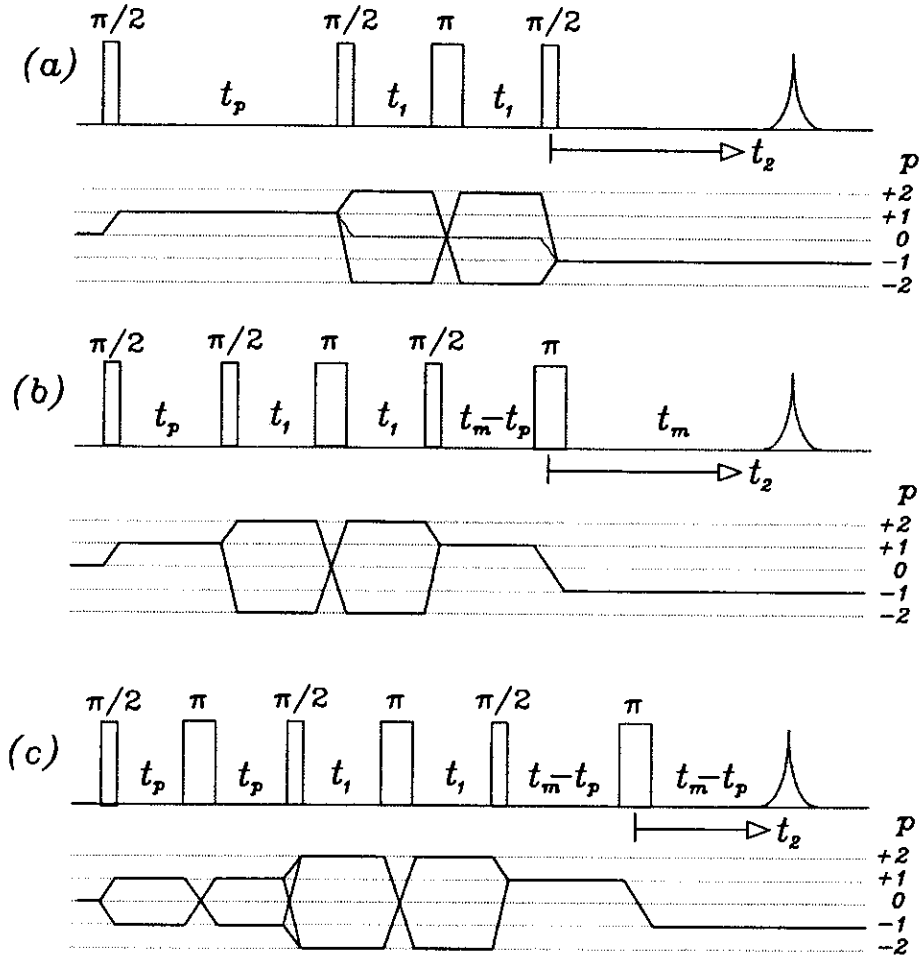

Figure 5. The 4-, 5- and 6-pulse schemes with the corresponding coherence pathways. (a)- the basic 4-pulse sequence leading to an echo at $t_2 = t_p$ from the coherence pathways illustrated. (b) - a 5 pulse variant wherein a π-pulse is added to the 4 pulse sequence to refocus the signal. This yields an echo at $t_2 = t_m$ for the coherence pathways shown. (c)- the 6 pulse sequence and associated relevant coherence pathways. It yields an echo for $t_2 = t_m - t_p$.

The 5-pulse sequence of Figure 5(b) employs an additional refocusing π-pulse. In this sequence, t_m is kept constant and t_p is varied. This eliminates the decay of the signal due to T_2 relaxation, since the echo is detected at a constant time: $2t_m+2t_1$ after the first pulse, independent of t_p.

The 6-pulse sequence of Figure 5(c) contains the 3-pulse preparation sequence $(\pi/2)_x - t_p - \pi_x - t_p - (\pi/2)_x$ which generates DQ coherence that is again refocused by the $t_1 - \pi - t_1$ sequence. The fifth pulse produces anti-phase coherences which evolve into observable SQ coherences, and the sixth

pulse refocuses them to form an echo. This sequence is used with fixed t_m, and t_p is varied. The signal envelope is recorded as a function of $t_\xi \equiv t_m - 2t_p$.

The latter two cases allow for "zero dead-time" signals, which result from refocusing of antiphase coherences in the middle of the data acquisition interval. For example, for Fig. 5(c), when one steps out t_p in the range $0 \le t_p \le t_m$ keeping t_m fixed, this yields a signal vs. t_ξ which ranges from $-t_m \le t_\xi \le t_m$. Keeping t_m fixed also has the effect of canceling out the role of phase (or T_2) relaxation on the echo at $t_2 = t_m - t_p$, since the total duration of the pulse sequence is independent of t_p for both the five pulse (see above) and the six pulse sequences.

2.2 Product Operator Analysis for Arbitrary Pulses

In this section we drop the assumption of ideal or non-selective pulses, since this is rarely the case in ESR. The Hamiltonian for a radical pair in the case of nitroxides can be written in the form:

$$H/\hbar = (\beta/\hbar)\mathbf{B}\cdot\mathbf{g}_1\cdot\mathbf{S}_1 + \mathbf{I}_1\cdot\mathbf{A}_1\cdot S_{1z} + (\beta/\hbar)\mathbf{B}\cdot\mathbf{g}_2\cdot\mathbf{S}_2 + \mathbf{I}_2\cdot\mathbf{A}_2\cdot S_{2z} + D\left(3\cos^2\theta - 1\right)\left(S_{1z}S_{2z} - \frac{\mathbf{S}_1\cdot\mathbf{S}_2}{3}\right) + J\left(\frac{1}{2} - 2\mathbf{S}_1\cdot\mathbf{S}_2\right). \quad (16)$$

Here, $\mathbf{g}_1$, $\mathbf{g}_2$ are the g-tensors and $\mathbf{A}_1, \mathbf{A}_2$ are the *hfi* tensors of the nitroxides, $D = 3\gamma_e^2\hbar/2r^3$ is the dipolar spin-spin interaction constant, and $J(r)$ is the electron exchange integral. The non-secular terms were dropped as is appropriate at high field. In addition, as is appropriate for the systems under study (Saxena and Freed, 1997a; Raitsimring and Salikhov, 1985; Milov *et al.*, 1998) nuclear Zeeman and quadrupole interactions were neglected. We shall use the Hamiltonian of Eq. 16 in the form:

$$H/\hbar = \Omega_1 S_{1z} + \Omega_2 S_{2z} + a S_{1z}S_{2z} + b_p(S_1^+S_2^- + S_1^-S_2^+)/2 \quad (17)$$

where $a = b + 2J$, $b_p = -b/2 + 2J$, with $b \equiv d(1-3\cos^2\theta)$, (cf. Sec. 2.1.4). Here Ω_1 and Ω_2 represent the Larmor frequencies of electron spins 1 and 2 due to their respective *g* and *hfi* tensors and their respective orientations, the details of which (Saxena and Freed, 1997a; Lee *et al.*, 1993) we suppress for compactness.

A rigorous treatment of DQ ESR for the nitroxide biradicals using the Hamiltonian of Eq. 16 was developed by (Saxena and Freed, 1997a). Detailed expressions, suitable for computer simulations, were provided for the cases of two and five-pulse "forbidden" echo sequences, as well as for the six-pulse "allowed" DQ sequence. This approach can be adapted to the other

"allowed" pulse sequences used in the present study, and we have derived appropriate expressions. However, this again necessitates numerical solutions, and they do not provide much insight into the essence of the experiment until certain assumptions are made to render them more manageable. Instead, we employ an approximate approach (Borbat and Freed, 1999), suitable when dipolar and exchange couplings are weak in comparison with the electron spin Zeeman and hyperfine tensors. More precisely, the exited spectral extent should be much broader then dipolar and exchange couplings. This is the case for nitroxides with interspin distances exceeding 15 Å when B_1 is greater than ca. 30 G.

Given the reasonable approximation that for sufficiently broad spectral excitation $|\Delta\Omega_1 - \Delta\Omega_2| >> |a|$ as noted above, the pseudo-secular terms (i.e. terms in $S_1^{\pm} S_2^{\mp}$) can be ignored as is commonly done in analyses of weak dipolar and exchange interactions in pulsed ESR, (Salikhov *et al.*, 1976; Maryasov *et al.*, 1998), since they would only enter into the eigen-energies to order $a^2/(\Delta\Omega_1 - \Delta\Omega_2)$. Thus we end up with the weak-coupling Hamiltonian of Sec. 2.1.1, which we write in the rotating frame as:

$$H/\hbar \approx \Delta\Omega_1 S_{1z} + \Delta\Omega_2 S_{2z} + a S_{1z} S_{2z} . \qquad (18)$$

The more complex case with the pseudo-secular term preserved (Borbat, Freed, 2000) can be treated as outlined in Appendix A.

We shall assume that the microwave pulses are intense enough that $|\gamma_e B_1/2| >> a$, so that during the pulse we have in the frame rotating at ω_{rf}, the applied microwave frequency:

$$H_r/\hbar \approx \Delta\Omega_1 S_{1z} + \Delta\Omega_2 S_{2z} + \frac{\gamma_e B_1}{2}[(S_1^+ + S_2^+)e^{-i\varphi} + (S_1^- + S_2^-)e^{i\varphi}] \qquad (19)$$

where $\Delta\Omega_k \equiv \omega_{rf} - \Omega_k$. Here ϕ is the phase of the pulse such that for ϕ=0 (π/2), B_1 is along the rotating x (y) axis.

Whereas the standard PO method (Slichter, 1990) can now be applied to obtain the solution for the various pulse sequences for the case of non-selective pulses, as was done in Secs. 2.1.2-2.1.4, we must utilize Eq. 19 for ESR experiments, which is suitable for pulses of arbitrary strength, subject to the above condition $|\gamma_e B_1/2| >> |a|$. We must thus adapt the PO method to the case of arbitrary pulses.

To accomplish this, we first need to select a convenient set of basis operators with which to represent the density operator for the two interacting electron spins, and then to determine the transformation rules for the basis operators under the action of the arbitrary pulses and during the free evolution periods.

There are several convenient choices for the PO basis set:

$$\begin{gathered}(E_1,S_{1z},S_{1x},S_{1y})\otimes(E_2,S_{2z},S_{2x},S_{2y})\\(S_1^{\alpha},S_1^{\beta},S_1^{+},S_1^{-})\otimes(S_2^{\alpha},S_2^{\beta},S_2^{+},S_2^{-})\\(E_1/2,S_0^{(1)},S_{+1}^{(1)},S_{-1}^{(1)})\otimes(E_2/2,S_0^{(2)},S_{+1}^{(2)},S_{-1}^{(2)})\\S_0^{(j)}=S_{jz},\qquad S_{\pm1}^{(j)}\equiv\mp S_j^{\pm}/\sqrt{2}\end{gathered}\tag{20}$$

which are the Cartesian, single-element, and spherical bases respectively. The symbol $\otimes$ implies the direct product. E_j, and S_{jz},S_j^{+},S_j^{-} are respectively the identity matrix and spin matrices of dimension 2 for the k^{th} electron spin, as in Eqs. 1-3. Both Cartesian and spherical basis operators are very handy in describing coherences. In NMR the Cartesian basis is widely used due to its convenience in handling coherences under the action of non-selective *rf* pulses[1], whereas the spherical basis is more convenient for the description of the evolution of coherences. However, for the case of arbitrary pulses, which is typical for ESR, we found that the spherical basis is more convenient at all stages of the calculation especially for the complicated case of a full dipolar Hamiltonian. We actually used the modified spherical basis (Borbat and Freed, 1999) in the form of

$$(E_1/2,S_{1z},S_1^{+},S_1^{-})\otimes(E_2/2,S_{2z},S_2^{+},S_2^{-}).\tag{21}$$

The pulse propagator superoperator $\tilde{R}$, is associated with H_r, as:

$$\tilde{R}\rho\Leftrightarrow e^{-i\frac{H_r t}{\hbar}}\rho e^{i\frac{H_r t}{\hbar}}.\tag{22a}$$

Here ρ is the density operator for two coupled spins and can be represented as:

$$\rho=\sum_i c_i B_i\,.\tag{22b}$$

Here, the complete basis set of 16 operators B_i is given by the following direct product operators:

[1] Only the Cartesian basis has the property $e^{-i\chi A}Be^{i\chi A}=B\cos\chi-i[AB]\sin\chi$ that makes it possible to express effect of multipulse sequences in terms of composite linear and bilinear rotations (Ernst *et al.*, 1987).

$$\begin{array}{c} S_1^+E_2, S_1^-E_2, E_1S_2^+, E_1S_2^- \\ 2S_1^+S_{2z}, 2S_1^-S_{2z}, 2S_2^+S_{1z}, 2S_2^-S_{1z} \\ E_1E_2/2, S_{1z}E_2, E_1S_{2z}, 2S_{1z}S_{2z} \\ 2S_1^-S_2^+, 2S_1^+S_2^-, 2S_1^+S_2^+, 2S_1^-S_2^-. \end{array} \tag{22c}$$

The matrix multiplication in the 16 terms of Eq. 22c should be understood as the direct product. Consequently, these 16 direct product operators are represented by 4×4 matrices.

The basis sets given by Eqs. 20, 21, and 22c, after simple normalization are orthonormal in Frobenius trace metrics:

$$\mathrm{Tr}\{B_i^\dagger B_j\} = \delta_{ij} \tag{22d}$$

where $B_i^\dagger B_j$ implies simple matrix multiplication of the 4×4 matrices and Tr is the trace of this matrix product.

The pulse propagator superoperator $\tilde{R}$ becomes a direct product of the individual pulse propagator superoperators for the individual spins $\tilde{R} = \tilde{R}_1 \otimes \tilde{R}_2$ in the case when we can neglect the dipolar Hamiltonian during the pulse. In other words, we implicitly exclude "forbidden" coherence effects in this treatment. The next step is to determine the rules for transforming the basis operators. Rotational superoperators $\tilde{R}_1$ and $\tilde{R}_2$ can be represented in a matrix form using the Cayley-Klein parameters associated with a rotation about the x-axis by the k^{th} rf pulse by a nominal rotation angle β_k (Bloom, 1955). The appropriate matrices $R_1(\beta_k)$ and $R_2(\beta_k)$ for the transformation of the operator basis set $(E_j/2, S_{jz}, S_j^+, S_j^-)$ are:

$$R_j(\beta_k) = \begin{pmatrix} 1 & 0 & 0 & 0 \\ 0 & C^{(j)}(\beta_k) & -\dfrac{S^{(j)}(\beta_k)^*}{2}e^{-i\varphi_k} & -\dfrac{S^{(j)}(\beta_k)}{2}e^{i\varphi_k} \\ 0 & -S^{(j)}(\beta_k)^* e^{i\varphi_k} & C_2^{(j)}(\beta_k)^* & S_2^{(j)}(\beta_k)e^{i2\varphi_k} \\ 0 & -S^{(j)}(\beta_k)e^{-i\varphi_k} & S_2^{(j)}(\beta_k)e^{-i2\varphi_k} & C_2^{(j)}(\beta_k) \end{pmatrix} \tag{23}$$

where the asterisk indicates complex conjugation. $\tilde{R}(\beta_k)$ is represented by a 16×16 matrix whose elements can be written out by expanding the direct product of $R_1(\beta_k)$ and $R_2(\beta_k)$. The elements of $R_j(\beta_k)$ are given by:

$$\begin{array}{ll} C_2^{(j)}(\beta_k) = a_{jk}^2, & S_2^{(j)}(\beta_k) = -b_{jk}^2 \\ S^{(j)}(\beta_k) = 2a_{jk}b_{jk}, & C^{(j)}(\beta_k) = |a_{jk}|^2 - |b_{jk}|^2. \end{array} \tag{24}$$

Here a_{jk} and b_{jk} are the Cayley-Klein parameters associated with a nominal rotation by angle β_k about the rotating x-axis, and they are:

$$a_k = \cos\beta_{ek}/2 - i\cos\psi_k \sin\beta_{ek}/2, \quad b_k = -i\sin\psi_k \sin(\beta_{ek}/2) \tag{25}$$

where

$$\beta_{ek} = \beta_k[1+(\Delta\Omega_k/\gamma_e B_1)^2]^{1/2} \text{ and } \tan\psi_k = \gamma_e B_1/\Delta\Omega_k . \tag{26}$$

For non-selective pulses Eq. 24 becomes:

$$C_2^{(j)}(\beta_k) = \cos^2\beta_k/2, \quad S_2^{(j)}(\beta_k) = \sin^2\beta_k/2$$
$$S^{(j)}(\beta_k)^* = i\sin\beta_k, \qquad C^{(j)}(\beta_k) = \cos\beta_k .$$

The evolution of the density operator between pulses is given by the free evolution propagator superoperator associated with Eq. 18, which includes dipolar and exchange effects. This superoperator can be represented by a matrix of dimension 16 by 16 in the PO basis. We need to know only a few of its elements here. Its relevant sub-block is given by Eqs. A5-A7. For example, for the transformation of $S_1^{\pm}$ and $2S_1^{\pm}S_{2z}$ we find from Eqs. A5-A7 for the case of zero pseudo-secular term (cf. App. A):

$$\begin{aligned} S_1^{\pm} &\xrightarrow{H t/\hbar} [S_1^{\pm}\cos\frac{at}{2} \mp i(2S_1^{\pm}S_{2z})\sin\frac{at}{2}]e^{\mp i\Delta\Omega_1 t} \\ (2S_1^{\pm}S_{2z}) &\xrightarrow{H t/\hbar} [(2S_1^{\pm}S_{2z})\cos\frac{at}{2} \mp iS_1^{\mp}\sin\frac{at}{2}]e^{\mp i\Delta\Omega_1 t}. \end{aligned} \tag{27}$$

Eqs. 23 and 27 are sufficient for deriving expressions for the signals for each pulse sequence in the weak-coupling limit. The computational effort is greatly reduced by only tracking those coherence pathways of interest shown in Fig. 5, which are selected by the phase-cycling.

The general expressions for DQC and ZQC signals associated with the coherence pathways in Fig. 5 (Borbat and Freed, to be published) can now be written down.

One finds that all the signals may be written in the following form (or else as a sum of terms of this form):

$$V_{n,DQ(ZQ)}(\Delta\Omega_1, \Delta\Omega_2, \mathbf{r}_{12}, t_p) = G_n(\Delta\Omega_1)H_n(\Delta\Omega_2)F_n(\mathbf{r}_{12}, t_p)R_{n,DQ(ZQ)} . \tag{28}$$

The $F_n(\mathbf{r}_{12},t_p)$ represent the oscillations due to the dipolar interactions:

$$F_4(\mathbf{r}_{12},t)=-(1/2)\sin^2(at_p/2)$$
$$F_5(\mathbf{r}_{12},t)=-(S^{(2)}/2)\left(\sin^2(at_m/2)-\sin^2[a(t_m-t_p)]\right)+(C^{(2)}/2)\sin^2(at_p/2)$$
$$F_6(\mathbf{r}_{12},t)=-\sin at_p\sin[a(t_m-t_p)]=(\cos at_m-\cos at_\xi)/2,\ (t_\xi\equiv t_m-2t_p) \tag{29}$$

where for nominal $\pi/2$ and π pulses $S^{(2)}\equiv S_2^{(2)}(\pi)$, $C^{(2)}=1-S^{(2)}$. The $G_n(\Delta\Omega_1)$ and $H_n(\Delta\Omega_2)$ represent the excitation functions for spins 1 and 2, respectively. Also the $R_{n,DQ(ZQ)}$ represent the spin relaxation.

The detailed forms of the signal amplitudes, $V_{n,DQ(ZQ)}$ are given below. Since they are somewhat lengthy, we show here only the results when the nominal pulse rotation angles are set to $\pi/2$ and π as shown in Fig. 5. In the absence of relaxation they are for the 4, 5, and 6 pulse sequences (Borbat and Freed, 1999) :

$$\begin{aligned}V_{4DQ}(\Delta\Omega_1,\Delta\Omega_2,\mathbf{r},t_p)&=V_{4ZQ}(\Delta\Omega_1,\Delta\Omega_2,\mathbf{r},t_p)\\&=-(1/2)\,\mathrm{Im}\{S^{(1)}(\pi/2)^*\}S_2^{(1)}(\pi)S_2^{(2)}(\pi)\\&\times[|C_2^{(1)}(\pi/2)|^2+S_2^{(1)}(\pi/2)^2]\,|S^{(2)}(\pi/2)|^2\sin^2(at_p/2)\\&\equiv\overline{V}_4(\Delta\Omega_1,\Delta\Omega_2)\sin^2(at_p/2)\end{aligned} \tag{30a}$$

$$\begin{aligned}V_{5,DQ}(\Delta\Omega_1,\Delta\Omega_2,\mathbf{r},t_p)&=V_{5,ZQ}(\Delta\Omega_1,\Delta\Omega_2,\mathbf{r},t_p)\\&=\overline{V}_4(\Delta\Omega_1,\Delta\Omega_2)\\&\times S_2^{(1)}(\pi)[S_2^{(2)}(\pi)\sin^2 at_m/2-(S_2^{(2)}(\pi)\sin^2[a(t_m-t_p)/2]\\&\quad+(1-S_2^{(1)}(\pi))\sin^2 at_p/2]\end{aligned} \tag{30b}$$

$$\begin{aligned}V_{6,DQ}(\Delta\Omega_1,\Delta\Omega_2,\mathbf{r},t_p)=&-\mathrm{Im}\{S^{(1)}(\pi/2)^*\}[S_2^{(1)}(\pi)S_2^{(2)}(\pi)]^3\\&\times|S^{(2)}(\pi/2)|^2\sin at_p\sin a(t_m-t_p).\end{aligned} \tag{30c}$$

Superscripts (j) for j = 1 or 2 are used in Eqs. 30 to label terms associated with the j^{th} spin. We have set $\phi=0$ for convenience. In the derivation of Eqs. 30 it was assumed that the spectrum is sufficiently broad, so that any unrefocused signals decay away rapidly, and any accidental refocusing is unlikely. [There are residual FID-like terms, which can be ignored, (cf. App. A), so they are not included in Eqs. 30]. Note that the dependence on $\Delta\Omega_1$ and $\Delta\Omega_2$

enters via the above definitions of β_{ek} and ψ_k. Note also that for Eqs. 30 there is an equivalent expression obtained from permuting the superscripts (1) and (2). The two give identical results, thus we write out only one term.

Amplitude factors $|C_2^{(1)}(\pi/2)|^2+S_2^{(1)}(\pi/2)^2|, |S^{(2)}(\pi/2)|^2$ in Eqs. 30 with good accuracy are nearly unity for the nitroxide experiments discussed in Sec. 4 and only $S_2^{(k)}(\pi)$ and $S^{(k)}(\pi/2)$ will determine the spectral excitation. We can account for the time evolution with respect to t_2 (Fig. 5) by simply multiplying the rhs of Eqs. 30 by:

$$\exp[i(\Delta\Omega_1+a/2)\delta t_2]e^{-\delta t_2/T_{2,SQ}} \tag{31}$$

where $\delta t_2 \equiv t_2 - t_p$ for Eq. 30a; $\delta t_2 \equiv t_2 - t_m$ for Eq. 30b, and $\delta t_2 \equiv t_2 - (t_m - t_p)$ for Eq. 30c. For the present, we are mainly interested in the case of $\delta t_2 = 0$. Note that in the limit of non-selective pulses (i.e. $B_1 \rightarrow \infty$) these equations simplify considerably and become:

$$\begin{aligned} V_{4,DQ} &= -(1/4)\sin^2(at_p/2) \\ V_{5,DQ} &= -(1/4)[\sin^2 at_m/2 - \sin^2 a(t_m - t_p)/2] \\ V_{6,DQ} &= -\sin at_p \sin a(t_m - t_p). \end{aligned} \tag{32}$$

These represent the ideal cases, where the signal, as a function of t_p, just shows the coherent oscillations due to dipolar (plus exchange) interactions, independent of $\Delta\Omega_k$. However, more generally, the $V_{n,DQ}$, n = 4, 5 or 6, signals will depend upon $\Delta\Omega_k$ via the spectral coverage factors associated with the finite pulses.

To account for relaxation we shall multiply Eqs. 30 by:

$$\begin{aligned} R_{4,DQ(ZQ)} &= \exp(-2(t_p T_{2,SQ}^{-1} + t_1 T_{2,DQ(ZQ)}^{-1})) \\ R_{5,DQ(ZQ)} &= \exp(-2(t_m T_{2,SQ}^{-1} + t_1 T_{2,DQ(ZQ)}^{-1})) \\ R_{6,DQ} &= \exp(-2(t_m T_{2,SQ}^{-1} + t_1 T_{2,DQ}^{-1})) \end{aligned} \tag{33}$$

respectively and Eq. 32 accordingly. Here $T_{2,SQ}$, $T_{2,DQ}$, and $T_{2,ZQ}$ refer to the T_2 decay constants characteristic of SQC, DQC, and ZQC, respectively (T_1 processes are neglected). This approach to the treatment of relaxation is a simplified one, (Saxena and Freed, 1997a). A rigorous approach is to include the relaxation superoperator in the Liouville-von Neuman equation for the density matrix as was done in the work of Lee *et al.*, (1993, 1994). This would help to account for any orientationally dependent relaxation effects and any correlation between magnetic tensors of the coupled radicals.

We shall choose Euler angles $\lambda_i \equiv (\alpha_i, \beta_i, \gamma_i)$, with γ_i set to zero, to represent the transformation from the dipolar frame to the magnetic frame of the i^{th} nitroxide fragment (i = 1 or 2), and Euler angles $\eta \equiv (0, \theta, \zeta)$ to represent the transformation from the lab frame to the dipolar frame (Saxena and Freed, 1997a). Then the $G_n(\Delta\Omega_1)$ of Eq. 28 will depend upon λ_1 and η, while $H_n(\Delta\Omega_2)$ depends upon λ_2 and η, and $F(\mathbf{r}_{12},t_p)$ just upon η as well as the magnitude $|\mathbf{r}_{12}| \equiv r$. It is then necessary to average the signal over an appropriate distribution in these variables, which we represent by angular brackets as:

$$D_n(t_p) = \left\langle G_n(\Delta\Omega_1(\lambda_1,\eta)) H_n(\Delta\Omega_2(\lambda_2,\eta)) F_n(r,\eta,t_p) \right\rangle_{r,\lambda_1,\lambda_2,\eta}. \tag{34}$$

The relaxation function $R_{n,DQ(ZQ)}(\Delta\Omega_1, \Delta\Omega_2, \lambda_1, \lambda_2, \eta)$ which has been dropped for convenience in Eq. 34 can be placed outside the angular brackets, since for nitroxides, which are the major application of our DQ methods, at the reduced temperatures used, T_2's are not substantially dependent upon λ_1, λ_2 nor upon η. In the nitroxide biradicals that we have studied so far, the contribution of the modulation of dipolar coupling to T_2 is very small, (Saxena and Freed, 1997b). Therefore there should not be noticeable dependence on η or r. Moreover, we have not seen a noticeable angular variation of the T_2's in the experiments with macroscopically aligned biradicals nor a significant variation of T_2 across a 2D-ELDOR spectrum (Saxena and Freed, 1997b), implying only a weak dependence on λ_1, and λ_2. We shall not include the factors of Eq. 32 in the sequel for brevity.

It is easy to see that when there is no correlation between the λ_i and η, then Eq. 34 yields the expected simpler form, Eq. 35:

$$\begin{aligned} D_n(t_p) &= \left\langle G_n(\Delta\Omega_1(\lambda_1,\eta)) \right\rangle_{\lambda_1} \left\langle H_n(\Delta\Omega_2(\lambda_2,\eta)) \right\rangle_{\lambda_2} \left\langle F_n(r,\eta,t_p) \right\rangle_{r,\eta} \\ &\equiv G_n^{AV} H_n^{AV} \left\langle F_n(r,\eta,t_p) \right\rangle_{r,\eta}. \end{aligned} \tag{35}$$

Thus one can simply integrate over the distribution of orientations and magnitudes of r in the sample. A FT with respect to t_p or t_ξ will then yield familiar Pake doublets. Another simple limiting case occurs when the pulses can be regarded as non-selective, so that

$$G_n(\Delta\Omega_1) \rightarrow G_n^{\infty} \text{ and } H_n(\Delta\Omega_2) \rightarrow H_n^{\infty} \tag{36}$$

independent of $\Delta\Omega_1$, $\Delta\Omega_2$, which follows immediately from the $B_1 \rightarrow \infty$ limiting forms of Eqs. 30 given in Eq. 29.

Then Eq. 34 becomes:

$$D_n(t_p) = G_n^{\infty} H_n^{\infty} \left\langle F_n(r,\eta,t_p) \right\rangle_{r,\eta}. \tag{37}$$

This is the case when all the spins in the sample contribute to the signal. We can thus write as inequalities:

$$G_n^{\infty} \geq G_n^{AV} \text{ and } H_n^{\infty} \geq H_n^{AV}. \tag{38}$$

2.3 Approach for General Analysis

When the condition $|\Omega_1 - \Omega_2| \gg |a|$ no longer holds, the weak-coupling approach should be corrected. For nitroxides, this includes distances under 10-12 Å for non-selective pulses, corresponding to a large coupling, or exotic cases of mutual arrangement of the nitroxide moieties such that the magnetic axes substantially coincide, thereby leading to small frequency differences for a significant fraction of pairs. The full expressions for the signal in the 6-pulse sequence can be found in (Saxena and Freed, 1997a). They are obtained by tracking down the density matrix elements along the relevant coherence pathways using the complete spin-Hamiltonians instead of the approximate forms of Eqs. 18 and 19. As a result they become substantially more complex. In Appendix A we outline a suitable approach for obtaining expressions for the signals from "allowed" coherence pathways. The only assumption that is made in App. A is that the dipolar coupling during the pulse has only an insignificant effect on the signals. This is indeed the case for very intense pulses and longer distances, ≥12-15 Å.

2.4 Relation to Other ESR Techniques

A detailed review of cw ESR methods for determining distances using nitroxide bilabeling is given in (Hustedt and Beth, 1999). Cw ESR methods are very useful in the range of distances from 5 Å to 15 Å, and provide the opportunity to report on the mutual orientation of the nitroxide moieties under certain conditions. Even somewhat larger distances can be assessed by using perdeuterated ^{15}N spin-labels. A number of studies have emerged with use of cw-ESR due to its wide availability (Hustedt *et al.*, 1997; Rabenstein and Shin, 1996; Hanson *et al.*, 1996; Budker *et al.*, 1995). A summary of various cw and pulsed ESR distance measurement techniques is given in Ch.1 of this volume.

Here we note the relationships between pulsed ESR techniques which deal with the distance between the electron spins[2] and share common features.

The relevant techniques can be divided into the following categories:

1. *Incoherent techniques*:

These include double electron-electron resonance (DEER) (Milov *et al.*, 1998; Pannier, *et al.*, 2000; cf. Ch. 11). It usually makes use of selective pulses at two well-separated microwave frequencies, and hence it is applicable to systems with sufficiently broad ESR spectra, including nitroxides. It is practical in cases of broad spectra (e.g. $\geq$ ca. 50 G). It is the only sensible alternative in cases of widely separated spectra like the case of pairs of semiquinone radicals interacting with hydrogen atoms (Milov *et al.*, 1981). A further advantage of multiple-frequency techniques is the insignificant role played by the "pseudo-secular" part of the dipolar Hamiltonian. Also, nuclear modulation effects can be virtually absent if there is no spectral overlap from the selective pulses at the separated frequencies.

The "2+1" technique (Kurshev and Raitsimring, 1989; Ch. 10) can also be included in this group. It is closely related to the 3-pulse DEER technique, except for its use of only a single frequency (or else a large spectral excitation overlap in the 3-pulse DEER).

2. *Coherent techniques* which include:

i) Techniques that select a particular order of MQC. They include "allowed" and "forbidden" DQC and ZQC pulse sequences (Saxena and Freed, 1996; 1997a; Borbat and Freed, 1999).

ii) Techniques that manipulate SQ coherences and do not select MQC but instead detect indirectly the effect of generation of MQC's on the SQ echo amplitude. Thus, they do not display selectivity with respect to a given order of coherence. Examples include 5(6)-pulse sequences (cf. App. C; Borbat and Freed, 1999a, 2000) and 4-pulse sequences (Jeschke *at al.*, 2000).

3. INSTRUMENTATION:

3.1 2D-FT Pulse ESR Spectrometer

The multi-frequency pulsed two-dimensional FT-ESR spectrometer described elsewhere (Borbat and Freed, 1997) was used in all DQ experiments. Initial experiments were performed at both 9.2 and 17.3 GHz, but most results were obtained at the higher frequency, since it provided 4 times higher

[2] We do not consider here important distance measurement techniques which utilize relaxation phenomena (Ichikawa *et al.*, 1985; Dzyuba and Kawamori, 1996; Rakowsky *et al.*, 1998).

SNR, the maximum B_1~ 30 G and the shortest spectrometer dead-times $\tau_d \approx$ 30 ns. [The effective B_1 has been estimated using a technique based on a well-known method (Raitsimring and Salikhov, 1985)]. At X-band the maximum B_1 in the BLGR resonator with Q ≈ 50 was about 20 G and the dead-time was 5-10 ns longer. At 17.3 GHz the minimum $\pi/2$ (π) pulse widths were 3-3.5 ns (5-6 ns) in the low-Q dielectric resonator used. One more reason to prefer Ku-band was in the higher frequency and reduced magnitude of ESEEM. The signal acquisition unit includes two 200 Msps flash ADC converters with fast averaging capability. The repetition rate is 6-12 kHz depending on the record length. For sampling of the signals at time intervals shorter than 5 ns an interleaving technique was employed. The signal from the microwave bridge was detected in quadrature, and CYCLOPS phase cycling (Hoult and Richards, 1975; Gorcester and Freed, 1988; Ohba *et al.*, 1993) was always used to eliminate image signals in 2D collections.

For the successful implementation of DQ ESR the most important features are the intense pulses and the sensitivity, and to a somewhat lesser extent the dead time. The latter follows, because the most favorable DQ-ESR pulse sequences are based on the principle of "remote detection", i.e. they have "apparent" zero dead time.

3.1.1 Intense Pulses

Spectral excitation depends on the available B_1 and the type of signal. As we mentioned in Sec. 2.2, the expressions for the signal given by Eqs. 30 contain terms of the type $|S(\pi/2)|^2$ or $2(|C_2(\pi/2)|^2 + S_2(\pi/2)^2)$ which are close to unity for a broad range of $\Delta\Omega$'s, so they may be ignored in analyses of spectral excitation. The major factor limiting the spectral excitation arises from the products of terms as:

$$S_2(\pi) = \sin^2(\pi u/2)/u^2$$

where $u^2 \equiv 1 + \Delta\Omega^2/\gamma_e^2 B_1^2$. A small additional effect is from $S(\pi/2)$. In Fig. 6 we plot the amplitude factors G_6^{AV}, H_6^{AV} of Eq. 35, and their product M_6^{AV} calculated for an uncorrelated pair of ^{14}N nitroxides at X-band. At Ku-band the difference is marginal.

The product of three $S_2(\pi)$ functions arising from the π pulses in the 6-pulse sequence yields very reasonable values of about 0.5 for the amplitude factors given by G_6^{AV} or H_6^{AV} for a B_1 of 30 G, for which the overall amplitude factor, M_6^{AV}, is about 0.3. It is useful to note that the width of the spectral excitation predicted for a product of N $S_2(\pi)$ terms decreases slowly with N, as $N^{-1/2}$. For B_1 under 20 G the growth of M_6^{AV} is faster than linear, thus achieving $B_1 \geq 30$ G is essential for producing substantial DQ signals. We

find that spectral distortions caused by correlations are determined by the H function of Eq. 35, whereas G only influences the overall signal strength.

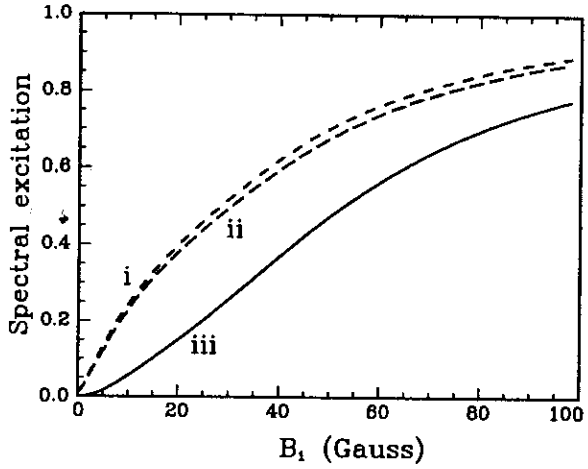

Figure 6. Spectral excitation in the 6-pulse DQ sequence as a function of B_1 calculated for an uncorrelated pair of ^{14}N nitroxides excited at the center of gravity of the ESR spectrum. (i) - G_6^{AV}, (ii) - H_6^{AV}, and (iii) - their product $H_6^{AV}\,G_6^{AV}$. Note that as $B_1 \rightarrow \infty$ one obtains $H_6^{\infty} = G_6^{\infty} = 1$. These results were calculated for 9.3 GHz. At 17.3 GHz differences are small, so the results are approximately valid at this frequency as well.

In the case of short distances (under 15 Å) the distortions of the Pake pattern caused by the pseudo-secular term (cf. App. A) are less significant at large B_1. For correlated nitroxides, we expect that by increasing B_1 to ca. 60 G and consequently H to 0.75 would greatly decrease the correlation effects (cf. Sec. 2.2). Further increases in B_1 only yield a steadily decreasing improvement as the asymptotic limiting value of unity is only slowly approached with increasing B_1.

We have studied the effects of weaker B_1's and shorter distances, (Borbat and Freed, 2000). With a B_1 of only 12 G (at 9.2 GHz using a TE_{012} resonator) we found that all the DQ and coherent SQ sequences yielded only weak signals for rigid biradical R-II, which displays a 16.2 Å distance (cf. Sec. 4.2). Strong signals are, however, obtained for longer distances under these conditions (e.g. with rigid biradical R-I, with a distance of 28.8 Å, cf. Sec. 4.2). At 17.3 GHz smaller B_1's still yield strong signals, but they are severely distorted by several factors (cf. App. A). Above about 25 Å there is no problem with using weaker pulses. Thus a large B_1 is very important for all these sequences to work reliably.

Simple estimates would indicate that for ^{15}N nitroxides only about 70% of the B_1, needed for ^{14}N, is required in order to achieve the same degree of spectral excitation.

The spectral excitation that has already been achieved corresponding to $B_1 = 30$ G is sufficient for producing strong DQ signals even in samples with a small number of spins, (cf. Sec. 4). Figure 7 shows an example of the SNR obtained under typical conditions (i.e. sample volume V_s of 15 μL, spin concentration C of 1 mM, data acquisition time, 9 s) for the biradical R-II (cf. Sec. 4.2).

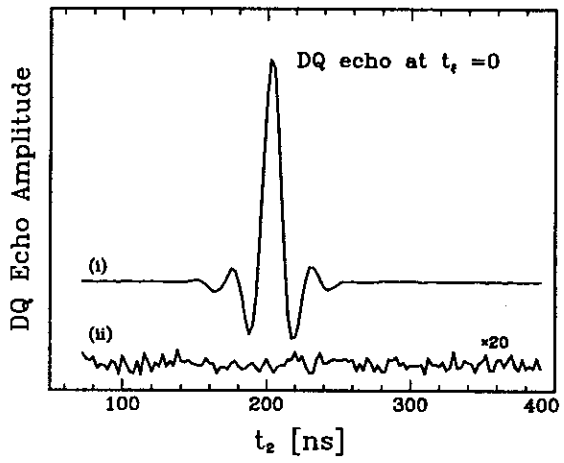

Figure 7. Example of signal to noise ratio for DQ echo detected for biradical R-II randomly oriented in liquid crystalline Phase-V at -66° C using the 6-pulse sequence. (i)- DQ echo was acquired at the signal maximum which occurs at the t_ξ=0. (ii)- Off resonance baseline vs. t_2 amplified by a factor of 20. SNR (ratio of echo amplitude to rms noise) is about 500.

The DQ echo envelope was recorded for the 6-pulse sequence at a temperature of -66° C. At this temperature, T_2 is 0.5 μs, which is about 4 to 8 times shorter than is typical for nitroxides at 77 K (Lindgren *et al.*,1997; Zecevic *et al.*, 1998).The amplitude of the DQ echo after correction for T_2-decay was about 0.15 of the COSY (Gorcester and Freed, 1988) signal, which is about 50% of the maximum expected for a B_1 of 30 G. The discrepancy is believed to be due to the effect of correlation of orientations of the nitroxide *hfi* tensors, so it should decrease with further increase of B_1 in the π-pulses

3.1.2 Short Dead-Times

The short dead times that were achieved are typically in the range of 30-35 ns at Ku-band (Borbat and Freed, 1997), although with careful adjustments we can obtain 22-25 ns. This is important for the 4-pulse DQ experi-

ment and also for the COSY or 2D-ELDOR experiment. It is less important for 5 and 6 pulse DQ, where the DQ signal is detected when sufficient time has elapsed after the *rf* pulses. Of course, one must keep this elapsed time to a minimum to avoid signal loss due to T_2-type relaxation.

3.1.3 Signal Acquisition Schemes; 1D vs. 2D

It is sufficient to utilize only one-dimensional acquisition for most of the experiments. However, with our 2D FT spectrometer, we always acquire the whole echo shape, since we use a transient digitizer. The quadrature signals from the microwave bridge are fed into the digitizer, and they are accumulated for each step of the phase cycle. The data records are then combined according to the phase cycle table for selection of the desired DQ signal (cf. App. D). To obtain the 1D signal from the 2D data set we sample the signal amplitude as a function of t_p or t_ξ by selecting the necessary number of points from the data records. This "digital sampling window" serves the same function as a boxcar integrator.

In a 2D experiment all collected data are stored. Fourier transformation of the 2D time-domain signal with respect to t_p or t_ξ and t_2 yields the Pake pattern along the ESR spectrum (cf. Sec. 4.2.3). This information can be utilized to study correlations in the mutual orientation of the nitroxides. However the 2D experiment is more time consuming, because the sampling interval needed for 2D-FT ESR is larger than the sampling window in 1D data processing. The sampling window in the 1D experiment is about 0.5-1 times the full width at half height of the echo signal and typically is in the range of 5-15 ns. In the 2D experiment the sampling interval is ca. 100-150 ns. Thus, most of the echo is at a signal level well below its maximum, which is all that needed in 1D experiment. The larger window is essential for adequate spectral resolution in a 2D spectrum. As a result, the SNR in the 2D spectrum is several times worse than for the 1D Pake pattern. In order to compensate for this the acquisition time for the 2D experiment should be increased. In Sec. 4.2.3 we show results for 2D data collection with the nitroxide biradicals R-I and R-II.

3.1.4 Coherence Pathway Selection

3.1.4.1 Phase Cycling

Phase cycling is a powerful method for suppressing unwanted coherence pathways by alternating the phases of the *rf* pulses and then combining the detected signals appropriately. It was introduced in NMR and has become widely employed for the selection of desired coherence pathways in numerous types of 1D and 2D experiments (Ernst *et al.*, 1987). This method was

brought into the ESR field (Fauth *et al.*, 1986; Gorcester *et al.*, 1988) in order to select desired signals in 1D and 2D pulsed electron spin-echo experiments.

The general rule for the selection of a particular coherence pathway is based on the fact that if a pulse propagator U, acting on the density matrix according to

$$\rho(t) = e^{iUt}\rho(0)e^{-iUt} \tag{39}$$

produces a change in the given coherence order p by Δp, then the same pulse propagator, but with the phase shifted by φ, i.e. $U(\varphi)$, will multiply $\rho(t)$ by $e^{-i\Delta p\varphi}$. Consequently, a sequence of pulse propagators ($U_1(\varphi_1)$, $U_2(\varphi_2)$ ... $U_N(\varphi_n)$)) will multiply the density matrix and hence the signal produced by a particular coherence pathway (Δp_1, Δp_2 .... Δp_n,) by:

$$\exp(-i\sum_k \Delta p_k \varphi_k)\,. \tag{40}$$

Stepping the phase by $2\pi l/N$ (l = 0, 1 ,..., N-1) and combining the detected signals with weighting factors $e^{i\Delta p_k \varphi_l}$ selects signals with a change in the coherence order equal to $\Delta p_k \pm Nm$ (m = 0, 1, ...) (Ernst *et al.*, 1987). For the $\pi/2$ phase increment one has N=4. Hence a phase cycle that selects $\Delta p = \pm 2$ also selects pathways $\Delta p = (\pm 6, \pm 10, \ldots)$ and suppresses the others.

For a phase increment of π, N is 2. Thus $\Delta p = (0, \pm 2, \pm 4, \ldots)$ are selected. We see that $\Delta p = 2$ and $\Delta p = 0$ are both selected. Therefore a phase cycle based on just the π increment cannot separate DQC from ZQC. The more pathways there are containing a given Δp_k that can interfere with the desired signal, the more pulse propagators should be included in the phase cycling scheme. It is well known that a series of pulse propagators (which represents unitary transformations) can be replaced by a single propagator representing the cumulative effect of the series. This also applies to a series of pulse propagators interspersed by free evolution propagators representing the effect of the spin Hamiltonian, Eq. 18. Such a cumulative propagator is referred to as a composite propagator or rotation in NMR (Sørensen, 1983).

For example, the 2 and 3 pulse sequences for preparation of DQC (cf. Sec. 2.1.2) can be replaced by a single composite propagator which produces changes in the order of coherence of $\Delta p = 0, \pm 1, \pm 2$. It is the last value that corresponds to DQC. Thus a phase cycle that selects $\Delta p = \pm 2$ is required. The virtue of using the composite propagator is that it is sufficient to consider just its phase shifts in constructing the phase cycling. Then for a given phase shift φ for the composite propagator each pulse in its sequence must be given the identical phase shift, φ.

Consider as an example the 6-pulse DQ sequence. The first three pulses may be considered as a composite propagator that produces DQC. The subsequent change in the coherence order Δp is ± 2. We should select all four pathways depicted in Fig. 5(c) with this change. Using $N = 4$, with the understanding that the phases of the three pulses should be incremented simultaneously, we arrive at a 4-step phase sequence with the phases of these 3 pulses changing as follows (0, 0, 0), ($\pi/2$, $\pi/2$, $\pi/2$), (π, π, π), ($3\pi/2$, $3\pi/2$, $3\pi/2$) and each of the 4 signals are weighed by factors (1, -1, 1, -1), when they are added. This phase cycle is, in principle, sufficient because it suppresses all of the pathways that yield SQ or ZQ coherence.

This phase cycle for the 6-pulse sequence is satisfactory if the phases are very accurate, which is hard to achieve in practice. Therefore, it is usually necessary to cycle the phases of the other pulses in order to attain an improved suppression of unwanted signals. Additionally, the phase cycle should be combined with the CYCLOPS sequence for suppression of signals at the image frequency. This increases the number of phase steps by a factor of four. The typical phase cycling that we employ for the 6-pulse sequence consists of 64 steps, which combined with CYCLOPS yields 256 steps (cf. App. D). The 4-pulse and 5-pulse sequences have phase cycles with the number of steps ranging from 64 to 128.

With these phase cycles we could suppress unwanted echoes by a factor of 300-3000 depending on the sharpness of the SQ echoes, (e.g. the smaller figure applies for nitroxides, which have sharper echoes, and the larger to E'-centers).

3.1.4.2 Pulsed Field Gradients

In the previous section we learned that to select coherence orders with $p \geq 3$, phase increments less than $\pi/2$ would be necessary. This is not a standard feature of existing pulsed ESR spectrometers. Such a phase increment would need to have a smaller absolute error, bringing an extra challenge to the task. It may be useful to consider an alternative solution.

One well-known approach for selection of high orders of coherence relies on using pulsed field gradients (PFG). This is routinely done in NMR for a variety of purposes including suppression of unwanted coherence orders (Bax *et al.*, 1985) The same technique could in principle be employed in the DQ ESR experiment. There is not yet an experimental demonstration in ESR, but we include this topic for its potential.

An underlying principle is based on a key property of multiple-quantum transitions. The frequency of a multiple-quantum transition is the sum of the frequencies of all the single quantum transitions that can be considered as making up the multiple-quantum transition. Thus a shift of resonant frequencies of all relevant SQ transitions by the same amount shifts the frequency of

the multiple-quantum transition by p times that for the SQ transitions, with p the order of coherence of the multiple-quantum transition (Ernst *et al.*, 1987). When the field gradient pulse $G_z^{(i)}(\mathbf{r},t) = \nabla B_z^{(i)}(\mathbf{r},t)$, [with superscript i numbering the gradient pulse], is applied at a given point in a coherence pathway where the signal has coherence order p, the amplitude V of the observed signal becomes:

$$V = V_0 \int_{V_s} v_1(\mathbf{r}) \exp[-ip\Phi_i(r)] d\mathbf{r} \,. \tag{41}$$

We introduced the phase:

$$\Phi_i(\mathbf{r}) \equiv \int_{\Delta t_i} \gamma_e B_z^{(i)}(\mathbf{r},t) dt \tag{42}$$

where Δt_i is the duration of the ith gradient pulse. Also, $V_0 v_1(\mathbf{r})$ is the signal per unit volume in the absence of the gradient pulse. As a result, the signal amplitude decreases due to dephasing caused by a distribution of $\Phi_i(\mathbf{r})$ over the sample.

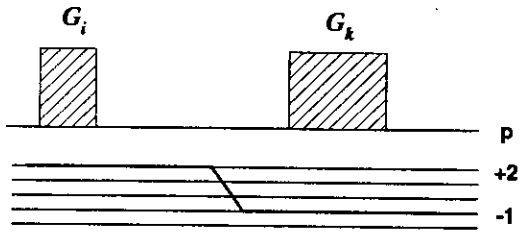

Figure 8. Selection of the coherence pathway using PFG's. Two field gradient pulses with equal field gradients but with widths of Δt and $2\Delta t$, respectively, are applied. The coherence pathway $2 \rightarrow -1$ is to be selected as is shown.

If a second gradient pulse with the same spatial distribution is applied, (cf. Fig. 8), then it is possible to refocus the phase introduced by the first gradient pulse. This occurs when the condition $p_i\Phi_i(\mathbf{r}) = -p_k\Phi_k(\mathbf{r})$ is satisfied. Here, p_i and p_k are the orders of coherence for the selected pathway when the i^{th} and k^{th} gradient pulses are applied, and $\Phi_i(\mathbf{r})$ and $\Phi_k(\mathbf{r})$ are the phases introduced by PFG's i and k.

In the examples given in Sec. 4 for DQC a strong suppression of unwanted signals has been achieved using phase cycling. An estimate for suppression by PFG's can be made, assuming a sample with the dimensions of $(2X, 2Y, 2Z)$, uniform square gradient pulses with components $(G_X, G_Y, 0)$, and $v(\mathbf{r}) = \text{const.}$

The condition for refocusing $2\Phi_i(\mathbf{r}) = -\Phi_k(\mathbf{r})$ is met for the signal from the DQ coherence pathway 2 → -1 depicted in Fig. 8. Alternatively, for the SQ pathway 1 → -1, which is to be suppressed, we find from Eq. 41:

$$V = V_0 \frac{\sin(\gamma_e G_X X \Delta t)\sin(\gamma_e G_Y Y \Delta t)}{\gamma_e^2 G_X G_Y XY \Delta t^2} \quad . \tag{43a}$$

For a gradient pulse with a width Δt of 20 ns, sample dimensions of 1.5×6×1.5 mm, and PFG of (70, 70, 0) G/cm, we find $V/V_0 \approx 0.063$. (The 0 → -1 pathway would be suppressed by a factor of 4 greater). Past work on PFG's for FT-ESR Imaging (Ewert *et al.*, 1991) suggests that such specs are not unreasonable. Suppression can be improved by fine tuning of gradients, such as to bring the sine functions in the numerator of Eq. 43a closer to zero. For selection of high orders of coherence this value would be adequate. Note also that signal selection with PFG's is highly specific with respect to the given order of coherence.

For such experimental conditions, PFG's would not provide as great a suppression as phase cycling does. Nevertheless PFG's could be very useful in the case of small spin clusters where, for spin-counting, it is necessary to separate higher orders of coherence. This would be a challenging task for phase cycling. PFG's could also be used in conjunction with phase cycling to improve the suppression of unwanted pathways by phase cycling in experiments with nitroxides.

4. EXAMPLES

4.1 Random Radicals (E' Centers in Fused Silica)

Paramagnetic centers with narrow lines are ideally suited as a model system to examine the features of DQC. The model system of E' centers in γ-irradiated silica has been studied by Borbat and Freed, (1999). E' centers have a narrow ESR spectral extent (ca. 5 G at Ku-band), thereby posing few instrumental challenges. This system provides a good illustration for all the pulse sequences. It was used for initial studies in order to work out the proper pulse sequences and to optimize phase cycling schemes. Because paramagnetic centers are randomly distributed, this system can also serve as an illustration for DQ experiment on random distributions. The weak-coupling approximation is adequate for magnetically dilute solids (Feldman and Lacelle, 1996).

Due to the small spectral extent Eq. 37 readily applies to the experiments on E'-centers in γ-irradiated fused silica shown in Figs. 9-11. To interpret

such an experiment, we must sum over all the individual random radical-pair interactions. Formally, this averaging over the random distribution of pairs of spin is done by configurational averaging of

$$\left\langle \prod_j \cos a(\mathbf{r}_{1j})t \right\rangle_{\{\mathbf{r}_{1j}\}} . \tag{43b}$$

Such averaging has previously been performed by the Markov method (Chandrasekhar, 1943) for SQ coherence (Abragam, 1961), but it can be performed for DQC as well (Borbat and Freed, 1999). It yields, for example, for the envelope of the 4 and 6-pulse signals:

$$\begin{aligned} D_4(t_p) &= -\frac{1}{8}[1-\exp(-kt_p)] \\ D_6(t_\xi) &= \frac{1}{2}[\exp(-kt_m)-\exp(-k\,|t_\xi|)] \end{aligned} \tag{44}$$

where, $k = (4/3^{5/2})\pi^2\gamma^2\hbar C$ and C is the concentration (i.e. number density) of spins. In a 4-pulse sequence we observe exponential growth of the DQ signal that is faster at higher concentrations.

Note that for random distributions, all orders of coherence are produced by the preparation sequence. This results in the loss of amplitude of the DQ signal by a mechanism that is referred to as "instantaneous diffusion" in the literature (see for example, Salikhov, *et al.*, 1976; Raitsimring and Salikhov, 1985), and Eqs. 44 should be modified accordingly by multiplying them by $\exp(-k_1 t_m)$ where $k_1 = (4/3^{5/2})\pi^2\gamma^2\hbar CH$ where in this case $H_n = H_n^{\infty}$ $(n = 4, 6)$

The simple time behavior expressed by Eq. 44 in conjunction with complete excitation was convenient for demonstrating some key features. We compared the DQ signals from different DQ sequences as well as with SQ signals.

The ratio 1:4 for the amplitude of the 4 (or 5) pulse vs. the 6-pulse DQ echoes predicted by Eq. 32 is experimentally demonstrated in Fig. 9. The result in this figure was obtained by the 6-pulse sequence of Fig. 5(c). It is a 2D acquisition in which the echo shape is obtained as a function of t_2; then the acquisition is repeated as the time interval t_{p1} in the preparation period is stepped out. Here we label the first t_p period in Fig. 5(c) as t_{p1} and the second as t_{p2}. The sum of t_{p1} and t_{p2} is kept constant. When $t_{p1} = t_{p2}$, the 6-pulse DQ echo is successfully refocused. This echo is in the center of the plot. When $t_{p1} \neq t_{p2}$ we detect two echoes from the upper and lower SQC pathways with $p = \pm 1$ in the t_{p1} portion of the preparation sequence. These two echoes are positioned symmetrically with respect to the 6-pulse echo, and their magni-

tudes are the same as expected for a 4(5)-pulse echo, i.e. ¼ of the 6-pulse DQ echo (cf. Fig. 9). The first and last π pulses of the 6-pulse sequence now only change the sign of these two echoes. Splitting of the 6-pulse echo into two 4(5) pulse type DQ echoes yields a factor of 2 reduction. Another factor of 2 emerges because half of the coherence pathways of the type

$$S_1^{\pm} S_{2z} \rightarrow S_2^{-} S_{1z},\ S_2^{\pm} S_{1z} \rightarrow S_1^{-} S_{2z}$$

are lost, since they cannot satisfy the refocusing conditions with such a timing arrangement.

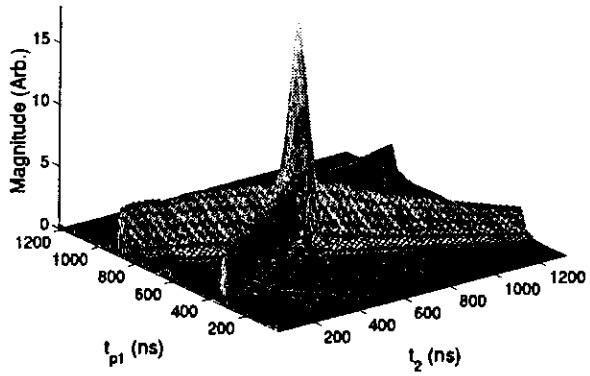

Figure 9. The relative amplitudes in the 4(5) and 6-pulse DQ echoes as exemplified by results on E'-centers. A modified 6-pulse acquisition scheme was used in 2D format. In the plot t_2 is the spectral coordinate and t_{p1} is the length of the first time interval in the preparation sequence.

In Fig. 10 we show results from samples of E' centers in γ-irradiated fused silica for the 4 pulse sequence. Again uniform coverage was obtained. By varying t_2 we record the actual shapes of the echoes. We show the 4-pulse SQ echo [signal (i)] and the 3-pulse stimulated echo [signal (v)] (arising from eliminating the π-pulse of Fig. 5(a)). They are equal but opposite in sign. Note, that both have magnitudes equal to COSY (cf. Sec. 4.2.5), if relaxation can be neglected. By phase cycling we separate the DQ signal from the sum of ZQ and SQ signals. Also, it was possible to suppress the ZQ signal from the latter sum yielding just the 4-pulse SQ by "detuning" the ZQ signal. This is achieved by setting the two t_1 periods in Fig. 5 to be unequal. The DQ signal (iv) is close to 25% of that for the stimulated echo at this t_p. By "retuning", (i.e. resetting the refocusing condition for DQC by equalizing the lengths of the two intervals t_1), we get the algebraic sum of the SQ and ZQ signals, (cf. ii). Finally with a modified phase cycle, we get the algebraic sum of SQ + ZQ + DQ, (cf. iii). One sees that the ZQ and DQ signals are

equal, and they are opposite in sign to the SQ signal. These relationships are consistent with the theory given in the Sec. 2.2.

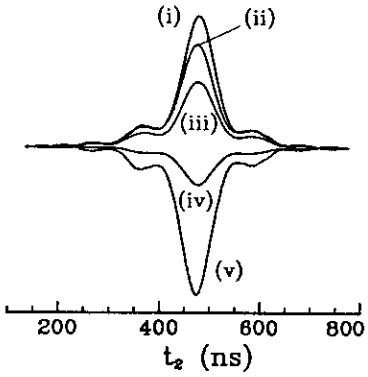

Figure 10. DQ, SQ, and ZQ signals observed for E' centers in γ-irradiated fused silica with the 4-pulse sequence of Fig. 5(a); t_p =475 ns and t_1= 50 ns with t_2 varied to give the echo shape: Case (i) the SQ signal; (ii) the algebraic sum of the SQ and ZQ signals; (iii) the algebraic sum of the SQ, ZQ, and DQ signals; (iv) the DQ signal; (v) the 3 pulse stimulated echo.

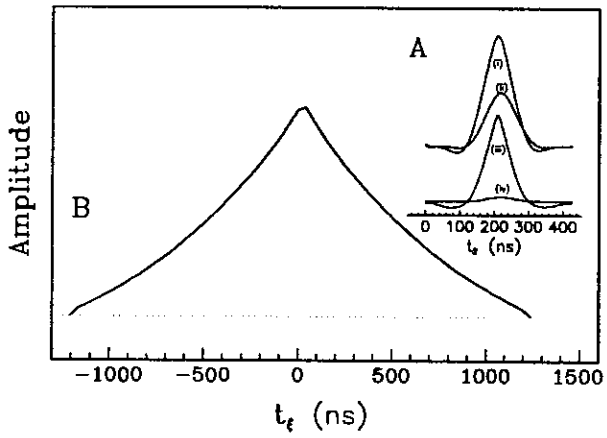

Figure 11. E' centers in γ-irradiated fused silica. The 6-pulse sequence of Fig. 5(c) was used. The $\pi/2$ pulses were set to 6.8 ns and the π-pulses to 13.2 ns. t_m = 1,200 ns, t_1 = 50 ns and the DQ signal is shown in B vs. t_ξ for a step size in t_p of 20 ns.A) echo shapes vs. t_2 for (i) the two-pulse COSY echo; (ii) the DQ echo at t_p= 200 ns. Cases (iii) and (iv) are respectively the COSY and DQ echoes for a more dilute sample.

Fig. 11 shows DQ echo shapes vs. t_2 for the 6-pulse sequence, as well as echoes from the two pulse COSY signal, for both a low and high concentra-

tion of E' centers. [Results from the latter sample were shown in Fig. 10] The DQ signal vs. t_ξ in Fig. 11(b) is also shown for the more concentrated sample. This figure illustrates refocusing of dipolar interactions for randomly distributed spins. An analysis of this signal in terms of a random distribution of interacting spins given by Eq. 44 yields a sample concentration of $1.7 \cdot 10^{18}$ spins/cm^3. This value is close to the value $2.0 \cdot 10^{18}$ spins/cm^3 that we obtained from a standard instantaneous diffusion measurement (Eaton and Eaton, 1993) for this sample.

One sees from Fig. 11(A) that for the high concentration sample, the DQ signal reached about 50% of its maximum value at this t_p (200 ns) by comparison with the COSY signal, (which is produced by two successive $\pi/2$ pulses), whereas it is relatively much smaller for the low concentration sample due to its considerably slower signal growth (cf. Eq. 44).

4.2 Bilabeled Organic Molecules

As an example of a system that exhibits a large distance, ca. 30 Å, the nearly linear rigid nitroxide biradical: piperidinyl-CO_2-$(Phenyl)_4$-O_2C-piperidinyl, (R-I), (Borbat and Freed, 1999) was studied. It could be aligned in the liquid-crystal mixture: Phase V (Meirovitch *et al.*, 1982), by slowly cooling the 0.5 mM solution into the nematic phase in an orienting magnetic field of 13.5 kG. The nematic phase persists to low temperatures, and the sample remained fully aligned in the temperature range from -57°C to -66°C, where the experiments were performed. For comparison, the sample was also quickly frozen in zero magnetic field to yield an isotropic powder (glass). As a model system with a shorter distance, ca. 16 Å, the biradical (R-II) piperidinyl-CO_2-Phenyl-O_2C-piperidinyl was used. It was studied in the LC phase V.

4.2.1 4, 5, and 6 Pulse Sequences: Oriented Samples

We show in Figs. 12 and 13 a series of DQ signals obtained with the pulse sequences in Fig. 5. In Fig. 12A (curves (i) - (ii)) we show the DQ signal from the 4-pulse sequence of Fig. 5(a) for the biradical R-I for the cases of 0° and 90° alignment respectively. The t_p minimum here was 35 ns and one observes that for 0° alignment a significant build-up of signal has occurred during this "dead-time". The experiments are affected by decay due to a T_2 of about 0.8 μs. In addition, there is ESEEM, due to matrix and nitroxide protons, which does not pose a problem, since it occurs at 26.2 MHz. This is still much greater than the dipolar modulation we discuss next. In addition, the relative intensity of the ESEEM is low. The modulation of the DQ signals due to dipolar interaction is strong for both orientations. Fourier

transformation yields frequencies of 2.13±0.15 MHz and 4.2±0.15 MHz respectively for 90° and 0° tilt angles for both the 4 and the 5-pulse sequences. The decay of the oscillations, which is more pronounced at 0° tilt, is presumably due to a small distribution of interspin distances, as well as to an order parameter close to, but not exactly unity. In Fig. 12(B) (iii, iv) we show signals obtained with the 5-pulse sequence of Fig. 5(b). These signals have the characteristic features of no decay due to T_2, a baseline offset, and they are a sum of two components, (cf. Sec. 2.2). The second component is considerably weaker and can be noticed in (iii) for large t_m-t_p.

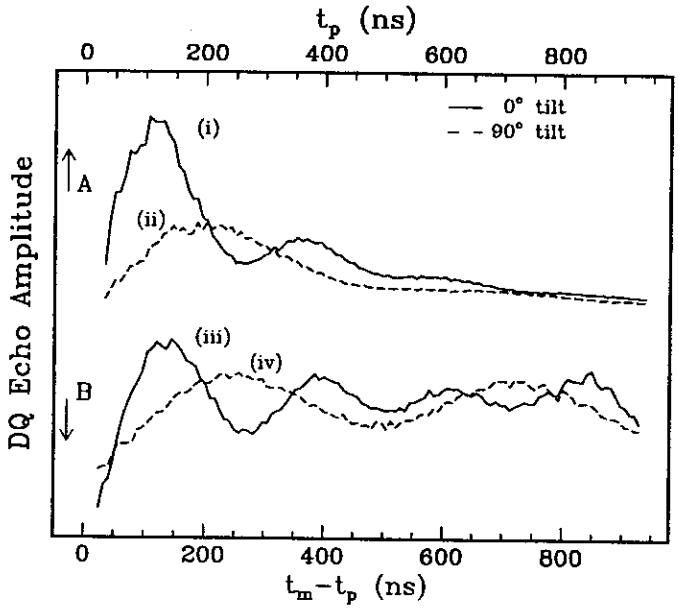

Figure 12. 4 and 5-pulse DQ signals from an oriented sample of biradical R-I dissolved in Phase V at about 0.5 mM concentration (limited by solubility). The 4-pulse sequence of Fig. 5(a) is shown in A, and the 5-pulse sequence of Fig. 5(b) is shown in B. Results were obtained at 0° (i, iii) and 90° (ii, iv) tilt angles. The spectrometer frequency was 17.358 GHz; the sample temperature was -57°C. In both experiments the pulse widths were set to 6.2 ns for the π pulses and 3.6 ns for the $\pi/2$ pulses; t_1 was set to 26.5 ns, and the step size in t_p was 8 ns. A total of 200 points yielding a t_p maximum of 1.6 μs were sampled in 9 min for the 4-pulse sequence (only the first 114 points are shown), and 114 points were sampled in 49 min for the 5-pulse sequence. The signal for the 5-pulse sequence is plotted as a function of t_m-t_p, so as to correspond to the graph of the 4-pulse sequence.

The characteristic dipolar modulation frequencies of 2.13 and 4.2 MHz for 90° and 0° tilt angles respectively, readily yield the distances from Eq. 15c and Eqs. 30a and 30b. For the 4-pulse sequence the modulation obeys $\sin^2(at_p/2) = (1-\cos at_p)/2$. From Eq. 15d, $a(90°) = \gamma_e^2\hbar/r^3$ and

$a(0°) = -2\gamma_e^2\hbar/r^3$ corresponding to the 1:2 ratio observed. These results are readily converted into r. We obtain r = 28.8 Å using the conversion r[Å] = $10(51.9/f\,[\mathrm{MHz}])^{1/3}$.

Fig. 13 shows the results obtained with the 6-pulse sequence for the same aligned sample of R-I.

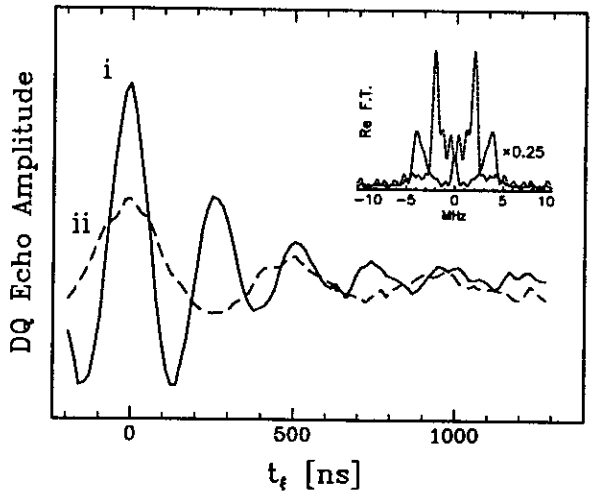

Figure 13. Rigid biradical R-I aligned in LC Phase-V. Data collected with 6-pulse sequence are plotted for two orientations (i) 0° and (ii) 90°. Only part of the signal was collected, given its symmetry vs. t_ξ. Inset shows Fourier transforms of the corresponding envelopes. Solid lines: 0°; dashed lines: 90°.

For the oriented samples DQ echoes are quite strong and the signal can be collected in a matter of minutes even over an interval as long as 1 μs. We obtained the same characteristic frequencies in the 6-pulse scheme as with the 4 and 5 pulse schemes, since its signal oscillates as $\cos(at_\xi)$. The DQ echo is stronger for 0° tilt angle, which is qualitatively consistent with the proposed geometrical structure of the biradical (cf. below), where the z-axes of the respective *hfi* tensors of nitroxides are nearly perpendicular to the interspin vector. For such a case at the 0° tilt angle $\Delta\Omega \approx A_\perp$ for the $m = \pm 1$ nuclear manifolds. Hence with limited spectral excitation stronger signals are produced. This observation is supported by comparison of ESR spectra obtained by Fourier transformations of the COSY signal at both tilt angles.

The above results indicate how macroscopically aligned samples provide the greatest opportunity for accurate distance measurements: the dipolar line shape from the FT (cf. Inset to Fig. 13) is just a narrow line. This also leads to increased sensitivity. Macroscopically aligned samples are ideally suited for extracting distance distributions, order parameters, and structural parameters.

Also, the range of measurable distances would be broader, since at 0° tilt the dipolar splitting is larger (cf. App. B). In addition, the relative angles between interspin vectors of different types of radical pairs could be determined from the angular dependence of their dipolar splitting (Astashkin *et al.*, 1997).

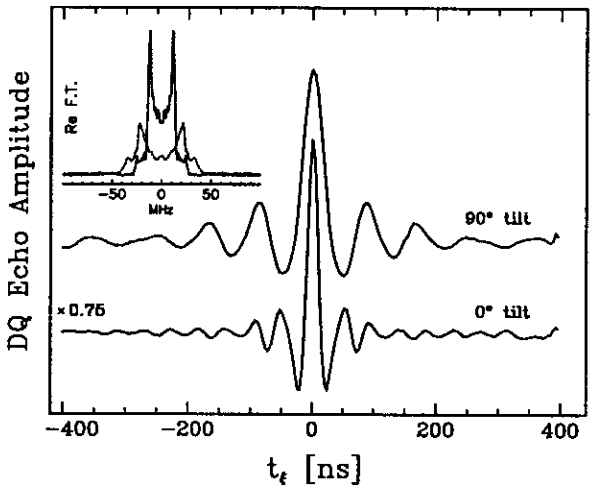

Figure 14. Biradical R-II aligned in Phase-V at -69°C. Signal envelopes in the 6-pulse sequence are shown for 0° and 90° tilt angles. Inset: Real FT of the left halves of the signal envelopes for 0° tilt (dashed line) and 90° tilt (solid line). Concentration is about 1 mM. The collection time was 15 min, and we show unprocessed signals.

Next, we show the results for the shorter biradical R-II, also aligned in Phase-V in Fig. 14. The signal is detected with high SNR. The frequency of 11.9 MHz at 90° tilt angle can be readily read from the FT spectra (Inset) and it translates into a distance of 16.2 Å. We note that at this relatively short distance, effects caused by the pseudo-secular term of the dipolar Hamiltonian can be noticed (cf. App. A). While they are small for 90° tilt angle, for 0° tilt angle the frequency $3\nu_I/2 = 36$ MHz ($\nu_I \equiv \omega_I/2\pi$) is clearly seen. These pseudo-secular effects plus small deviations from perfect alignment and also the weak ESEEM line at 13 MHz (cf. Sec. 4.2.4) lead to the Pake-like appearance in Fig. 14.

4.2.2 Random vs. Oriented Samples

We have shown in Figs. 13 and 14 the DQ signals obtained from the 6-pulse sequence of Fig. 5(c) for aligned samples. The same samples can be converted to disordered ones by rapid freezing. Figs. 15 and 16 show the disordered cases, which are the ones more typically encountered. We see the

DQ modulation pattern plotted vs. t_ξ. The signals, of course, have zero dead time as a function of t_ξ, and they are symmetric about $t_\xi = 0$. They represent the "dipolar echo" which occurs at $t_\xi = 0$, when refocusing conditions for dipolar interaction are met. We also show the real part of the FT of the time domain signals.

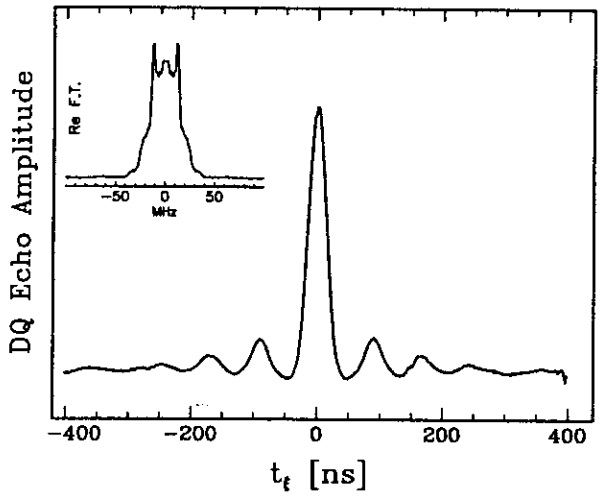

Figure 15. Results from the 6-pulse DQ sequence. Biradical R-II was studied in disordered LC Phase V at -69° C. Inset shows Fourier transform of the left half of the signal envelope. The two characteristic frequencies of the Pake doublet (cf. Insert) 11.9 and 25 MHz translate into a distance between NO groups of 16.2 Å, and the exchange integral, J is -0.25 MHz. The biradical concentration is about 1 mM. (A signal at 0 MHz corresponds to a residual baseline vs. t_ξ). Data collection took 1 hour for 400 points in t_ξ, but with improved time sweep capabilities it can be performed in about a minute. We show the unprocessed signal.

The DQ signal for R-II is strong with a SNR of about 300 at the signal maximum. The concentration could be reduced to 100 μM and would still permit an accurate distance determination. The Pake doublet is well-resolved and both canonical frequencies $\nu_\parallel$ and $\nu_\perp$ can be accurately determined. From Eq. 15c,d using the experimental values for $\nu_\parallel$ and $\nu_\perp$ equal to 25 MHz and 11.9 MHz, respectively, we can find that d is 12.3 MHz and J is -0.25 MHz. The value of 12.3 MHz for d yields the distance of 16.2 Å between the NO groups. The shape of the Pake doublet shows characteristics due to non-negligible effects of the pseudo-secular terms (cf. App. A), but at the distance ca. 16 Å these effect can be noticed only at 0° tilt angle where d is ca. 8.2 G.

The DQ signal for R-I (cf. Fig. 16) was acquired over a long enough sampling interval of 1.56 μs to produce a nearly ideal Pake doublet after subtraction of a very weak linear slope, that is caused by the DQ signal from the

interaction of nitroxide spins on different molecules (cf. Sec. 4.3). The intermolecular DQ signal from the randomly distributed spins, is quite small in comparison to the DQ signal caused by the intramolecular coupling. While the DQ signal in Fig. 16 is a very good one, it is not yet optimal, because full spectral excitation has not yet been achieved. The Pake doublet can readily be interpreted (cf. above) to yield a distance between nitroxides of 28.8±0.5 angstroms.

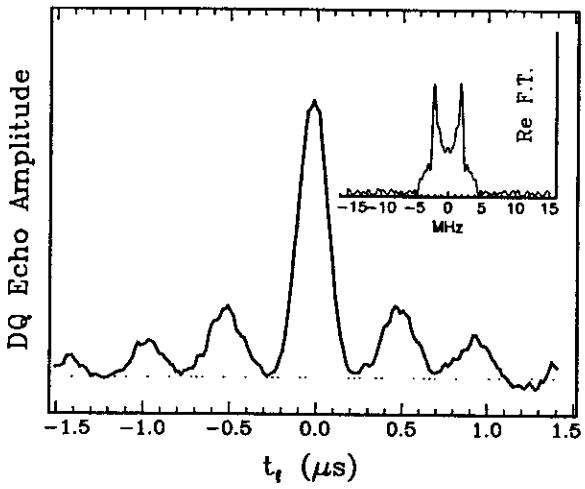

Figure 16. DQ signal using 6-pulse sequence at -62° C for disordered sample of rigid biradical R-I in LC Phase-V. Data were collected over a sampling interval of 1.56 μs with 6 hours of acquisition. No data smoothing or filtering was applied. Inset shows the Pake doublet obtained by the real Fourier transformation of the sum of the left and right halves of the signal envelope after folding the spectrum over the point $t_\xi = 0$ and subtracting a linear baseline. The concentration was 0.5 mM.

Molecular modeling by means of the PCMODEL v.7 software package yielded a value of 28.06 Å (27.81 Å) for the H-H (N-N) distance between the diamagnetic NH groups, which had to be used in the modeling instead of NO.

The data collection for Fig. 16 took a substantial but reasonable time, for this not very concentrated sample, (≈0.5 mM), but it could be made shorter since the S/N in Fig. 16 is greater than necessary. A reasonable upper limit for the sampling interval for this sample with its T_2 of 0.8 μs is about 2 μs. Note that the 1.56 μs sampling interval used in Fig. 16 is already sufficient to measure a 43 Å distance with ±5 Å accuracy, and a 2 μs interval increases it to 47 Å. Such estimates are based on the simple assumption that one needs at least one full period of oscillation of the frequency $\nu_\perp = d$, the singular component of the Pake doublet. Larger distances can be assessed with longer T_2's. With a T_2 of 2 μs a distance of 70 Å could be determined

with the same relative error, whereas for T_2 in the range of 1 - 1.5 μs such a distance could be estimated with tolerable accuracy.

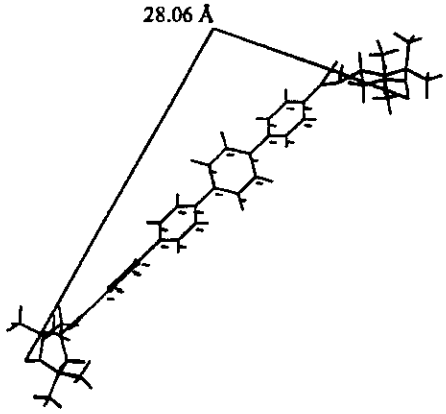

Figure 17. Geometrical model of the rigid biradical R-I, generated by PCMODEL v7.0 software package

For aligned samples the upper range of distances extracted from $\nu_{\parallel} = 2d$ would be about 80 Å. Further discussion relating to the upper range of distances, can be found in App. B.

4.2.3 Correlation of Orientations (2D Experiments)

We found (cf. Sec. 3.1.1) that even with a B_1 as large as 30 G, π-pulses did not provide uniform excitation for the ^{14}N-labeled nitroxides. FT's of our data for 4, 5, and 6-pulse sequences for the aligned sample of R-I show that the amplitude ratios of the spectral peaks for the 90° orientation relative to that for the 0° orientation are about 1.5, 1, and 0.65, respectively. This indicates that the nitroxide moieties are correlated and indicates the steady decline in spectral excitation with increasing number of pulses in the sequence. When there is spatial correlation between *hfi* tensors of the nitroxides and $\boldsymbol{r}$, then Eq. 34 needs to be used for simulations. It has been shown in DEER (Maryasov *et al.*, 1998) that selective excitation gave rise to modulation of the Pake doublet by a function $\xi(\cos\theta)$ which they called the geometrical form-factor. It was also shown there that in the case of inhomogeneous broadening typical for nitroxides, $\xi(\cos\theta)$ is a fairly smooth function of $\cos\theta$ and typically varies within a factor of 2. It can badly distort Pake doublets, but does not change characteristic frequencies. Maryasov *et al.* (1998) suggested that by varying B_0 it could be possible to extract some structural information related to the mutual orientations of the nitroxides *hfi* tensor principal axes by modeling variations of $\xi(\cos\theta)$ with magnetic field. It is rea-

sonable to expect that a 2D DQ experiment can be utilized for obtaining this kind of information. Such an experiment provides the shape of a Pake pattern as a function of position in the ESR spectrum. That is, a 2D Fourier transformation of the echo shapes $F(\omega_1,\omega_2)=FT\{D_n(T,t_2)\}_{T,t_2}$ collected as a function of the time T (which is t_ξ for the 6-pulse sequence and t_p for 4-pulse sequence) would yield variations of the Pake doublet displayed along $f_1 = \omega_1/2\pi$ as a function of position in the ntroxide spectrum, (i.e. along $f_2 = \omega_2/2\pi$) due to orientational correlations. Let us consider how this can happen. Let us first ignore any variation in spectral coverage of the second spin for simplicity. Excitation of the first spin at a certain frequency offset $\Delta\Omega_1(\lambda_1,\eta)$ selects a range of orientations (λ_1,η) corresponding to this frequency offset, if the orientations of the magnetic tensors of this nitroxide is correlated with the orientation of interradical vector, $\boldsymbol{r}$, (cf. discussion of Eqs. 34 and 35). Only biradicals with a certain range of angles $\eta \equiv (\theta,\varphi)$ will be excited corresponding to a non-uniform distribution for $(3\cos^2\theta - 1)/2$. This will result in a variation of the Pake pattern over the ESR spectrum. [Clearly, this type of argument holds equally well when there is correlation for both nitroxides with $\boldsymbol{r}$].

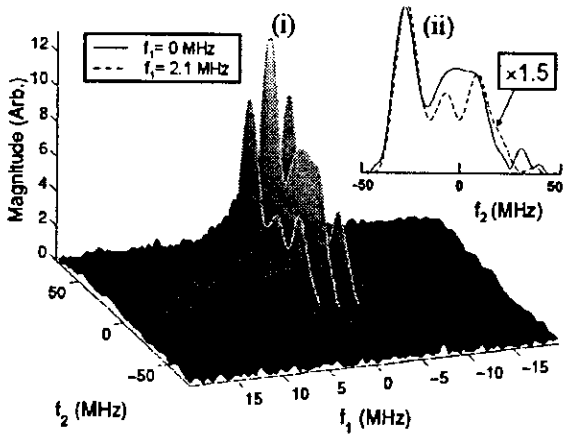

Figure 18. The 2D 6-pulse DQ experiment with biradical R-I disordered in the LC Phase-V at -62° C. (i) - The 2D data were collected in this experiment, which also provided the data in the 1D format depicted in Fig. 16. The spectrum is the magnitude FT vs. f_1 and f_2, which are the respective FT variables of t_ξ and t_2. No baseline correction was made. The inset (ii) displays the $f_1 = 0$ MHz slice (solid) and the $f_1 = 2.1$ MHz slice (dashed) superimposed. The latter is at the maximum of the DQC Pake doublet whereas the former is mainly a background that depends only on $\langle G_6(\Delta\Omega_1)\rangle_{\Delta\Omega_1}\langle H_6(\Delta\Omega_2)\rangle_{\Delta\Omega_2}$. Hence the difference between them is a result of correlation between $\mathbf{r}_{12}$ and the nitroxide magnetic tensors.

We show in Fig. 18 such a 2D spectrum, which clearly shows variations in the Pake pattern along f_1 with spectral resonant frequency, f_2. Fig. 18 is

from a disordered sample of R-I. A detailed analysis of these 2D spectra should enable important structural information to be obtained. In Fig. 18 we can clearly see substantial variations of the intensity of the $\nu_\perp$ component of the Pake doublet. This component is visible as a sideband in the stack plot. The line at zero frequency has its origin from the FT of the slope, which is caused by the DQ signal from interactions with the other spins in the sample, and therefore corresponds to the uncorrelated case. The sidebands vary quite substantially, with a lower intensity of $\nu_\perp$ in the center of the spectrum. This indicates that the z-axes of the *hfi* tensors are oriented at an angle that is substantially different from the interspin vector. This conclusion is consistent with the molecular model of the biradical (cf. Fig. 17).

4.2.4 ESEEM Effects

So far, we have not discussed ESEEM effects in this chapter. As long as oscillations from ESEEM occur at significantly different frequencies from those resulting from DQ modulation, simple Fourier transformation methods can easily separate them. However, ESEEM can interfere with the relevant signal in some cases. At this point it seems appropriate to give an aproximate picture of ESEEM in the DQ experiment. Nuclear modulation is known to be a potential problem not only in other coherent distance measurement techniques such as "2+1" (Kurshev *et al.*, 1988) but also in 4-pulse DEER, when overlap of spectral excitations at the two applied frequencies is not negligible, (Pannier *et al.*, 2000).

A rigorous treatment of ESEEM for radical pairs could yield very cumbersome expressions for DQ pulse sequences even for the case of non-selective pulses, for which it should be possible to arrive at a closed form expression. This is why we give a more approximate picture of ESEEM effects with the example of the 6-pulse sequence. We assume that ESEEM is determined predominantly by the SQ pathways, i.e. by preparation and detection periods where it attains the well-known form for a 2-pulse echo (Dikanov and Tsvetkov, 1992):

$$M(t)=\prod_{n=1}^{N}(1-2k_n^2\sin^2(\omega_{\alpha,n}t/2)\sin^2(\omega_{\beta,n}t/2)) \qquad (45a)$$

where $\omega_{\alpha n}$, $\omega_{\beta n}$, k_n are given by

$$k_n^2=\frac{\omega_{I,n}^2(T_{zx,n}^2+T_{zy,n}^2)}{\omega_{\alpha,n}^2\omega_{\beta,n}^2}$$
$$\omega_{\alpha,n},\omega_{\beta,n}=[(\omega_{I,n}\pm T_{zz,n})^2+(T_{zx,n}^2+T_{zy,n}^2)/4]^{1/2}. \qquad (45b)$$

Here t is either t_p or t_m - t_p, N is the number of interacting nuclei with their respective *hfi* tensors $\mathbf{T}_n$ and Zeeman frequencies $\omega_{I,n}$. We shall ignore the action of the DQC refocusing pulse sandwich $(\pi/2)$ - t_1 - π - t_1 - $(\pi/2)$, which introduces constant phase and amplitude factors. The signal envelope in the 6-pulse sequence is then modulated by $M(t_p)M(t_m - t_p)$ and can be rewritten as:

$$M(t_m,t_\xi) \approx 1 - 4\sum_n k_n^2 (1 - \cos\frac{\omega_{\alpha,n}t_m}{2}\cos\frac{\omega_{\alpha,n}t_\xi}{2} - \cos\frac{\omega_{\beta,n}t_m}{2}\cos\frac{\omega_{\beta,n}t_\xi}{2} + \frac{1}{2}\cos\frac{\omega_{n+}t_m}{2}\cos\frac{\omega_{n+}t_\xi}{2} + \frac{1}{2}\cos\frac{\omega_{n-}t_m}{2}\cos\frac{\omega_{n-}t_\xi}{2}). \quad (46a)$$

Here $\omega_{n\pm} = \omega_{\alpha,n} + \omega_{\beta,n}$ and the terms in k_n^4 are neglected. For matrix nuclei and weakly-coupled nuclei of nitroxides, $\omega_{\alpha,n}, \omega_{\beta,n} \approx \omega_I$ and Eq. 46a becomes:

$$M(t_m,t_\xi) \approx 1 - k(\frac{3}{4} + \frac{1}{4}\cos\omega_I t_m \cos\omega_I t_\xi - \cos\frac{\omega_I t_m}{2}\cos\frac{\omega_I t_\xi}{2}) \quad (46b)$$

with k is a spatial average of the k_n^2 over all interacting nuclei. One immediately finds that the modulation frequencies are scaled down by a factor of 2, and that "blind spots" will emerge, where the ESEEM at a given frequency is suppressed. (Such blind spots occur in ESEEM for sequences with more than two pulses (Schweiger, 1990).

With respect to ESEEM, we note that the 4-pulse DQ sequence resembles HYSCORE (Höfer *et al.*, 1986; Gemperle *et al.*, 1990). Using an expression for HYSCORE from Dikanov and Tsvetkov, (1992) for weakly-coupled protons we derived:

$$M(t,t_1) \approx 1 - 2k\sin^2(\omega_I t/2)\sin^2[(\omega_I(t+2t_1)/2].$$

The line at ω_I will be suppressed by the effect of "blind spots" when $2\omega_I t_1 = \pi(2n+1)$, $(n = 0, 1, \ldots)$, i.e. for $t_1 = 9.5$ ns, 28.5 ns, etc. at 17.3 GHz. We typically set $t_1 \approx 28$-30 ns and have successfully suppressed the line at ω_I. The same type of "blind spots" effect can take place in the 6-pulse sequence as well, (cf. Eq. 46b).

Experiments we have performed have confirmed that Eq. 46b gives a qualitatively correct picture. In some of our experiments, we made use of the blind spots in order to suppress ESEEM at the proton Zeeman frequency, by adjusting t_m. Finally, we remind the reader that ESEEM of the DQ signal

from electron spin pairs in diluted systems does not constitute a problem for two reasons. First, at Ku-band the modulation frequencies from matrix nuclei, which are typically protons, occur well outside the Pake doublet. [In the 4 or 5 pulse sequences at 17.3 GHz, the proton ESEEM at 26.3 MHz is higher in frequency than the dipolar modulations for $r > 15$ Å. In the 6-pulse sequence the proton ESEEM frequency is 13.1 MHz and is outside the doublet for $r > 20$ Å]. Second, the modulation is shallow in the DQ experiment, and we often do not see it. At X-band, the modulation due to solvent nuclei is about 4 times stronger and nuclear modulation frequencies are about 2 times lower than at 17.3 GHz.

A problem arises when a weak DQ signal from electron spin pairs is imposed on a strong DQ signal from randomly distributed radicals or from the radicals grouped in small clusters, (e.g. in cases of very high concentration). In the case of randomly distributed spins at high concentration, the DQ signal from pairs decreases due to generation of higher orders of coherence, and the intermolecular DQ signal from radicals in the bulk becomes larger. With increase of the sampling interval t_m, the DQ signal from the randomly distributed spins grows according to Eqs. 44. This signal appears as a nearly linear slope modulated by ESEEM. At sufficiently high concentration, this modulation can become comparable to the DQ signal from pairs. Prior to Fourier transformation this signal should be removed. For reliable subtraction, it is advantageous to reduce the modulation depth, which is accomplished by using the suppression effect of the "blind spots".

4.2.5 Comparison with COSY, etc.

It is clear that the simplest pulse experiment from which it is possible to extract distance information is just the two pulse Hahn echo sequence. In the weak coupling limit the expression for the primary echo signal amplitude (under the same conditions that Eqs. 30 for DQ signals were derived) is[3] :

$$V_{2,SQ}(\Delta\Omega_1,\Delta\Omega_2,\mathbf{r},t_p) = -\mathrm{Im}\{S^{(1)}(\beta_1)^*\}S_2^{(1)}(\beta_2) \times[1-2S^{(2)}(\beta_2)\sin^2(at_p/2)]. \quad (47)$$

In COSY $\beta_1 = \beta_2 = \pi/2$. In the limit of non-selective $\pi/2$ pulses, Eq. 47 becomes:

$$-V_{2,SQ}(\Delta\Omega_1,\Delta\Omega_2,\mathbf{r},t_p) \approx (1+\cos at_p)/4 \quad (48a)$$

[3] A somewhat lengthy expression for the 2-pulse echo for coupled spins was derived by Yudanov et al. (1969) in the limit of non-selective pulses. In the weak coupling limit it simplifies to Eq. 47 if FID-like terms (cf. App. A) are ignored.

which is to be compared with Eq. 32. Note that

$$-V_{4,DQ}(\Delta\Omega_1,\Delta\Omega_2,\mathbf{r},t_p)\approx(1-\cos at_p)/8 \qquad (48b)$$

from Eq. 32 as $S^{(2)}(\pi/2)\approx 0.5$ for sufficiently non-selective pulses. (The actual value is 0.454 for a B_1 of 30 G for ^{14}N at X-band), Therefore Eq. 48a holds even for realistic pulses. However for B_1=30 G at X-band the factor $\mathrm{Im}\{S^{(1)}(\pi/2)^*\}S_2^{(1)}(\pi/2)$ for COSY is 0.75, whereas the factor

$$2\,\mathrm{Im}\{S^{(1)}(\pi/2)^*\}S_2^{(1)}(\pi)S_2^{(1)}(\pi)[|C_2^{(1)}(\pi/2)|^2+S_2^{(1)}(\pi/2)^2]|S^{(2)}(\pi/2)|^2$$

for $V_{4,DQ}$ (cf. Eq. 30a and Sec. 3.1.1) is 0.44. This means that $V_{4,DQ}$ will be about 4 times less than $V_{2,DQ}$ under realistic conditions.

Thus, it would appear that in the case of ^{14}N nitroxides, the COSY sequence can be effectively used, given sufficient spectral excitation and short dead-times. We examine this with examples using biradicals R-I(II).

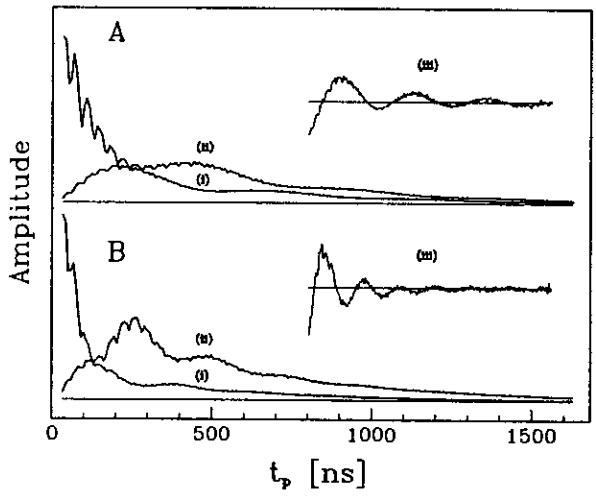

Figure 19. Comparison of the COSY and 4-pulse DQM experiments with the rigid biradical R-I aligned in LC phase V at -57° C. Results are shown for 90° (A) and 0° (B) tilt angles, respectively. (i) – DQM, [scaled up by a factor of 4 in (A)]; (ii) – COSY; (iii) - DQM with exponential decay removed. Pulse widths are 3.5/3.5 ns for COSY and 3.5/3.5/6/3.5 for the DQ experiment.

In Fig. 19 we show COSY and 4-pulse DQ signals for macroscopically aligned biradical R-I for two orientations. Note that both show the low-frequency oscillations due to dipolar coupling (DQM), but COSY shows

relatively larger ESEEM effects (which are seen as high frequency noise in insets), and both show effects from T_2 decay.

The situation is totally different in the case of disordered samples. Fig. 20 shows the envelope of the primary echo [$\beta_1 = \pi/2$, $\beta_2 = \pi$] for R-II. It follows from Eq. 47 that for the primary echo sequence the relative effect of DQ modulation must be stronger than for COSY, since $S_2(\pi) \approx 1$ for strong pulses. Despite this, it is very difficult to obtain the dipolar modulation from the primary echo. After removing the decaying background the residual signal is Fourier transformed and shown in the inset of Fig. 20. In addition to the strong ESEEM pattern that is typical for weakly coupled protons, a weak solitary peak at 11.9 MHz is clearly visible. Even if we believe that it is the singular component of the Pake doublet (i.e. $\nu_\perp$), we cannot reliably translate it into a distance without a prior knowledge of J. That is we need both $\nu_\perp$ and $\nu_\parallel$ to extract J (cf. Eq. 15d), but the latter frequency is buried under the ESEEM line at the proton Zeeman frequency.

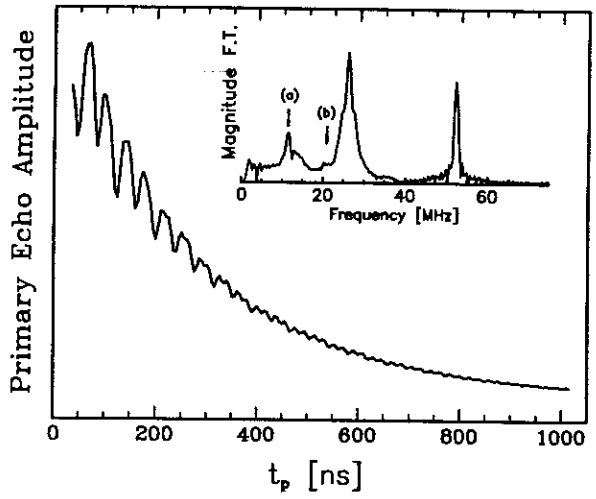

Figure 20. Primary echo ($\pi/2$-τ-π-τ) for the R-II in disordered LC Phase V at -66° C. Pulse widths were 3.5 and 6 ns. Inset: Fourier transformation of the primary echo after removing the decay. The weak solitary peak at 11.9 MHz (a) is likely the singular component of the Pake doublet and the small feature (b) at 22 MHz could be the $\nu_\parallel$.

The reader can compare this result with that obtained using the 6-pulse sequence for the same radical (cf. Fig. 15). In the 6-pulse sequence we obtained a Pake doublet with high SNR and extraction of the distance is a routine task. The electron exchange integral, (small in this case), was also obtained. In the 2-pulse echo (cf. Fig. 20) as we have pointed out above, matters are much more problematic. Even for this Ku-band experiment, this peak is weaker than the ESEEM component at ν_I (26.2 MHz). The second

characteristic frequency of the Pake doublet (25 MHz for R-II) is hidden under the line at ν_I. Note that at X-band both lines will be buried under the ν_I (ca. 13.5 MHz) and $2\nu_I$ lines, respectively. [These lines will be about 4 time more intense at X-band]. Furthermore, the subtraction of the decaying component of the signal practically always produces spurious low-frequency components in the spectrum.

A range of low frequencies of instrumental origin are typically in the signal envelope, as well. All these frequencies yield a low-frequency band which could overlap with the dipolar spectrum in the case of long distances, leaving little hope for extraction of useful data. The situation becomes especially poor in the case of weak pulses. Thus in favorable cases, e.g. aligned systems, one can utilize COSY for distance measurements. When dipolar modulation is shallow, it becomes progressively more difficult to extract distance information from the COSY experiment, even with a dead-time of 35 ns, in cases where distances are sufficiently short (<20 Å) or else distributions in distance damp the oscillations quickly (cf. Sec. 4.3.1). The same problem exists with the 4-pulse DQ signal but to a lesser extent, because in this pulse sequence ESEEM effects can be reduced (cf. 4.2.4). The situation can be improved by adding refocusing pulses to both sequences, and thereby eliminating T_2 decay and to some extent reducing dead time problems. This produces a "2+1" SQ sequence, or the 5-pulse DQ sequence. Coherent 5(6) pulse SQ sequences are also useful (Borbat and Freed, 1999a; 2000), but we found them less convenient unless B_1 is large and/or the spectrometer frequency is high. However, greater benefits can be found in the 6-pulse DQ sequence, which entirely eliminates "apparent" dead-time, deeply suppresses background, and yields stronger signals, given adequate B_1.

4.3 Bilabeled Peptides

In addition to rigid biradicals, spin-labeled synthetic peptides have been studied, (Borbat and Freed, 1999). They are described in (Saxena and Freed, 1996) and have the structure: MTSL-CPPPC-MTSL, (R-III), MTSL-CPPPPC-MTSL, (R-IV), where MTSL is the (1-oxyl-2,2,5,5,-tetramethyl-pyrroline-3-methyl) methanethiosulphonate spin label, and C and P are amino acids cysteine and proline, respectively. The concentration was about 1.0 mM for R-III and 0.75 mM for R-IV in glycerol/water/trifluoroethanol mixture, which was buffered with MOPS (3-[N-morphilino] propane sulphonic acid). They were studied at about -82°C. All samples were about 15-20 μL in volume. In Fig. 21 we show the DQ signal, arising from the 6-pulse sequence, from the polyproline biradical R-IV, where T_2 is 340 ns. The Pake pattern generated by Fourier transforming the left half of the original signal is also shown. There are no well-defined Pake components of the type seen

in Figs. 15-16 for R-I(II), which indicates that there may be a range of distances between the two ends in this synthetic peptide.

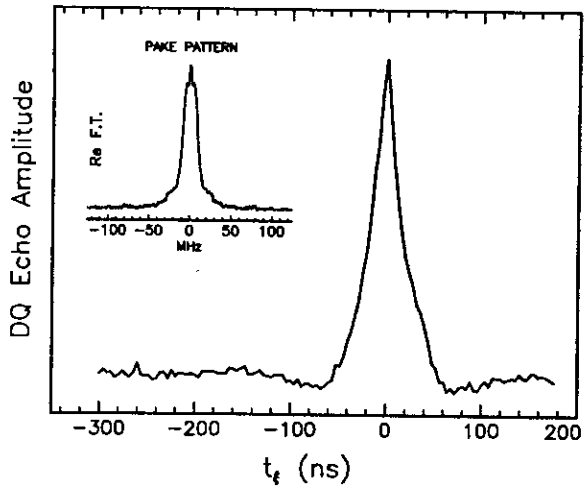

Figure 21. DQ signal, obtained at -82°C for the biradical R-IV dissolved in a glycerol-H_2O-trifluoroethanol mixture. The 6-pulse sequence of Fig. 1(c) was used at 17.35 GHz. Pulse widths were 3.2 ns for $\pi/2$ pulse and 6.0 ns for π pulses. The Pake doublet from the real part of the FT of the signal is shown in the inset. No components are well resolved, suggesting a distribution of distances.

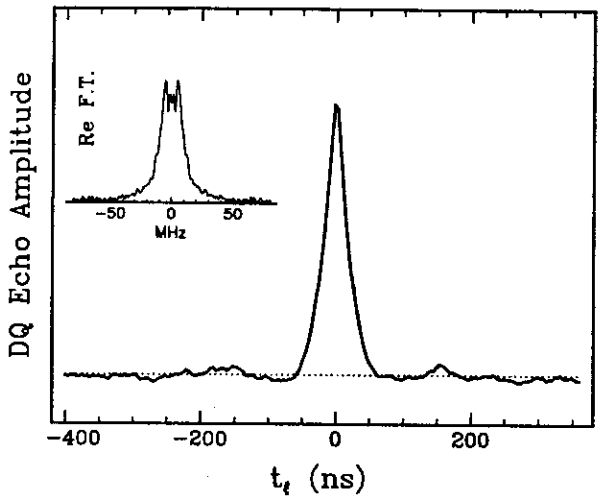

Figure 22. DQ signal, obtained at -82°C for the biradical R-III dissolved in a glycerol-H_2O-trifluoroethanol mixture. Concentration was 0.75 mM. The 6-pulse sequence of Fig. 1(c) was used at 17.35 GHz at the conditions of Fig. 21. The Pake pattern generated by taking the real part of the FT of left half of the signal is shown in the inset.

One can interpret the weak splitting frequency of 4.5 MHz and the half-width of the doublet (9 MHz) to yield an average distance of 22.6 Å with a distribution of distances characterized by a half width of 2 Å by simulating the line shape using distance distributions of different width. This is consistent with the value previously found for R-IV (Saxena and Freed, 1996, 1997). We also found that a 4-fold increase in the concentration of this peptide to 3 mM leads to peptide aggregation, such that the DQ signal from the intramolecular pairs is imposed on the larger signal from intermolecular interactions. This larger signal yields the nearly linear slope that is characteristic of random spin distributions with sufficiently high local concentrations[4]. We did not observe this kind of aggregation for R-III at 3 mM, but could not rule out other possibilities, e.g. dimerization. The Pake pattern for R-III also does not exhibit pronounced singularities of the classical Pake doublet and a small distribution of distances similar to that found for R-IV can well account for this. The distances found for these two peptides are very close, with that for R-III about 1 Å less. We found it difficult to reproduce the shape of the signal envelope in the time domain for R-III(IV) using simple considerations. Also, the DQ signal was not as strong as in the case of R-I or R-II. Two possible explanations are as follows. 1) There are two (or more) conformers one with (or more) separated by a shorter distance (especially for R-IV). This can yield a sharp featureless signal for the latter. 2) The presence of dimers with one of the distances short could also yield a similar result. In this case detection of higher orders of coherence can help to clarify the matter. These are matters for future study.

As an additional note, by analogy to other methods of distance measurements (Milov *et al.*, 1999; Rabenstein and Shin, 1995), one can attempt to subtract out the DQ signal arising from intermolecular dipolar interactions by obtaining the DQ signal from singly-labeled peptides under identical conditions. We have had some preliminary success in this way.

4.3.1 Distribution of Distances

Our examples above, as we have interpreted them, indicate the challenges when there is a distribution of distances. For this case one has to sum over the dipolar line shapes using the proper distance distribution in addition to consideration of possible correlations between nitroxide *hfi* tensors. The net result is a rapid damping of oscillations in the time-domain and a featureless line in the Pake pattern from which it may be very difficult to extract the radial distribution. An estimate of the half width of the distribution can certainly be made from the width of the Pake doublet. The situation can be even more challenging if electron exchange is not negligible. Obviously, our two

[4] Precisely, the slope is exponential in the case of uniform spatial distributions (cf. Eq. 44).

peptide examples cannot be fit reliably with many parameters. In the case of macroscopically aligned systems the situation is predicted to be more encouraging, because distance distributions will show up directly in the form of the observed line shape especially in the limit of non-selective pulses. A study of the angular dependence of the line shape would yield data sufficient to address more complex cases of spatial distributions.

The 6-pulse sequence with sufficiently non-selective pulses seems to be the most suitable technique in the case of distance distributions: it yields the least distorted signals in the time-domain due to virtually zero apparent dead-time, its high time resolution, and its remarkable filtering properties (Borbat and Freed, 2000). It is relatively insensitive to the correlation of *hf* tensors, given adequate spectral excitation. Thus, only the distribution of distances and the dipolar line shape need to be considered. The role of the latter can be minimized by using an oriented sample as we already noted. Current spectral excitation should be improved, and we see several reliable ways of achieving this, (cf. Sec. 5.2).

4.4 "Forbidden" Coherences

4.4.1 "Forbidden" Coherence Pathways

The coherence pathways discussed in Sec. 2 are not the only ones that can give rise to DQC. They are based upon "allowed" coherence pathways, i.e. those that yield DQC which are then converted to detectable SQC by means of hard or non-selective pulses. Even when arbitrary pulses were considered in Sec. 2.2 the coherence pathways remained the same "allowed" ones. The arbitrary pulses referred to the fact that the B_1 was not necessarily large enough to cover the whole nitroxide spectrum; it still ignored the dipolar interaction during the pulse.

In fact, in the case of arbitrary pulses, the dipolar interaction can, in conjunction with the *rf* pulse, produce DQC, as was shown in the extensive numerical analysis of Saxena and Freed (SF), (1997a). In particular, a two-pulse sequence is sufficient to first produce the DQC and then convert and detect it as SQC. In this case the first pulse becomes the full preparation period, i.e. the equivalent of Fig. 3 for non-selective pulses. How can that be? SF found that the first pulse should be a selective one; i.e. a long weak pulse. In particular, of the cases that they considered, the best was in the region of $\tau = 80$ ns and $B_1 = 1.8$ G for an $r \approx 18.5$ Å (D=4.4 G). Thus the dipolar interaction can act during the pulse.

A relatively simple way of analyzing this pulse is by a method due to Salikhov *et al.*, (1996), based on the Suzuki-Trotter (S-T) formula (Suzuki, 1985). They show that the arbitrary pulse can be split up into a series of n

small $\Delta\tau$ segments (where $n\Delta\tau = \tau_{pulse}$). Within each segment, the role of the pulse and of H (Eq.18) can be treated as separate. Then Fig. 3 becomes the n = 2 approximant to this pulse, (except that if the selective pulse is nominally $\pi/2$, then each sub-pulse for n = 2 is just $\pi/4$). As a result, the forbidden coherence (FC) becomes weakly allowed. SF estimate that FC will range from 14 to 60 times weaker than the allowed pathways from their simulations, which assumed both pulses to be identical. Actually, it would be better to use a strong second $\pi/2$ pulse to more effectively convert the DQC into anti-phase SQC. In addition, preliminary experiments have indicated that this FC approach would be better achieved by adding refocusing π pulses after the first and second pulses, by analogy to what is done for the "allowed" pulse sequence of Fig. 5(b). In fact, it would yield the 4-pulse FC pathway analogue of the 5-pulse allowed coherence pathway of Fig. 5(b), where the first two pulses of Fig 5(b) are replaced by a single selective pulse.

The low order analysis based on the S-T formula (n=2) outlined above shows that the "mixing in" of DQC depends on the ratio:

$$|D/\gamma_e B_1| = \frac{3\gamma_e \hbar}{2r^3 B_1}|1-3\cos^2\theta| \qquad (50)$$

It thus favors those biradicals with interspin vector parallel to B_0, for which the magnitude is maximized. This can provide some orientational selectivity by analogy to that provided by aligning the sample (cf. Sec. 4.2.1), but it corresponds to a weak partial alignment. However, higher order S-T theory (i.e. $n > 2$) can predict FC pathways where $|D/\gamma_e B_1|$ appears to a power greater than unity, implying stronger orientational selectivity.

In their original work, SF (1996) found that they could obtain a FC from a 5-pulse sequence, which is a modified form of Fig. 5(b), from R-IV which shows a more substantial modulation pattern than what is seen in Fig. 21, but exhibits much weaker overall S/N. It was fit by numerical simulations by the rigorous theory of SF (1997a), but the effects of distributions in angles λ_1 and λ_2 and distance, r were not considered due to extensive computation times. Clearly, further exploratory work is required before FC can be usefully applied to distance measurements.

5. DISCUSSION

The studies described in the previous section have shown that DQC experiments on bilabeled nitroxide molecules yield the Pake doublets from which one can readily extract distances. This is most successful if there is no correlation between the orientations of the nitroxide moieties relative to $\mathbf{r}_{12}$,

(i.e. Eq. 35). In general this need not be true, so that one has, in principle, to perform a complex analysis based upon Eq. 34 that is analogous to rigorous analyses of any other cw or pulsed ESR method. However, in the DQC experiment it is possible, by using a large enough B_1 field relative to the spectral extent, to almost completely suppress any effects of the nitroxide moieties, (i.e. Eq. 37). Current experimental conditions should be somewhat closer to this limit for ^{15}N labeled nitroxides. Additional improvements (cf. Sec. 5.2) should enable approaching this limit for ^{14}N nitroxides. This "decoupling" is a virtue of the DQC experiment not shared by DEER or "2+1" based upon selective pulses, or by cw-ESR methods (Hustedt and Beth, 1999). Fortunately, such matters have negligible effects in our DQC experiments on the characteristic frequencies, $\nu_\perp$ and $\nu_\parallel$ but do affect the shape of the dipolar spectra. Such matters become of greater concern in the case of biological systems that in our experience show broad distributions of r, so the Pake patterns become poorly resolved or completely unresolved. In such cases, any and all distortions due to correlations and other effects cannot be ignored. *The best way to deal with them is to supply nonselective excitation and double-quantum filtering*. Our experience has indicated that selective pulses should be used with great caution.

Correlation can probably be best addressed by 2D experiments such as illustrated in Fig. 18. Alternatively, the first pulse of the sequences of Fig. 5 could be made selective, and its field position stepped out in a series of experiments. The 2D method, however, provides minimal unwanted effects due to broad spectral excitation with the multiplex advantage. It promises better frequency resolution, that is only limited by the sampling window, and consequently would be expected to result in a more reliable analysis.

Another important advantage of the DQC experiment is that the (nearly) non-selective pulses lead to (nearly) complete excitation of all the spins thereby enhancing signal strength, which is not the case for techniques based upon selective pulses. This should be of considerable value for spin-labeled biomolecules available only in small amounts and typically at low concentrations. In addition, we note that, unlike other ESR methods, the DQC experiment is unaffected by any singly labeled molecules (unless they are present at high concentrations, which in turn will produce more substantial problems to other ESR techniques).

We have seen how the 6-pulse sequence effectively provides zero deadtime. This is achieved by refocusing dipolar coupling at the (virtual) zero time[5], $t_\xi = 0$. In addition, the extremely narrow pulses employed in the method means that they do not contribute significant uncertainty to the time periods for spin evolution. The 4-pulse DQ sequence lacks the zero deadtime feature, (but can yield stronger signals in some cases when there is re-

[5] This is analogous to a 4-pulse DEER sequence (Pannier *et al.*, 2000)

duced coverage from the finite B_1). We do observe ESEEM in the DQC experiments due to surrounding nuclei. It has a small or no effect on the signal in dilute systems (cf. Sec. 4.3.4). In the case of concentrated systems, as we have shown, it is possible to use the suppression effect that results in "blind spots" in the proton modulation in the 4 and 6-pulse sequences.

All in all, we believe these results show how the development of multiple quantum coherences in ESR can lead to a range of new and useful techniques, especially in applications to distance measurements.

5.1 Comparison with Other Pulsed ESR Techniques

When dipolar coupling between two electron spins is present, virtually any SQ signal carries distance information in some form, because its amplitude becomes modulated by the dipolar coupling as antiphase coherences are created (cf. Eq. 27). The simplest technique is of course the Hahn echo, which, in the case of a short dead time, can yield at least one of the two canonical frequencies of the Pake doublet, as we demonstrated with the example of the biradical R-II (cf. Fig. 20). ESEEM is not an unavoidable problem for nitroxides, especially at higher spectrometer frequencies. With very short dead-times a 2-pulse echo technique could be successful (cf. Sec. 4.2.5). Nevertheless, it was instructive to compare the results obtained on the same sample using a Hahn echo and the 6-pulse DQ sequence, (cf. Sec. 4.2.5) to show that the latter is superior.

An improvement to the 2-pulse SQ technique can be made by adding one or more pulses. Several SQ pulse sequences for distance measurement emerge, including DEER and "2+1" sequences (cf. Sec. 2.2).

In the 3-pulse SQ technique known as the "2+1" pulse sequence (Kurshev *et al.*, 1989; cf. Ch. 10), the added pulse has in the past been mainly a selective one, (but this is not necessary). An advantage of this sequence in comparison with the 2-pulse echo is that it eliminates decay due to T_2 and any artifacts that emerge from incrementing the interpulse distance. However, the informative part of the signal consists of two overlapping signals depending on different time variables. These signals are difficult to separate, and there is a large background. As a result, an FT of the signal does not result in a Pake pattern. ESEEM could be strong in "2+1" and it has received special consideration, (Kurshev *et al.*, 1988, Raitsimring *et al.*, 1995). However, in the limit of hard pulses, the nuclear modulation will disappear (Raitsimring, Freed *et al.*, 1995), albeit this is hard to achieve due to the spectral excitation challenges in this sequence.

Coherent SQ sequences (Borbat and Freed, 1999a, 2000; cf. App. C) have also been proposed. They essentially use the refocusing of dipolar coupling in the same fashion as was done in the DQ 6-pulse sequence. Another

SQ sequence has been reported recently by Jeschke *et al.*, 2000. The deficiency of these SQ sequences is that they cannot provide DQ filtering, thus they are useful mainly with very high B_1's and/or well-defined distances (as opposed to distributions in distance).

DEER is a viable SQ technique with many advantages. First of all, ESEEM is virtually absent in 3-pulse DEER, which is an incoherent experiment. The apparent dead-time in 3-pulse DEER is typically limited by the pulse widths, which for a B_1 of 2-4 G are in the range of 40-20 ns, making it difficult to detect ν_I or to obtain the Pake doublet when there is a distribution of distances, because this leads to a rapid damping or even an absence of oscillations (cf. Sec. 4.3).

The 4-pulse version of DEER largely eliminates the dead-time problem of 3-pulse DEER, at the expense of using only part of the pulse sequence length available for evolution of coherences due to dipolar interactions. This should reduce the maximum measurable distance (R_{max}) up to a factor of $2^{1/3}$ as compared to other techniques, (cf. App. B). Nevertheless, the benefits gained due to shortening of the dead-time will be more important. It was clearly demonstrated that this method produces reliable distance information over a broad range of distances and for a variety of systems, (Pannier *et al.*, 2000). The same advantage of zero dead-time is shared by the 6-pulse DQ sequence, but with a much finer time resolution enabling measurements of distances as short as ca. 10 Å.

In most typical cases that we have encountered, the strong dipolar oscillations seen for bilabeled molecules with very rigid structures are rarely observed. For broad distance distributions the oscillations are shallow or completely smoothed out. With weak pulses it becomes problematic, if at all possible, to separate this small smooth signal from the large baseline, which has a steep slope that can be modulated by low ESEEM frequencies, as we have observed in some solvents.

DEER utilizes selective pulses and the signal amplitude is proportional to the product of the excitation profiles at both frequencies (Maryasov *et al.*, 1999). The desirability of increasing B_1 is limited by the rapidly increasing overlap in the spectral excitations at the two irradiating frequencies. Our estimates show that even for ^{14}N nitroxides, B_1 is limited by ca. 4.0 G even when pulses are placed at opposite ends of the spectral bandwidth (the most favorable case). (Here we used a criterion that the spectral overlap should be no more than 10% of the useful signal). The corresponding amplitude factor for the DEER signal was estimated to be about 0.005 of the ideal primary echo signal from all of the spins. The signal amplitude of DEER could be improved by a factor of 5-10 if a high Q resonator were used. However, Pannier *et al.* (2000) found it necessary to use a low-Q LGR to enable excitation at both frequencies. The reduced receiver bandwidth in DEER should

yield an improvement by a factor of 2 or 3 (to about 0.01). In making this estimate, we assumed that in DEER the sampling window, pulse widths, and Q are all set to their optimum values, matching the maximal permissible B_1, (cf. above). More considerations about sensitivity can be found in App. B.

Note that in DEER a pulse that is too wide would ultimately lead to a distortion of the Pake pattern when $0.5\gamma_e B_1 \sim d$. This corresponds to ~20 Å at a B_1 of 4 G. As we noted above, the DQ technique is virtually free from this limitation.

A small amplitude factor in DEER necessitates using higher concentrations and/or large samples, in order to acquire the signal in a reasonable time, especially for larger distances. This may be a reason why, in DEER, the small dipolar modulation is usually imposed on the steep slope of a larger signal (Milov *et al.*, 1999; Pannier *et al.*, 2000) which is caused by intermolecular interactions amongst the randomly distributed spins in the sample. The slope can be removed by conducting experiments at different concentrations (Milov *et al.*, 1999). However this introduces noise and one cannot be fully confident that the separation of useful signal from the large offset is reliably obtained.

By contrast, the DQ technique, due to its sensitivity, is most beneficial for low-concentration samples, which can be of small size. Along with cw ESR methods it can become the technique of choice in distance measurements for many biological systems, which normally are neither concentrated nor available in large quantities.

Finally, there should be large distortions and a reduction of signal with selective pulses, when the *hfi* tensors of the nitroxides are correlated (Maryasov *et al.*, 1998). The DQ sequences are potentially free from this problem, which would virtually disappear at sufficiently large B_1's.

It is appropriate to compare the key equipment used in the pulsed ESR techniques. Although they are different, the equipment is similar in many aspects. In 3-pulse DEER it is better to use 2 high-power pulse sources, [usually TWTA's], to avoid interference between pulses that occurs in the source when the pulses are close to each other. Nevertheless, single high-power sources, have been successfully used (Larsen and Singel, 1993; Pfannebecker *et al.*, 1996). In 4-pulse DEER or in the DQ technique one source is adequate, because the pulses do not need to be very close. "2+1" typically uses the standard ESE equipment "as is" or with minor modifications, but an optimal performance, as that in DEER, can be achieved with use of two TWTA's. The source in the DQ experiment should have an output of at least 2 kW, which is in fact readily available. TWT's with 0.5-1 GHz bandwidth and even greater power are found on the market.

One important difference concerns the probes. Different types of resonators are in use. Bimodal cavity resonators with the modes tuned to different

frequencies have the advantage of high Q in the modes and an opportunity of tuning the modes independently in DEER. The samples can be conveniently studied at low-temperatures using standard fingertip dewars or gas-flow systems (Milov *et al.*, 1998). However, the filling factor is rather poor leading to a loss of SNR. In the DQ experiment low-Q structures including dielectric, loop-gap, and other types of small resonating and delay structures are the most appropriate. Thus low-Q single-mode resonators are in routine use, and they are simpler devices than bimodal structures. However cavity resonators could also be used, and they are more convenient for cryogenic temperatures. We have successfully employed a standard Varian rectangular resonator at X-band for DQC and SQC distance measurements (Borbat and Freed, 2000). It was possible to achieve $\pi/2$ pulses as short as 7.0 ns with our TWT for this cavity. Nevertheless, for best results one should use a high-power source and a small low-Q resonator.

The unavoidable reduction of Q, needed to provide the wide spectral bandwidths to accommodate the short pulses in the DQ experiment (or the different frequencies in DEER), decreases the SNR. This is more than offset by the rapid growth of the amplitude of DQ signals (as the pulse width is decreased) which is a product of the spectral excitations of the two spins as well as by the suppression of destructive effects of correlation and the pseudo-secular term on the signal intensity. This growth is limited only by reaching the condition of full spectral excitation (B_1 of 10 G for E'-centers) or by the available B_1, whichever comes first.

Experimentally DQC is less laborious than other distance measurements by pulsed ESR, because the relevant signal is not overwhelmed by a large unwanted signal.

It is not surprising that we conducted most of our experiments at Ku-band due to its advantages for this technique. Other techniques, including DEER, could also benefit from higher frequency. Commercial spectrometers working at X-band can be used 'as is' for the DQ experiment, but for best results with nitroxides a somewhat smaller loop-gap or dielectric resonator would be highly desirable in order to enhance B_1.

Finally we wish to point out a unique advantage of DQ, or more precisely MQ techniques. More complex structures, such as aggregates of spin-labeled proteins, would involve several interacting electron spins. One should be able to generate and detect the higher orders of coherence that emanate, by analogy to NMR (Baum *et al.*, 1985). This would provide additional insight into such systems.

5.2 Improvements in the Future

As we have seen, given sufficient spectral excitation, the DQ distance measurement technique offers the best sensitivity in comparison to other pulsed methods. It is fully capable of providing accurate distance information over a broad range of distances from 10-15 Å to about 80 Å (cf. Appendix B).

It has been demonstrated that we can generate strong DQ signals at conditions (190-230 K) that are far more challenging than those at cryogenic temperatures (i.e. below ca. 100 K), and can extract distances using small samples (ca. 10 μL) with concentrations of spin even as low as 0.1 mM. This is equivalent to 50 μM concentrations and 500 pmoles of doubly-labeled species. A worst case situation of short T_2's (ca. 0.3-0.5 μs) and distances larger than 25 Å would require about 5-10 nmoles of doubly-labeled molecules. It is also important that solutions of bilabeled proteins are at low enough concentrations, especially, for large molecular weight proteins. This is especially true for measurement of large distances, when concentrations should be low. The DQ experiment can meet this challenge. There is much potential for future improvements of the technique, and we expect that the current limits can be reduced with the additional improvements, that we now describe.

The most important improvement would be the generation of more intense pulses. It greatly improves not only DQC experiments but coherent SQ techniques as well. Using as an example the 6-pulse sequence, we found that there would be a significant increase in the signal amplitude if the B_1 were increased from 30 to 60 G. This increase would be even greater for correlated nitroxides.

The coverage is mainly determined by the π-pulses. It would be sufficient to increase B_1 just for the π-pulses by a factor of 2 and make them of the same length as the $\pi/2$-pulses. As we described, we employ a TWTA with rather typical parameters. It delivers about 2 kW at X and Ku bands and can be boosted up to 3 kW at X-band. For the two-fold increase of B_1 in the resonators that are currently used, the required power would need to be increased by a factor of 4 to the level of about 8 kW. One can use either a more powerful traveling-wave tube or else utilize output pulse compression (Farkas *et al.*, 1989) in order to complete the task.

Another possibility is to explore the applicability of composite pulses, (Levitt, 1979; Crepeau *et al.*, 1989) in DQ sequences. Another improvement, which is being implemented, is to use a higher working frequency, i.e. Ka-band corresponding to 35 GHz (which would also further improve the sensitivity). At this frequency, B_1's can be created as large as 60 G with 1 kW pulses in a dielectric resonator of small size, This would be sufficient for

both ^{15}N and ^{14}N nitroxides at this frequency. The amount of sample could be reduced by a factor of 4 to 5, with a small gain in concentration sensitivity being likely.

Additionally, ESEEM will provide practically no problem at this frequency even in those special cases (small clusters of spin-labeled molecules) that might be expected to pose difficulties, such as when there are long distances (35-80 Å) and when perdeuterated spin-labels and solvents may be desirable or even necessary. At 35 GHz the deuterium ESEEM frequencies are about 4 and 8 MHz in the 6-pulse DQ experiment, and therefore outside the Pake doublet for distances exceeding 30 Å. The ESEEM modulation depth also would decrease as the frequency squared.

Additional improvements should include better phase cycling with a smaller increment to enable one to separate higher orders of coherences in cases of clusters of spin-labeled molecules. Also, pulsed field gradients could be employed to ease the task of separation of high orders of coherence in this case.

ACKNOWLEDGMENTS. We are grateful to Professor A. Rassat for the gift the sample of nitroxide biradical, R-I, and to Professor I. A. Grigorev who kindly supplied the biradical R-II. We thank Dr. M. Ge for help in preparing samples of spin-labeled polypeptides R-III(IV), Professor C. F. Wilcox for help with the molecular modeling of R-I, Drs. S. Saxena and Bosong Xiang for useful discussions, and C. R. Dunnam who brought to our attention the binary pulse compression technique.

The study was supported by NIH Grants RR07126 and GM25862 and NSF Grant CHE9615910.

APPENDICES

A. Effects of the Pseudo-Secular Terms.

In Sec 2.2 we described the theory for DQC pulse sequences, where (1) the pseudo-secular dipolar terms in H were neglected, (cf. Eq. 18), and (2) the dipolar interaction was completely neglected during the pulse, (cf. Eq.19). If both of these approximations are removed, then the solution to the resulting general problem requires numerical simulations (Saxena and Freed, 1997a). Since we are primarily interested in allowed coherence pathways and strong pulses, assumption (2) remains a good approximation (with the pulses that we used ($B_1 \cong 30$ G) for $r \geq 11.5$ Å using estimates from perturba-

tion theory). Thus, in this Appendix we shall remove assumption (1) so that Eq. 17 transformed to the rotating frame will need to be used for H:

$$H/\hbar = \Delta\Omega_1 S_{1z} + \Delta\Omega_2 S_{2z} + aS_{1z}S_{2z} + b_p(S_1^+S_2^- + S_1^-S_2^+)/2. \qquad \text{(A1)}$$

This admits of analytic, though complicated solution. The approach is to utilize the basis set of Eqs. 21 and 22c to describe the free evolution periods when H, given by Eq. A1, is acting. Then by analogy to Eq. 22a:

$$\tilde{Q}\rho \Leftrightarrow e^{-i\frac{H}{\hbar}t}\rho e^{i\frac{H}{\hbar}t} \equiv P\rho P^\dagger. \qquad \text{(A2)}$$

The superoperator $\tilde{Q}$ is represented by a matrix with dimension 16×16 in the operator space with the basis vectors of Eq. 22c. The Hamiltonian H can be diagonalized by a suitable unitary transformation U: $U^\dagger HU = \Lambda$. The propagators on the rhs of Eq. A2 become $P = Ue^{-i\Lambda t}U^\dagger$.

The matrix elements of $\tilde{Q}$ can be determined by applying $\tilde{Q}$ to the basis vectors $\tilde{Q}B_i = Q_{ij}B_j$. Using the scalar product as described by Eq. 22d we can write:

$$Q_{ij} = \mathrm{Tr}\{B_j^\dagger PB_iP^\dagger\}. \qquad \text{(A3)}$$

For evolution of SQC coherences one may reduce the dimension of the problem by considering only the relevant sub-block of Q. We also use only the relevant sub-blocks of the pulse propagator superoperator $\tilde{R}(\beta_k)$ (cf. Eqs. 22a-23) in the derivations. To account for evolution of SQC we introduce the relevant super vectors **I**, **O** of inphase and antiphase SQC's respectively:

$$\begin{aligned} \mathbf{I} &\equiv (\mathbf{I}^+, \mathbf{I}^-), & \mathbf{O}^\pm &\equiv (\mathbf{O}^+, \mathbf{O}^-) \\ \mathbf{I}^\pm &\equiv (S_1^\pm, S_2^\pm), & \mathbf{O}^\pm &\equiv (2S_1^\pm S_{2z}, 2S_2^\pm S_{1z}). \end{aligned} \qquad \text{(A4)}$$

With these definitions, we can write for the free evolution of SQC during a time interval t using the relevant sub-block of Q:

$$\begin{pmatrix} \mathbf{I}' \\ \mathbf{O}' \end{pmatrix} = \begin{pmatrix} \mathbf{V}_t & \mathbf{W}_t \\ \mathbf{W}_t & \mathbf{V}_t \end{pmatrix} \begin{pmatrix} \mathbf{I} \\ \mathbf{O} \end{pmatrix} \qquad \text{(A5)}$$

where the prime denotes the coherences at the end of the evolution period.

The sub-blocks $\mathbf{V}_t$ and $\mathbf{W}_t$ are :

$$\mathbf{V}_t = \begin{pmatrix} \mathbf{V}e^{-i\Delta\Omega_s t} & 0 \\ 0 & \mathbf{V}^* e^{i\Delta\Omega_s t} \end{pmatrix}, \quad \mathbf{W}_t = \begin{pmatrix} \mathbf{W}e^{-i\Delta\Omega_s t} & 0 \\ 0 & \mathbf{W}^* e^{i\Delta\Omega_s t} \end{pmatrix} \tag{A6}$$

which in turn contains the 2×2 matrices:

$$\mathbf{V} = \begin{pmatrix} \alpha c & -i\beta s \\ -i\beta s & \alpha^* c \end{pmatrix}, \quad \mathbf{W} = \begin{pmatrix} -i\alpha s & \beta c \\ \beta c & -i\alpha^* s \end{pmatrix}. \tag{A7}$$

Here

$$\begin{aligned} &\Delta\Omega_s = (\Delta\Omega_1 + \Delta\Omega_2)/2, \quad s = \sin(at/2), \quad c = \cos(at/2) \\ &\alpha = \cos(Rt/2) - ic_{2\Phi}\sin(Rt/2), \quad \beta = -is_{2\Phi}\sin(Rt/2) \\ &c_{2\Phi} = \Delta\Omega/R, \; s_{2\Phi} = b_p/R, \; R^2 = b_p^2 + \Delta\Omega^2, \; \Delta\Omega = \Delta\Omega_1 - \Delta\Omega_2. \end{aligned} \tag{A8}$$

We assumed that $\Delta\Omega_1 > \Delta\Omega_2$ for a positive sign of R. When the pseudo-secular term in b_p of Eq. A1 can be neglected, $\mathbf{V}_t$ and $\mathbf{W}_t$ become diagonal, since $\beta \to 0$; also $\alpha \to \exp(-i\Delta\Omega t/2)$. Then the matrix form is no longer needed and we arrive at Eq. 27 for the evolution. The pulse propagators have a similar block form; details may be found in (Borbat and Freed, 2000), where we also provide the super vector forms of DQ and ZQ coherences and the matrix form for the double quantum filter. This matrix form of the PO formalism allows implementation in "Mathematica" (Wolfram Research) although many of the derivations were easily performed by hand.

After straightforward matrix multiplication one obtains the signal as the scalar product :

$$V = Tr\{\rho^\dagger I^-\}. \tag{A9}$$

The calculations are generally lengthy and somewhat complicated, but they simplify considerably when we use the 6 pulse sequence of Fig. 5(c), i.e. nominal rotation angles $\pi/2$ and π. In this important case the expansion is straightforward, given the assumption that for the terms caused by pseudo-secular part of the dipolar coupling we should take $\Delta\Omega_1 \approx \Delta\Omega_2$. This greatly simplifies calculations and results in more compact expressions. We found that we should modify the $F_n(\mathbf{r}_{12}, t_p)$ of Eqs. 29. For example, the signal enve-

lope in the 6-pulse sequence is now given by $F_6(\mathbf{r}_{12},t_p) = F(t_p)F(t_m-t_p)$, where now $F(t)$ has the form :

$$F(t)=[c_{2\Phi}^2+s_{2\Phi}^2\cos(Rt)]\sin(at)-s_{2\Phi}\sin(Rt)\cos(at)\,. \qquad \text{(A10)}$$

The expressions for the other DQ and SQ signals that are used in distance measurements have similar forms, but we do not give them here. Eq. A10 (and Eqs. 30) do not include "FID-like" terms that occur at $t_\xi \approx 0$. They are caused by the transfer of antiphase coherences between coupled spins that is possible with non-ideal first and last refocusing π pulses and they have the form:

$$\left\langle K(\Delta\Omega_1,\Delta\Omega_2)e^{i(\Delta\Omega_1-\Delta\Omega_2)t_\xi}\right\rangle_{\lambda_1,\lambda_2} \qquad \text{(A11)}$$

where $K(\Delta\Omega_1,\Delta\Omega_2)$ is an unwieldy function of the $\Delta\Omega_i$. They do not carry useful information on the dipolar interaction. Such terms are minimal for nominally π refocusing pulses. Moreover, we found that for the 6-pulse sequence there is a factor of 1/64 in this "FID-like signal", As a result, it is typically two orders of magnitude smaller than the "useful" signal.

Numerical simulations, which we have performed for uncorrelated nitroxides, have shown that, as the distance between the spins becomes shorter, the shape of the Pake doublet changes in an expected way due to the pseudo-secular term in Eq A10. The general tendency is to reduce the intensity of the singular part of the spectrum and ultimately to produce a featureless Pake pattern, as the distance becomes very short (<10 Å). The characteristic frequencies $3d/2$ emerge from Eq. A10. One finds from Eq. A10 that when $\Delta\Omega_1$ is equal to $\Delta\Omega_2$, $F(t) = \sin(3dt/2)$. This is expected for dipolar coupled like spins (Slichter, 1990). These results explain the slightly smoothed shape of the Pake doublet for R-II and the appearance of weak peaks at $\pm 3d/2$ on the Pake doublet (cf. Fig. 16). In the simulations for the distance of 16.2 Å, the effect was distinct, but relatively small for B_1 ca. 30 G. The situation can be different for correlated *hfi* tensors, but this has yet to be explored in detail. This effect becomes pronounced for distances under 15 Å, where the dipolar broadening is very distinct in the ESR spectra of coupled nitroxides. This range of distances is readily studied by cw ESR, (cf. Ch. 3-Ch. 7). For longer distances, where cw methods are difficult to apply, the effects of the pseudo-secular term are not very significant, and it becomes appropriate to utilize the simple treatment given in the Sec. 2.2. With the example of biradical R-II we have seen that we should account for its effects when the distances are under 20 Å. But what is perhaps most significant, these simulations have also shown that an increase in B_1 to 60 G reduces the scale of distortions sub-

stantially. This is one more reason for developing ways to increase B_1 (cf Sec. 5.2). As we have already observed in a number of experiments (Borbat and Freed, 2000), great caution should be exercised in using weak B_1 pulses in coherent experiments, especially in the case of sufficiently broad distance distributions. The dipolar signals from spins at insufficiently large separations (e.g. $r \leq 20$-25 Å) may decrease by orders of magnitude and/or the dipolar spectrum could be too distorted to reflect distances correctly. We observed this for both SQ and DQ methods, i.e. irrespective of the presence of a DQ filter. Signals in most practical cases, when there are distributions of distances, are usually non-oscillating, and it is practically impossible to reliably separate them from the background in SQ coherent sequences and "2+1" if the pulses are weak.

B. Sensitivity and the Upper Range of Measurable Distances

The important issue of sensitivity in a pulsed ESR distance measurement experiment has not been discussed so far in this chapter. Therefore, it seems appropriate to make this estimate and in addition to evaluate an upper range of distances that can be reliably determined in the DQC experiment. We also wish to compare the DQ and DEER experiments with respect to concentration sensitivity. We consider the relevant case of coupled nitroxides, which we assume have uncorrelated *hfi* tensors. For the SNR we can write as an estimate:

$$\begin{aligned} \mathrm{SNR} &= S_1\sqrt{ft}K\exp[-(\frac{2t_m}{T_2})^{\kappa} - 2kCH^{AV}t_m], \\ K &= \mu G^{AV}H^{AV}. \end{aligned} \tag{B1}$$

Here, μ is a constant, S_1 is the SNR in a single-shot data acquisition for a standard SQ sequence, such as COSY, for the condition where the signal intensity is at its maximum [i.e. $t_m \approx 0$]. Other parameters are as follows: f is the repetition rate of the pulse sequence, t is the duration of the experiment, $2t_m$ is the time between the first pulse in the pulse sequence and the echo. This time is assumed to be fixed, and it is measured by the duration of the SQC pathways, (since the DQ pathway is relatively short). K is the ratio of the signal of interest (the DQ echo amplitude or the decrease of the echo intensity in the case of DEER) to a standard signal which for example can be COSY at $t_m = 0$ in the limit of hard pulses. Note that $K \propto G^{AV}H^{AV}$ where G^{AV} and H^{AV} are the spectral excitations for the first and the second spins, respectively, in both methods. The first term in the exponent is due to T_2 relaxation, which for nitroxide radicals at low temperatures is mainly determined by

nuclear spin diffusion and methyl group rotations (Milov *et al.*, 1973; Zecevic *et al.*, 1998; Saxena and Freed, 1997b). The second term in the exponent is due to instantaneous diffusion, with C is the concentration of electron spins, and k is a constant (cf. Sec. 4.1). For S_1 we use the estimate from Borbat and Freed, (1997)

$$S_1 \propto \omega^{3/2} C V_s (Q / V_c \Delta\omega)^{1/2} . \qquad \text{(B2)}$$

Here Q is the Q-value for the working resonator, ω is the applied *mw* frequency, $\Delta\omega$ is the receiver bandwidth (bw), V_c is the effective volume of the resonator, $V_s = V_c\eta$ is the volume of the sample, with η is the filling factor. We assume that the following conditions $\omega Q^{-1} \approx \Delta\omega \approx G^{AV}\Delta\Omega_s$ should result in an optimal SNR. Here $\Delta\Omega_s$ is the total spectral extent. The first condition matches the resonator bw to the receiver bw, and the second matches them to the extent of the spectrum that is excited. Thus we have :

$$S_1 \propto \omega Q (\eta V_s)^{1/2} C \equiv \omega^2 (\eta V_s)^{1/2} C / (G^{AV}\Delta\Omega_s) . \qquad \text{(B3a).}$$

From Eqs. B1 and B3a we find that the SNR $\propto \omega^2 (\eta V_s)^{1/2} C H^{AV}$.

It is appropriate to define and discuss the concentration sensitivity at this point. We assume for the moment that resonators with the same V_c and η, and Q-values are used in both methods. For simplicity, we define the concentration sensitivity as the value of C for a short enough τ (such that instantaneous diffusion does not matter in Eq. B1), that yields a SNR = 1. From Eqs. B1 and B3a we find that

$$C_{\min} \propto [H^{AV} \omega^2 (\eta V_s)^{1/2}]^{-1} . \qquad \text{(B3b)}$$

Eq. B3b leads to two observations. First, the concentration sensitivity improves as ω^2, making it desirable to increase the working frequency at least up to the point where the spectral width starts to be mainly determined by the g-tensor anisotropy, (i.e. for frequencies substantially greater than 35 GHz for nitroxides). Second, in the DQC, H^{AV} could be close to unity (cf. Sec. 3.1.1), whereas in DEER it is about an order of magnitude smaller. Consequently, the concentration sensitivity of the DQ technique should be about an order of magnitude greater.

In DEER the volume of the resonator can be larger than in DQC in some cases (at X-band), thus narrowing the gap in concentration sensitivity for the samples that are not volume limited, due to the factor $V_s^{1/2}$. Cavity resonators can admit the largest samples but, due to the degradation of η, they cannot compete favorably with DR or (B)LG resonators.

At Ku-band, DR or (B)LG resonators with $\eta \approx 1$ and maximal volumes V_c are used in DQC. Thus DEER, at this band, would not benefit from a larger sample. However, at X-band V_s has to be reduced by a factor of ca. 8 from the maximal possible volume ($V_s \approx V_c \approx 160$ μL) at this frequency range to attain sufficient B_1. Thus, this reduces the gain in sensitivity in comparison to DEER at X-band by a factor of 2.8. Of course, at Ku-band we have an additional increase in sensitivity, compared to X-band, of ~3.4[6].

The upper range of measurable distances is ultimately limited by the phase memory time which is determined by both T_2 and instantaneous diffusion. In measurements of very large distances in the range of 40-80 Å it is necessary to lower the concentration until the instantaneous diffusion becomes relatively unimportant in comparison with T_2 relaxation, and then to maximize T_2. In the case of nitroxides at cryogenic temperatures, nuclear spin diffusion of the solvent protons is the major process leading to a rapid phase relaxation with a time dependence $\exp[-(2t_m/T_2)^{\kappa}]$ (Milov *et al.*, 1973; Zecevic *et al.*, 1998; Lindgren *et al.*, 1997). For nitroxides, T_2's of 2-4 μs and κ ca. 1.5-2.5 are typical at temperatures under ca. 120 K, whereas for the temperature range in our studies, ($T \geq 190$ K) T_2's are in the range of 0.2-1 μs and $\kappa \approx 1$ (Saxena and Freed, 1997b). For biological systems, the use of D_2O as a solvent can considerably slow down phase relaxation, and it leads to a phase relaxation as $\exp(-2t_m/T_2)$ with T_2's of order tens of microseconds. It should be noted that our experiments were performed at a local maximum of T_2 for $T > 150$ K. For distances under 30 Å, these T_2's were sufficient, nevertheless, for longer distances than we have explored, temperatures under 100K would be advisable. At temperatures ca. 190 K, T_1 (ca. 25-30 μs) is short enough that the repetition rates of 10 kHz, that we used, allow for virtually complete spin relaxation between pulse sequences.

For extracting distance information with reasonable accuracy, it is necessary to determine, at the very least, the most prominent frequency in the Pake pattern, i.e. $\nu_\perp$. A minimum signal sampling interval could be $1/2\nu_\perp$ (Larsen and Singel, 1993). However, we do not consider this as sufficient, so we take $1/\nu_\perp$ as a more reasonable minimum (i.e. we set $t_m = 1/\nu_\perp$).

With these considerations in mind, we can deduce from Eq. B1 an estimate for an upper range of measurable distances R_{max} in our studies, (where $\kappa \approx 1$):

$$R_{\max}^3 = \frac{\gamma_e^2 \hbar T_2}{4\pi(1 + kCH^{\Delta V} T_2)} \ln\left[\frac{S_1\sqrt{ftK}}{\mathrm{SNR}_{acc}}\right]. \qquad \text{(B4)}$$

[6] Of course, one must take cognizance of the wall thickness of the sample tube relative to its diameter at higher frequencies.

We introduced into Eq. B4 an acceptable SNR denoted by SNR_{acc}. In our spectrometer at Ku-band at 200 K, $S_1 \approx 1$ occurs in the COSY with 30 G pulses at about 1 nmole of nitroxides in 20 μL. Thus, $S_1 \approx 10^9 CV_s$. Substituting into Eq. B4, C = 100 μM, V_s =20 μL, T_2 = 0.5 μs, S_{acc} = 10, f = 10 kHz, t = 10^4s, K = 0.4, we find from Eq. B4 an $R_{max} \approx 44$ Å for DQC. At temperatures below 80 K, T_2's are typically in range 2-4 μs, leading to an increase in R_{max}, (but one must consider κ as well).

In measurements of large distances, C should be sufficiently small. In fact, to avoid a significant contribution from instantaneous diffusion, we require $kCH^{AV}T_2 << 1$. However, if we just assume the weaker inequality:

$$q \equiv \ln[\frac{S_1\sqrt{fi}K}{SNR_{acc}}] >> kCH^{AV}T_2 \qquad \text{(B5)}$$

then to first order in $kCH^{AV}T_2/q$, we obtain

$$R_{max}^3 = \frac{\gamma_e^2 \hbar T_2 q^{\mu}}{4\pi(1+\mu kCH^{AV}T_2 q^{\mu-1})} \qquad \text{(B6)}$$

where $\mu \equiv 1/\kappa$. For T = 80 K, C = 100 μM, V_s = 20 μL, SNR_{acc} = 10, f = 2 kHz, t = 10^4 s, K = 0.4, k=$5 \cdot 10^8$ M^{-1} we find that for T_2 = 3 μs and κ=2 (nuclear spin diffusion), q is 6.8 and R_{max} = 58 Å and similarly for T_2 = 1 μs and κ = 1 (methyl group rotation) we have R_{max} = 55 Å. Thus we find that the upper range of distances by DQC is strongly limited to about 60 Å for a protonated or fluorinated solvent; (we remind the reader that Larsen and Singel's relaxed criterion for t_m (see above) yields 72 Å).

A larger range of distances can only be measured with acceptable accuracy if the solvent is perdeuterated. In this case T_2's may be in the range of tens of microseconds and κ=1. For T_2 =10 μs and C = 100 μM, one estimates an R_{max} = 110 Å, although a more conservative estimate might be somewhere in the range of 80 Å.

Another issue arises regarding the possibility of working with small samples at low concentrations. If the distances are not very large, relaxation is not a major problem. In this case the DQ technique, for a smaller sample, lowers the concentration requirement by at least an order of magnitude (cf. Sec. 5.1) compared to DEER, (in addition to providing less distorted spectra). At Ku-band, a sample with a C ≈ 200 μM and a volume of 10 μL has just 2 nmoles of spins and could easily be studied at T=100 K, for distances under 25 Å.

C. 5-PULSE SQ SEQUENCE

In addition to the 6-pulse DQ sequence (DQ6) which features zero dead-time with respect to the dipolar signal (as is the case in 4-pulse DEER), we also introduced at about the same time a 5-pulse SQ (SQ5) sequence, which was the first SQ sequence with such a property (Borbat and Freed, 1999a).

Here, we would like to briefly describe this sequence. The SQ5 sequence resembles the DQ6 sequence of Fig. 5c, except that the evolution period (consisting of the two t_1 intervals with a π pulse between them) is just replaced by a sufficiently long time interval T so that all coherences which contain frequency shift operators relax by T_2 - type relaxation processes.

The pulses are arbitrary in intensity and, as in the DQ sequences, the nominal rotation angles of the pulses, and their relative phases do matter. The only coherences which survive after T correspond to longitudinal magnetization and 2-spin longitudinal dipolar order which, in turn, are formed from corresponding in-phase and antiphase coherences at the end of the preparation period. Generally, we can describe the sequence as follows:

$$\begin{aligned} S_{1z}+S_{2z} &\xrightarrow{R(\alpha)Q(t_p)R(\beta_1)Q(t_p)} -(S_{1y}+S_{2y}),\, 2S_{1x}S_{2z}+2S_{2x}S_{1z} \\ &\xrightarrow{R(\beta)} S_{1z}+S_{2z},\, 2S_{1z}S_{2z},\, \ldots. \xrightarrow{Q(T)} S_{1z}+S_{2z},\, 2S_{1z}S_{2z} \\ &\xrightarrow{R(\beta)} S_{1y}+S_{2y},\, 2S_{1x}S_{2z}+2S_{2x}S_{1z} \xrightarrow{R(\beta)Q(t_2)R(\beta_1)Q(t_2)} -(S_{1y}+S_{2y}) \end{aligned} \qquad \text{(C1)}$$

Here α is the rotation angle of the 1st pulse, β_1 is that for the 2nd and 5th pulses, and finally β is for the 3rd and 4th pulses. (We use these arbitrary angles because different specific choices favor different pathways). In general, in this 5-pulse sequence with arbitrary pulses, there are 6 coherence pathways given in Eqs. C2 which cannot all be separated by setting proper phases and/or other means:

$$\begin{aligned} &(1)\ S_y \to -S_y \to S_z \to S_y \to -S_y \\ &(2)\ S_y \to -S_y \to S_z \to S_y \to -S_y \cos at_2 \\ &(3)\ S_y \to -S_y \cos at_p \to S_z \to S_y \cos at_p \to -S_y \cos at_p \\ &(4)\ S_y \to -S_y \cos at_p \to S_z \to S_y \cos at_p \to -S_y \cos at_p \cos at_2 \\ &(5)\ S_{1y} \to 2S_{1x}S_{2z} \sin at_p \to 2S_{1z}S_{2z} \to 2S_{1x}S_{2z} \sin at_p \to -S_{1y} \sin at_p \sin at_2 \\ &(6)\ S_{1y} \to 2S_{1x}S_{2z} \sin at_p \to 2S_{1z}S_{2z} \to 2S_{2x}S_{1z} \sin at_p \to -S_{2y} \sin at_p \sin at_2 \end{aligned} \qquad \text{(C2)}$$

Here, $t_2 \equiv t_m - t_p$. The first three pathways correspond to those cases where one or both of the π pulses do not flip the coupled spins. The first pathway is

dominant in the case of selective pulses and forms a "baseline". Pathways (2) and (3) are unwanted. Pathway (4) was our original interest in this sequence. All these pathways are suppressed in the DQC experiment. The pathways (5) and (6) resemble those in DQC as we can deduce from the following comparison.

$$\begin{aligned} &\text{SQ5: } 2S_{kx}S_{lz} \rightarrow 2S_{kz}S_{kz} \rightarrow 2S_{kx}S_{lz},\ 2S_{lx}S_{kz} \\ &\text{DQ6: } 2S_{kx}S_{lz} \rightarrow S_{kx}S_{ly} + S_{ky}S_{lx} \rightarrow 2S_{kx}S_{lz}, 2S_{lx}S_{kz} \end{aligned} \tag{C3}$$

In the general case, the signal can be expressed as a sum of two distinct signals V_1 and V_2 corresponding to pathways (1-4) and (5, 6) respectively. For arbitrary pulses, using our PO technique (cf. App. A) we find that

$$\begin{aligned} V_1 =& \frac{1}{2}\mathrm{Im}\{S(\alpha)^* |S(\beta)|^2 e^{i\Phi} + S(\alpha)S(\beta)^{*2} e^{-i\Phi}\}[S_{\beta 1}^{(1)}]^2 \\ &\times[C_{\beta 1}^{(2)} + S_{\beta 1}^{(2)}\cos(at_p)][C_{\beta 1}^{(2)} + S_{\beta 1}^{(2)}\cos(at_2)] \\ V_2 =& \frac{1}{2}\mathrm{Im}\{(S^{(1)}(\alpha)^* S^{(1)}(\beta)e^{i\Phi} - S^{(1)}(\alpha)S^{(1)}(\beta)^* e^{-i\Phi})(S^{(1)}(\beta)^* C^{(2)}(\beta) \\ &+ S^{(2)}(\beta)^* C^{(1)}(\beta))\} C^{(2)}(\beta)[S_{\beta 1}^{(1)} S_{\beta 1}^{(2)}]^2 \sin(at_p)\sin(at_2) \end{aligned} \tag{C4}$$

Here, $S_{\beta 1}^{(k)} \equiv S_2^{(k)}(\beta_1)$, $C_{\beta 1}^{(k)} \equiv 1 - S_{\beta 1}^{(k)}$, Φ is the relative phase of the 3rd and 1st pulses. Originally, we were primarily concerned with the signal V_1 (Pathway 4 in Eq. C2; $\Phi = 0$; $\alpha, \beta = \pi/2$, $\beta_1 = \pi$ in Eq. C4), which in the limit of nonselective pulses is just $\frac{1}{2}(\cos at_m + \cos at_\xi)$, and for selective pulses is about 1.4 times stronger than the 6-pulse DQC. Signal V_2 resembles the DQ6 signal but it is about a factor of 1.5 times weaker, as follows from simulations.

Why should one prefer one signal over the other? Signal (4) is typically about 2 times stronger and does not have any unwanted relaxation (cf. below). Thus, despite the presence of unwanted signals (1-3) it is useful. Signals (5 and 6) are similar to that in DQ6 but about 1.5-2 times weaker, and one of them (6) is subject to unwanted relaxation caused by nuclear spin diffusion, which is a major T_2 mechanism (cf. App. B and Eq. C5). Thus, in the case of very large distances, one may think of signal (6) as problematic, since the T_2 relaxation would usually be dominated by nuclear spin diffusion (cf. App. B). This signal can be removed by adjustment of the pulse sequence or by adding sufficiently nonselective inverting π pulses during T.

The advantage of the V_1 signal is that there is no extra relaxation with respect to t_ξ. This is the same useful property as in DEER. To explain how relaxation can enter into a constant time experiment, we consider the case

which arises when nuclear spin diffusion is causing T_2 decay given by (cf. App. B):

$$\exp[-(2t_m/T_2)^{\kappa}] \qquad \text{(C5)}$$

for the decay of Pathway (5), whereas for Pathway (6) the decay is :

$$\exp\left[-\left(\frac{t_m - t_\xi}{T_2}\right)^{\kappa} - \left(\frac{t_m + t_\xi}{T_2}\right)^{\kappa}\right] \qquad \text{(C6)}$$

This expression yields approximately a Gaussian signal envelope in t_ξ. For t_ξ=0 the exponent is $2(t_m/T_2)^{\kappa}$ in Eq. C6 while in Eq. C5 it is $2^{\kappa}(t_m/T_2)^{\kappa}$. For a typical case of $\kappa = 2$, the useful interval for sampling the dipolar interaction is reduced by a factor of 2 in the former case due to T_2 decay. Thus in the case (Eq. C6) the latter decay rate of the signal is substantially reduced. This special feature may be useful in order to detect the spin-echo signal at long times. At first glance, an increase of the interval allotted for the dipolar evolution leads to a corresponding increase in resolution of the dipolar spectrum. In fact, it may well be an illusion. Any appreciable increase in resolution does not occur, as is clear from Eq. C6. There is an additional (approximately) Gaussian broadening due to very rapid decay in t_ξ, which effectively shortens the useful interval in t_ξ to ca. $T_2/2^{\frac{1}{\kappa}}$. There is no such broadening in the basic SQ5 sequence (4).

Despite the flexibility of the 5-pulse SQ sequence it does not produce better results than the 6-pulse DQC sequence. With the intense pulses that we employ, it is more difficult to tune this sequence for a clean V_2 signal, as compared with DQ6. We have invariably ended up with better results using the 6-pulse DQC than with the 5-pulse SQC. Maybe in future work it will be possible to find cases where the SQ sequence would be more appropriate.

D. PHASE CYCLES

According to Fig. 5, the signal in the 4(5) pulse sequence is a sum of two signals from the pathways shown. In the 6 pulse sequence of Fig. 5c there are 4 pathways. We denote the pathways as *a*, *b* for 4(5) pulse sequence and *a*, *b*, *c*, *d* for the 6-pulse sequence. The phases for the signals from corresponding pathways are shown under phase tables; (recall ϕ_k is the phase of the k^{ith} pulse). The conditions for generation of DQ signal impose the restriction (cf. Sec. 3.1.4.1): $\phi_1 = \phi_2 = \phi_3$.

Phase cycling combines the signals *a*, *b* (*a*, *b*, *c*, *d*) constructively and suppresses unwanted pathways that interfere with the desired signal.

PHASE TABLE FOR 4-PULSE DQ SEQUENCE[a]

Step number	Phase				Memory address[b]	
	ϕ_1	ϕ_2	ϕ_3	ϕ_4	I	II
1	x	x	x	x	1	2
2	y	y	x	x	-1	-2
3	-x	-x	x	x	1	2
4	-y	-y	x	x	-1	-2
5	x	x	y	x	1	2
6	y	y	y	x	-1	-2
7	-x	-x	y	x	1	2
8	-y	-y	y	x	-1	-2
9	x	x	-x	x	1	2
10	x	y	-x	x	-1	-2
11	-x	-x	-x	x	1	2
12	-y	-y	-x	x	-1	-2
13	x	x	-y	x	1	2
14	y	y	-y	x	-1	-2
15	-x	-x	-y	x	1	2
16	-y	-y	-y	x	-1	-2
17	x	x	x	y	2	-1
18	y	y	x	y	-2	1
19	-x	-x	x	y	2	-1
20	-y	-y	x	y	-2	1
21	x	x	y	y	2	-1
22	y	y	y	y	-2	1
23	-x	-x	y	y	2	-1
24	-y	-y	y	y	-2	1
25	x	x	-x	y	2	-1
26	y	y	-x	y	-2	1
27	-x	-x	-x	y	2	-1
28	-y	-y	-x	y	-2	1
29	x	x	-y	y	2	-1
30	y	y	-y	y	-2	1
31	-x	-x	-y	y	2	-1
32	-y	-y	-y	y	-2	1

Phases ϕ_a, ϕ_b for selected pathways in 4 and 5-pulse sequences:

$$4-\text{pulse}:\ \phi_a = \phi_1 + \phi_2 - 4\phi_3 + \phi_4 \qquad \phi_b = \phi_1 - 3\phi_2 + 4\phi_3 - 3\phi_4$$

$$5-\text{pulse}:\ \phi_a = \phi_1 + \phi_2 - 4\phi_3 + 3\phi_4 - 2\phi_5 \qquad \phi_b = \phi_1 - 3\phi_2 + 4\phi_3 - \phi_4 - 2\phi_5$$

[a] This phase table is expanded by the addition of 2 step CYCLOPS to 128 steps.

[b] The memory addresses I and II are used to store the two quadrature signals. The factors in these columns indicate which quadrature output is stored (1 or 2) and the (+ or -) sign indicates whether they are added to or subtracted from I and II.

Step number	Phase				Memory address[b]	
	ϕ_1	ϕ_2	ϕ_3	ϕ_4	I	II
33	x	x	x	-x	-1	-2
34	y	y	x	-x	1	2
35	-x	-x	x	-x	-1	- 2
36	-y	-y	x	-x	1	2
37	x	x	y	-x	-1	-2
38	y	y	y	-x	1	2
39	-x	-x	y	-x	-1	-2
40	-y	-y	y	-x	1	2
41	x	x	-x	-x	-1	-2
42	x	y	-x	-x	1	2
43	-x	-x	-x	-x	-1	-2
44	-y	-y	-x	-x	1	2
45	x	x	-y	-x	-1	-2
46	y	y	-y	-x	1	2
47	-x	-x	-y	-x	-1	-2
48	-y	-y	-y	-x	1	2
49	x	x	x	-y	-2	1
50	y	y	x	-y	2	-1
51	-x	-x	x	-y	-2	1
52	-y	-y	x	-y	2	-1
53	x	x	y	-y	-2	1
54	y	y	y	-y	2	-1
55	-x	-x	y	-y	-2	1
56	-y	-y	y	-y	2	-1
57	x	x	-x	-y	-2	1
58	y	y	-x	-y	2	-1
59	-x	-x	-x	-y	-2	1
60	-y	-y	-x	-y	2	-1
61	x	x	-y	-y	-2	1
62	y	y	-y	-y	2	-1
63	-x	-x	-y	-y	-2	1
64	-y	-y	-y	-y	2	-1

PHASE TABLE FOR 5-PULSE DQ SEQUENCE:

This phase table is based on the first 16 steps of the 4-pulse DQ sequence given in Table 1. A 64 step sequence is generated as follows. For the first 16 steps, add $\phi_5 \rightarrow x$; for the 2nd 16 steps, just add $\phi_5 \rightarrow -x$; for the 3d 16 steps, just add $\phi_5 \rightarrow$ y; for the 4th 16 steps, just add $\phi_5 \rightarrow$ -y. The memory addresses for the first 16 steps are the same as in Table I; for the second 16 steps

[b] The memory addresses I and II are used to store the two quadrature signals. The factors in these columns indicate which quadrature output is stored (1 or 2) and the (+ or -) sign indicates whether they are added to or subtracted from I and II.

change signs of original entries in columns I, II; for the third 16 steps, exchange entries for I and II and then change signs of entries in column II; for the last 16 steps, again swap entries in I and II, but now change signs in column I. This 64 step phase table is also expanded to 128 steps by adding the 2 step CYCLOPS.

PHASE TABLE FOR 6-PULSE DQ SEQUENCE[c]

Step Number	Phase						Memory Array[d]	
	ϕ_1	ϕ_2	ϕ_3	ϕ_4	ϕ_5	ϕ_6	I	II
1	x	x	x	x	X	x	1	2
2	y	y	y	x	x	x	-1	-2
3	-x	-x	-x	x	x	x	1	2
4	-y	-y	-y	x	x	x	-1	-2
5	x	x	x	y	x	x	1	2
6	y	y	y	y	x	x	-1	-2
7	-x	-x	-x	y	x	x	1	2
8	-y	-y	-y	y	x	x	-1	-2
9	x	x	x	-x	x	x	1	2
10	y	y	y	-x	x	x	-1	-2
11	-x	-x	-x	-x	x	x	1	2
12	-y	-y	-y	-x	x	x	-1	-2
13	x	x	x	-y	x	x	1	2
14	y	y	y	-y	x	x	-1	-2
15	-x	-x	-x	-y	x	x	1	2
16	-y	-y	-y	-y	x	x	-1	-2
17	x	x	x	x	-x	x	-1	-2
18	y	y	y	x	-x	x	1	2
19	-x	-x	-x	x	-x	x	-1	-2
20	-y	-y	-y	x	-x	x	1	2
21	x	x	x	y	-x	x	-1	-2
22	y	y	y	y	-x	x	1	2
23	-x	-x	-x	y	-x	x	-1	-2
24	-y	-y	-y	y	-x	x	1	2
25	x	x	x	-x	-x	x	-1	-2
26	y	y	y	-x	-x	x	1	2
27	-x	-x	-x	-x	-x	x	-1	-2
28	-y	-y	-y	-x	-x	x	1	2
29	x	x	x	-y	-x	x	-1	-2
30	y	y	y	-y	-x	x	1	2
31	-x	-x	-x	-y	-x	x	-1	-2
32	-y	-y	-y	-y	-x	x	1	2

[c] This phase table is combined with 4 step CYCLOPS yielding 256 steps.
[d] See the Table for 4-pulse sequence, footnote b.

	ϕ_1	ϕ_2	ϕ_3	ϕ_4	ϕ_5	ϕ_6	I	II
33	x	x	x	x	y	x	2	-1
34	y	y	y	x	y	x	-2	1
35	-x	-x	-x	x	y	x	2	-1
36	-y	-y	-y	x	y	x	-2	1
37	x	x	x	y	y	x	2	-1
38	y	y	y	y	y	x	-2	1
39	-x	-x	-x	y	y	x	2	-1
40	-y	-y	-y	y	y	x	-2	1
41	x	x	x	-x	y	x	2	-1
42	x	y	y	-x	y	x	-2	1
43	-x	-x	-x	-x	y	x	2	-1
44	-y	-y	-y	-x	y	x	-2	1
45	x	x	x	-y	y	x	2	-1
46	y	y	y	-y	y	x	-2	1
47	-x	-x	-x	-y	y	x	2	-1
48	-y	-y	-y	-y	y	x	-2	1
49	x	x	x	x	-y	x	-2	1
50	y	y	y	x	-y	x	2	-1
51	-x	-x	-x	x	-y	x	-2	1
52	-y	-y	-y	x	-y	x	2	-1
53	x	x	x	y	-y	x	-2	1
54	y	y	y	y	-y	x	2	-1
55	-x	-x	-x	y	-y	x	-2	1
56	-y	-y	-y	y	-y	x	2	-1
57	x	x	x	-x	-y	x	-2	1
58	y	y	y	-x	-y	x	2	-1
59	-x	-x	-x	-x	-y	x	-2	1
60	-y	-y	-y	-x	-y	x	2	-1
61	x	x	x	-y	-y	x	-2	1
62	y	y	y	-y	-y	x	2	-1
63	-x	-x	-x	-y	-y	x	-2	1
64	-y	-y	-y	-y	-y	x	2	-1

Phases ϕ_a, ϕ_b, ϕ_c, ϕ_d for selected pathways in 6-pulse sequence:

$$\phi_a = \phi_1 - 2\phi_2 - \phi_3 + 4\phi_4 - \phi_5 - 2\phi_6 \qquad \phi_c = -\phi_1 + 2\phi_2 + \phi_3 - 4\phi_4 + 3\phi_5 - 2\phi_6$$

$$\phi_b = \phi_1 - 2\phi_2 + 3\phi_3 - 4\phi_4 + 3\phi_5 - 2\phi_6 \qquad \phi_d = -\phi_1 + 2\phi_2 - 3\phi_3 + 4\phi_4 - \phi_5 - 2\phi_6$$

REFERENCES

Abragam, A. (1961) The principles of nuclear magnetism. (Oxford Univ. Press, NY), Ch. 4.

Astashkin, A.V., Hara, H. and Kawamori A. (1997) The pulsed electron-electron double resonance and "2+1" electron spin echo study of the oriented oxygen-evolving and Mn-depleted preparations of photosystem II. *J. Chem. Phys.*, **108**, 3805-3812.

Bloom, A.L. (1955) Nuclear induction in inhomogeneous fields. *Phys. Rev.* **98,** 1105-1112.

Baum, J., Munowitz, M., Garroway. A.N. and Pines, A. (1985) Multiple-quantum dynamics in solid state NMR. *J. Chem. Phys.* **83**, 2015-2025.

Bax, A., de Jong, P.G., Mehlkopf, A.F. and Smidt, J. (1980) Separation of the different orders of NMR multiple-quantum transitions by the use of pulsed field gradients. *Chem. Phys. Lett.*, **69**, 567-570.

Borbat, P.P., Berdnikov, V.M., Milov, A.D. and Tsvetkov, Yu.D. (1977) Spatial distribution and diffusion of hydrogen atoms formed on photolysis of Fe(II) in frozen sulfuric acid water solutions. *Sov. Phys. Solid State*, **19**, 628-663.

Borbat, P.P. Crepeau, R.H. and Freed, J.H. (1997) Multifrequency two-dimensional Fourier transform ESR: X/Ku-band spectrometer. *J. Magn. Reson.*, **127**, 155-167.

Borbat, P.P. and Freed, J.H. (1999) Multiple-quantum ESR and distance measurements. *Chem. Phys. Lett.*, **313**, 145-154.

Borbat, P.P. and Freed J.H. (1999a) Progress in multiple-quantum ESR Spectroscopy: powerful tool for distance measurements, at *"41st Rocky Mountain Conference on Analytical Chemistry"*, Aug. 1-5, Denver, Colorado.

Borbat, P.P. and Freed, J.H. (2000) Double and single quantum coherence ESR for distance measurements: effects of microwave B_1 and frequency, (To be published).

Budker, V., Du, J.-L., Seiter, M., Eaton, G.,R., Eaton, S.S. (1995) Electron-electron spin-spin interaction in spin-labeled low-spin methemoglobin, *Biophys. J.*, **68**, 2531-2542.

Cavanagh, J., Fairbrother, W.J., Palmer III, A.G., Skelton, N.J. (1996) Protein NMR Spectroscopy. Academic Press, San Diego.

Chandrasekhar, S. (1943) Stochastic problems in physics and astronomy. Revs Modern. Phys. **15**, 165-191

Corio, P.L. (1966) Structure of high-resolution NMR spectra. Academic Press, NY.

Crepeau., R.H., Dulcic, A., Gorcester, J., Saarinen, T. and Freed, J.H. (1989) Composite pulses in time-domain ESR. *J. Magn. Reson.*, **84**, 184-190.

Dikanov, S.A., Tsvetkov, Yu.D. (1992) Electron spin echo envelope modulation (ESEEM) spectroscopy. CRC Press, 21.

Dzuba, S.A., Bosh, M.K., Hoff, A.J. (1996) Electron spin-echo detection of quantum beats and double-quantum coherence in spin-correlated radical pairs of protonated photosynthetic reaction centers. *Chem. Phys. Lett.*, **248**, 427-433.

Dzuba, S.A. and Kawamori, A. (1996) Selective hole burning in EPR: spectral diffusion and dipolar broadening. *Concepts in Magnetic Resonance* **8**, 49-61.

Eaton, S.S. and Eaton, G.R. (1993) Irradiated fused-quartz standard sample for time-domain EPR. *J. Magn. Reson.* **A. 102**, 354-356.

Emshwiller, M., Hahn, E.I., Kaplan, D. (1960) Pulsed nuclear resonance spectroscopy. *Phys. Rev.*, **118**, 414-424.

Ernst, R.R., Bodenhausen, G., Wokaun, A. (1987) Principles of nuclear magnetic resonance in one and two dimensions. Clarendon Press, Oxford.

Ewert, U, Crepeau, R.H., Lee, S., Dunnam C.R., Xu, D. and Freed, J.H. (1991) Fourier transform electron spin resonance imaging. *Chem. Phys. Lett.*, **184**, 25-33.

Farhbakhsh, Z.T., Huang, Q.-L., Ding, L.-L., Altenbach, C., Steinhoff, H.J., Horwitz, J. and Hubbell, W.L. (1995) Interaction of α-crystallin with spin-labeled peptides. *Biochemistry*, **34**, 509-516.

Farkas, Z.D., Spalek, G. and Wilson P.B. (1989) RF pulse compression experiment at SLAC, *Proceedings of the 1989 IEEE particle accelerator conference*. Chicago, March 20-23, vol. 1, 132-134.

Fauth, J.-M., Schweiger, A., Braunschweiler, L., Forrer, J. and Ernst, R.R. (1986) Elimination of unwanted echoes and reduction of dead time in three-pulse electron spin-echo spectroscopy. *J. Magn. Reson.*, **66**, 74-85.

Feldman, E.B., Lacelle, S. (1996) Configurational averaging of dipolar interactions in magnetically dilute spin networks. *J. Chem. Phys.* **104**, 2000-2009.

Gemperle , C., Aebli, G., Schweiger, A., and Ernst, R. R., (1990) Phase cycling in pulse EPR. *J. Magn. Reson.*, **88**, 241-256.

Gorcester, J. and Freed, J.H. (1988) Two-dimensional Fourier transform ESR correlation spectroscopy. *J. Chem. Phys.*, **88**, 4678-4693.

Hanson, P., Anderson, D.J., Martinez, G., Millhauser, G., Formaggio, F., Crisma, M., Toniolo, C. and Vita, C. (1999) Electron spin resonance and structural analysis of water soluble, alanine-rich peptides incorporating TOAC. *Mol. Phys.*, **95**, 957-966.

Hanson, P., Millhauser, G., Formaggio, F., Crisma, M., Toniolo, C. (1996) ESR characterization of hexameric, helical peptides using double TOAC spin-labeling. *J. Am. Chem. Soc.*, **118**, 7618-7625.

Hara, H., and Kawamori, A. (1997) A selective hole burning method applied to determine distances between paramagnetic species in Photosystems. *Appl. Magn. Reson.*, **13**, 241-257.

Höfer, P., Grupp, A., Nebenfuhr, H. and Mehring, M. (1986) Hyperfine sublevel correlation (HYSCORE) spectroscopy: A 2D ESR investigation of the squaric acid radical. *Chem. Phys. Lett.*, **132**, 279-282.

Hoult, D.I. and Richards (1975) Critical factors in the design of sensitive high resolution nuclear magnetic resonance spectrometers. *Proc. Roy. Soc.*, (*Lond*), **344**, 311-340.

Hustedt, E.J., Smirnov, A.I., Laub, C.F., Beth, A.H. (1997). Molecular distances from dipolar coupled spin-labels: the global analysis of multifrequency continuous wave electron paramagnetic resonance data. *Biophys. J.* **72**, 1861-1877.

Hustedt, E.J. and Beth, A.H. (1999) Nitroxide spin-spin interactions: applications to protein structure and dynamics. *Annu. Rev. Biophys. Biomed. Struct.*, **28**, 129-153.

Ichikawa, T., Wakasugi, S.Ichi and Yoshida, H. (1985) Structure of spurs in γ-irradiated alcohol matrices by electron spin-echo method. *J. Phys. Chem.*, **89**, 3583-3586.

Jeschke, G., Bauer C., Pannier M., Leporini D. and Spiess, H.W. (2000) Pulse high-field EPR on nitroxide spin probes in polymers, at *"High-frequency electron paramagnetic resonance: technology and applications"*, Amsterdam, April 12-14.

Kurshev, V.V., Astashkin, A.V., and Raitsimring, A.M (1988) Modulation Effects in 2+1 Electron spin echo pulse sequence. *J. Struct. Chem.*, **29**, 62-68.

Kurshev, V.V., Raitsimring, A.M. and Tsvetkov, Yu.D. (1989) Selection of dipolar interaction by the "2+1" pulse train ESE. *J. Magn. Reson.*, **81**, 441-454.

Larsen R.G. and Singel, D.J. (1993) Double electron-electron resonance spin-echo modulation. Spectroscopic measurement of electron spin pair separation in orientationally disordered solids. *J. Chem. Phys.*, **98**, 5134-5146.

Lee, S., Patyal, B.R. and Freed, J.H. (1993) A two-dimensional Fourier transform electron spin resonance (ESR) study of nuclear modulation and spin relaxation in irradiated malonic acid. *J. Chem. Phys.*, **98**, 3665-3689.

Lee, S., Budil, D.E. and Freed, J.H. (1994) Theory of two-dimensional electron spin-resonance for ordered and viscous fluids. *J. Chem. Phys.*, **101**, 5529-5558.

Levitt, M.H. (1979) Composite pulses. *Progr. NMR. Spectr.*, **18**, 61-122.

Lindgren, M., Eaton, G.R., Eaton, S.S., Johnsson, B-H, Hamarström, P., Svensson, M. and Carlsson, U. (1997) Electron spin echo decay as a probe of aminoxyl environment in spin-labeled mutants of human carbonic anhydrase II. *J. Chem. Soc., Perkin Trans.* **2**, 2549-2554.

Maryasov, A.G., Tsvetkov, Yu.D., Raap, J. (1998) Weakly-coupled radical pairs in solids: ELDOR in ESE structure studies. *Appl. Magn. Reson.*, **14**, 101.

Meirovitch, E., Igner, D., Igner, E., Moro, G. and J.H. Freed, J.H. (1982) Electron-spin relaxation and ordering in smectic and supercooled nematic liquid crystals. *J. Chem. Phys.*, **77**, 3915-3937.

Milov, A.D., Salikhov, K.M. and Tsvetkov, Yu.D. (1973) Phase relaxation of hydrogen atoms stabilized in an amorphous matrix. *Sov. Phys. Solid State.* 15, 802-806.

Milov, A.D., Salikhov, K.M., Shirov, M.D. (1981) Application of the double resonance method to electron spin echo in a study of the spatial distribution of paramagnetic centers in solids. *Sov. Phys. Solid State*, **23**, 565-569.

Milov, A.D., Maryasov, A.G. and Tsvetkov, Yu.D. (1998) Pulsed electron double resonance (PELDOR) and its applications in free-radical research. *Appl. Magn. Reson.*, **15**, 107-143.

Milov, A.D., Maryasov, A.G., Tsvetkov, Yu.D., Raap, J. (1999) Pulsed ELDOR in spin-labeled polypeptides. *Chem. Phys. Lett.*, **303**, 135-143.

Milov, A.D., Ponomarev, A.B. and Tsvetkov, Yu.D. (1985) Modulation beats of double electron-electron resonance in spin echo for biradical systems. J. Chem. Struct., **25**, 710-713.

Ohba, Y., Satoh, R., Kikuchi, T., Yamauchi. S. and Iwazumi. M. (1993) A new technique for accurate measurement and adjustment of the phase of the microwave pulse in pulsed EPR spectroscopy. *J. Magn. Reson.*, **A103**, 282-287.

Pake, G.E. (1948) Nuclear resonance absorption in hydrated crystals: fine structure of the proton line. *J.Chem.Phys.*, **16**, 327-336.

Pannier, M., Veit, S., Godt, A., Jeshke, G. and Spiess, H.W. (2000) Dead time free measurement of dipole-dipole interactions between electron spins. *J. Magn. Reson.*, **142**, 331-340.

Pfannebecker, V., Klos, H., Hubrich, M., Volkmer, T., Heuer, A., Wiesner, U. and Spiess, H.W. (1996) Determination of end-to-end distances in oligomers by pulsed EPR. *J. Phys. Chem.*, **100**, 13428-13432.

Rabenstein, M.D. and Shin, Y.-K. (1995) Determination of the distance between two spin labels attached to a macromolecule. *Proc. Natl. Acad. Sci., USA*, **92**, 8239-8243.

Rabenstein, M.D., Shin, Y.-K. (1996), HIV-1 gp41 tertiary structure studied by EPR spectroscopy. *Biochemistry*, **35**, 13922-13928.

Raitsimring, A.M. and Salikhov, K.M. (1985) Electron spin echo method as used to analyze the spatial distribution of paramagnetic centers *Bulletin of Magn. Reson.*, **7**, 184-217.

Raitsimring, A., Crepeau, R.H. and Freed, J.H. (1995) Nuclear modulation effects in "2+1" electron spin-echo correlation spectroscopy. *J. Chem. Phys.*, **102**, 8746-8762.

Rakowsky, M.H., Zecevic, A., Eaton, G.R. and Eaton, S.S. (1998) Determination of high – spin iron(II)-nitroxyl distances in spin-labeled porphyrins by time-domain EPR. *J. Magn. Reson.*, 11, 97-110.

Salikhov, K.M., Semenov, A.G. and Tsvetkov, Yu.D. (1976) Electron spin echo and its applications. Nauka, Novosibirsk, (in Russian).

Salikhov, K.M., Schneider, D.J., Saxena, S., Freed, J.H. (1996) A theoretical approach to the analysis of arbitrary pulses in magnetic resonance. *Chem. Phys. Lett.*, **262**, 17-26.

Saxena, S., Freed, J.H. (1996) Double quantum two-dimensional Fourier transform spin resonance: distance measurements. *Chem. Phys. Lett.*, **251**, 102-110.

Saxena, S., Freed, J.H. (1997a) Theory of double quantum two-dimensional electron spin resonance with applications to distance measurements. *J. Chem. Phys.*, **107**, 1317-1340.

Saxena, S. and Freed, J.H. (1997b) Two-dimensional electron spin resonance and slow motions. *J. Phys. Chem.*, **A101**, 7998-8008.

Schweiger, A. (1990) New trends in pulsed spin-resonance methodology. In *Modern Pulsed and Continuous-wave Electron Spin Resonance*, (Kevan, L., Bowman, M.K., eds), pp 43-118, Wiley, NY.

Shriver, J. (1992) Product operators and coherence transfer in multiple-pulse NMR experiments. *Concepts in Magn. Reson.*, **4**, 1-33.

Slichter, C.P. (1990) Principles of magnetic resonance, 3rd enl. and updated edn., Springer-Verlag, Berlin-Heidelberg-New-York.

Sørensen, O.W., Eich, G.W., Levitt, M.H., Bodenhausen, G. and Ernst, R.R. (1983) Product operator formalism for the description of NMR pulse experiments. *Progr. NMR Spectr.*, **16**, 163-192.

Suzuki, M. (1985) Decomposition formulas of exponential operators and Lie exponentials with some applications to quantum mechanics and statistical physics. *J. Math. Phys.*, **26**, 601-612.

Tang, J., Norris, J.R. (1995) Multiple-quantum EPR coherence in a spin-correlated radical pair system. *Chem. Phys. Lett.*, **233**, 192-200.

Thorgeirsson, T.E., Xiao, W., Brown, L.S., Needleman, R., Lanyi, J.K. and Shin, Y.-K. (1997) Transient channel-opening in bacteriorhodopsin: an EPR study. *J. Mol. Biol.*, **273**, 951-957.

Yudanov, V.F., Salikhov, K.M., Zhidomirov, G.M. and Tsvetkov, Yu.D. (1969) Modulation effects in the electron spin echo of biradical systems. *Theor. and Experim. Chem.*, *5*, 663-668.

Zecevic, A., Eaton, G.R., Eaton, S.S. and Lindgren, M. (1998) Dephasing of electron spin echoes for nitroxyl radicals in glassy solvents by non-methyl protons. *Mol. Phys.*, **95**, 1225-1263.